MODELLING AND DESIGN OF A LATENT HEAT THERMAL STORAGE SYSTEM

WITH REFERENCE TO SOLAR ABSORPTION REFRIGERATION

by

JOSEPH BASAKAYI KANTOLE

A dissertation submitted in fulfilment of the requirements for the degree of

MAGISTER INGENERIAE: MECHANICAL ENGINEERING

IN THE

FACULTY OF ENGINEERING AND THE BUILT ENVIRONMENT

AT THE

UNIVERSITY OF JOHANNESBURG

SUPERVISOR: PROFESSOR C.P. STORM

April 2012

DECLARATION

I, JOSEPH BASAKAYI KANTOLE, hereby declare that the work performed and the contents of this dissertation submitted for the Master Degree in Mechanical Engineering to the University of Johannesburg, apart from the help and guidance from my supervisor Professor C. P. Storm is my own work and has not previously been submitted to another university or institution of high education for a degree.

Date: _____ th day of _____of 2012

JOSEPH BASAKAYI KANTOLE

ABSTRACT

The research in this thesis focuses on the theoretical thermal modelling and design of a Latent Heat Storage system (LHS) for an absorption refrigeration machine. A shell-and-tube latent heat storage exchanger retaining any excess solar thermal energy is selected. Here, solar thermal energy supplied by a collector is transferred to and stored by the LHS. During low insolation, stored thermal energy is transferred by a Heat Transfer Fluid (HTF) into the generator, a component of an Ammonia Absorption Refrigerator (AAAR), to ensure efficiency of the cooling cycle.

The shell-and-tube LHS contains Phase Change Material (PCM) which fills space outside the tube heat exchangers. The HTF flowing through the tubes exchanges thermal energy with the PCM. The selection of a suitable PCM for a LHS is based on several factors. A primary criterion for an efficient, reliable storage unit is the correct melting point of the PCM at a desired operating temperature of the heating application.

An analytical model describing both the freezing process in the PCM and increased HTF temperature in the tube heat exchangers is investigated. The model is developed using energy balance equations. It is solved in terms of dimensionless parameters. The thermal resistance of the tube heat exchangers is considered for this model.

From the result of the analytical model, the design approach to size the LHS is provided and the different steps are given in order to determine the volume, mass, number of tube heat exchangers, inner and outer radius of the tube heat exchangers and other parameters of the LHS.

The dimensions of LHS are given as a function of a storage period, PCM properties, HTF properties, inner and outer radius of the tube heat exchangers, material of construction of the tube heat exchangers and the nature of load on the heating process.

Simulations from the analytical model developed are provided for the output thermal parameters of the storage system. These thermal parameters of the shell-and-tube latent exchanger are given in terms of the HTF outlet temperature, the front solidification of the PCM and the heat transfer rate during the solidification process of the PCM.

A case study to demonstrate the application of the design approach with respect to the size shell-and-tube latent heat exchanger is provided. The integration of the tube heat

exchangers thermal conductivity in the modelling of the LHS resulted in an increase of 2% in mass of the storage material compared to an analytical model neglecting the thermal conductivity of the tube heat exchangers.

The results of the model developed compared well with the results obtained from other analytical models at similar operating conditions.

Keywords: Phase Change Material; heat exchanger; storage; solar energy; Aqua Ammonia Absorption Refrigerator.

DEDICATION

This thesis is dedicated to my parents: my father, the late Marcel Basakayi Kanyama and my mother Jeanne Marie Ntumba for their endless love, support and encouragement.

I am grateful to my brothers, sisters and friends for all their love and support during my studies.

And I am grateful to God our Creator because only through His love and guidance are we capable of anything.

ACKNOWLEDGEMENTS

TABLE OF CONTENTS

LIST OF FIGURES

LIST OF TABLES

NOMENCLATURE

b — Dimension of the slab container of a PCM, [m]

Bi — Biot number

C — Specific heat capacity, [kJ/kg.°C]

D — Dimension of rectangular or slab container of a PCM, diameter of the tube, [m]

F — Fraction of the PCM solidified at the tube; Fourier number

G_0 — Function of F

G_1 — Function of F

h — Convection heat transfer coefficient, $[\dfrac{W}{m^2 °C}]$

k — Thermal conductivity, $[\dfrac{W}{m°C}]$; ratio of thermal conductivity

l — Length of the tube, [m];

m — Mass of the heat storage medium, [kg]

M — Mass of PCM, [kg]

m_f — Mass flow rate, $[\dfrac{kg}{s}]$

NTU — Number of Transfer Units

Nu — Nusselt number

Ph — Measure of the acidity or basicity of an aqueous solution

Pr — Prandtl number

r — Radius of solid-liquid interface; [mm]

R — Radius of tube, [mm]; universal gas constant $[\dfrac{kJ}{kg.K}]$; thermal resistance, $[\dfrac{°C}{W}]$

Re — Reynolds number

$\dot{Q}$ — Heat flow per unit length, $[\dfrac{W}{m}]$

Q — Heat transfer rate, [W]

$\hat{Q}$ Dimensionless heat flow

s   Ratio of the outer and inner radius of a tube heat exchanger

Ste Stefan number

t   Time, $[h]$

T   Temperature, $[^{\circ}C]$

V   Velocity, $[\frac{m}{s}]$; volume $[m^3]$, $[l]$

x   Axial distance along the tube exchanger, $[m]$

GREEK SYMBOLS

β Parameter function of convection heat transfer

ε Porosity, effectiveness

ξ Dimensionless axial distance along the tube exchanger

ρ Density, $[\frac{kg}{m^3}]$

τ Dimensionless time variable

SUBSCRIPTS

a   Ambient

ev   Evaporator

f   Fluid, final

G   Generator

i   Inlet, initial, inner

l   Liquid

m   Phase change material, melting

mol mole

o   Outlet, outer

p   Constant pressure, pump

r   Reacted

t   Total

s   Solid

w   Wall

ABBREVIATIONS

AAAR   Aqua Ammonia Absorption Refrigerator

ARU   Absorption Refrigerator Unit

CHTF   Cold Heat Transfer Fluid

COP   Coefficient Of Performance

DSC   Differential Scanning Calorimetry

HTF   Heat Transfer Fluid

HHTF   Hot Heat Transfer Fluid

LHS   Latent Heat Storage

n.a   not available

NTU   Number of Transfer Units

PCM   Phase Change Material

RSA   Republic of South Africa

SC   Solar Collector

SCILAB   Scientific Laboratory

SHS   Sensible Heat Storage

SS   Storage System

TES   Thermal Energy Storage

Chapter 1

INTRODUCTION

1.1   Background

Solar energy is among the most promising alternative sources of energy compared to traditional fossil fuels. It is available, there are no ongoing fuel costs and its environmental impact is low. Today, many solar energy systems able to convert solar radiation directly into thermal energy have been developed for low, medium and high temperature heating applications. Solar thermal power generation and solar space heating are examples of industrial applications; domestic applications include solar water heating and solar absorption refrigeration.

There are several options available which enable integration of solar energy into the process of "cold" production. For instance, solar absorption refrigeration can be accomplished by using either a thermal energy source supplied from a solar collector, or electricity from a photovoltaic panel. Photovoltaic refrigeration does not yet enjoyed widespread use because of low efficiency and the high cost of photovoltaic cells (Kalogirou, 2004).

A number of research work have been carried on solar absorption cooling in the past and the technology for their utilisation developed (Pridasawas, 2003; Duffie & Beckman, 2006), but further research is required to make solar thermal absorption refrigeration systems more competitive against conventional refrigeration equipment using electricity or gas.

Although solar energy has its advantages, it remains, however, intermittent and unpredictable (Mawire, 2009). Its total available value is seasonal and often dependent on meteorological conditions of a location. Therefore, solar energy cannot, for example, be trusted to produce cooling during periods of low solar energy irradiation. Some form of Thermal Energy Storage (TES) is necessary for effective utilisation of such an energy source, to meet demand on cloudy days and at night. TES, therefore, plays an important role in conserving thermal energy, leading to an improvement in the performance and reliability of a range of energy systems.

In an attempt to improve thermal performance of a solar thermal driven refrigeration system, a limited number of solar cooling designs with TES are recorded (Florides *et al.*, 2002; Duffie & Beckman, 2006; Mehling & Cabeza, 2008; Ajib, 2009).

Large scale solar cooling systems (40-300 kW) for large commercial buildings and for industrial applications have been successful demonstrated. However, given the increasing cooling demand in residential and small scale applications, a growing market persists for low cooling capacity equipment (less than 10 kW). Consequently, a Research Group in the Department of Mechanical Engineering at the University of Johannesburg investigated the design of a domestic Aqua Ammonia Absorption Refrigerator (AAAR) primarily dependent on solar radiation to function. It is thought that this machine may be of particular interest to the Republic of South Africa (RSA) since the RSA has one the highest levels of solar radiation in the world, ranging from around $1450\,\mathrm{kWh}/\mathrm{m}^2$ to about $1950\,\mathrm{kWh}/\mathrm{m}^2$ per year (http://www.pdcsolar.co.za, **Appendix A.1** and **Appendix A.2**).

The complete refrigeration system under development consists of three major units: a Solar Collector (SC), a Storage System (SS) and an Absorption Refrigerator Unit (ARU). The solar collector concentrates sunlight to heat a HTF to a high temperature which delivers the absorbed energy to the storage unit. This is the charge cycle. During the discharge cycle stored energy is extracted and conveyed to the generator. The acquired thermal energy is then used to drive the absorption cooling cycle.

Of the subsystems of the solar absorption refrigeration system, the SS of the solar absorption refrigeration system is of particular importance since it is required to adjust temporal mismatches between load and intermittent or variable solar energy.

Traditionally, low temperature domestic TES units make use of water because it has a high specific heat capacity. It is readily available and is cheap. In these systems Sensible Heat Storage (SHS) is used, by which the temperature of water or of another storage material is raised by solar radiation (or other thermal energy source) from which heat is later extracted by means of a heat exchanger or otherwise. The use of water as a heat storage medium in the AAAR is not viable, since the storage temperature can exceed $100^{\circ}\mathrm{C}$. At this temperature, a method of pressurising the system would be necessary to avoid the development of steam. Another problem is the size of the TES tank that would be required as the amount of stored energy depends on the product of the mass of water, the specific heat capacity and the temperature difference. Since a large thermal capacity is required to store an adequate amount of thermal energy, it will necessitate a large tank, so impacting on cost plus a potential rise in thermal losses that would require additional insulation.

An alternative method to SHS is changing the phase of a material during heating or cooling. The best known method is the use of ice or snow for cooling in cold storage. The material used in this case changes from solid to liquid and vice-versa. Melting and solidification

2

occur at a constant temperature. Storage materials which solidified or melted in this manner are called Phase Change Materials (PCMs). Because of the temperature remaining constant during this phase change, this heat storage method is referred to as Latent Heat Storage (LHS). PCMs present the largest storage densities compared to storage densities attainable through SHS, since with a small material volume, a larger amount of energy can be stored as against methods employing SHS. PCMs for LHS store 5 to 14 times more heat per unit volume than SHS materials (Sharma *et al.*, 2004).

These characteristics make LHS a prime candidate for use in SS units. The choice of an appropriate material, however, depends on many factors, such as the temperature range of use and the total amount of energy required to be stored in a SS (Mawire, 2009).

The storage of solar energy can be done in different ways. The use of PCM as an energy storage medium is now worldwide considered as an option with a number of advantages. The thermal storage of solar energy is particularly attractive in an AAAR. Any AAAR generator requires thermal energy to operate.

1.2 Problem statement

The sizing of a thermal storage system is one of the critical tasks for a given thermal system: It is a function of the space available, the weight and the load application.

The determination of the dimension of a LHS is a very complex problem because of the mechanisms of heat transfer that are involved in the storage unit during the charging and the discharging processes.
The need for more effective and reliable method of sizing a LHS is vital for any thermal system.

In order to quantify the volume of the PCM and other related dimensions of the LHS for a specific heating application, a simulation of the processes of heat storage (melting) or / and heat removal (freezing) that underlies this storage approach is required. Therefore, the quantitative study of any proposed LHS requires first modelling of the phase change process.

The purpose of the present study is to determine the dimensions of a latent heat storage system that would serve store solar thermal energy required to effectively power an absorption machine for a specific period.

1.3   Objective of the study

The specific objectives to address this problem are:

- To identify a suitable PCM to be used for TES (hot side) in the AAAR;
- To model the LHS unit for the AAAR;
- To size the LHS unit for the AAAR and,
- Evaluate the performance of the AAAR.

1.4   Layout of the study

This dissertation is divided into eight chapters, including an introduction as Chapter 1. The introduction presents some background to the problem of storage of solar energy. Chapter 2 focuses on some of the literature on related thermal storage technologies, to finding appropriate material candidates for TES, an efficient configuration of LHS, different approaches for solving and modelling the LHS and various methods of sizing a LHS.

In Chapter 3, the modelling of the LHS is presented. The solution of this model is then applied in the design of the LHS in Chapter 4. Moreover; the dimensions of the LHS unit are obtained. The description of the approach is described for sizing the LHS. Simulations for the designed LHS unit are given in terms of the outlet temperature of the working fluid from the storage unit, the front solidification (interface solid-liquid) of the selected PCM in the storage, the effectiveness of the storage unit and the heat transfer rate.

Chapter 5 applies the design method developed in Chapter 4 using a case study of storing solar energy for driving absorption refrigeration. The LHS for AAAR is dimensioned and simulated for a given set of design requirements.

Chapter 6 presents the simulations results of other analytical models for the design requirements of the unit dimensioned in Chapter 5.

Chapter 7 focuses on validation of the derived mathematical modelling through comparison of results obtained from the derived model (Chapter 3) and those acquired from other analytical modelling.

Chapter 8 concludes the dissertation as related to the objectives and provides suggestions for future work.

4

Chapter 2

LITERATURE SURVEY AND EXISTING STORAGE TECHNOLOGY

2.0   Introduction

In this chapter, previous work on thermal storage is presented with two focus areas. The first is on the basic thermodynamics of thermal energy storage and associated systems. The second focus area is on the application of thermal energy storage to solar absorption refrigeration.

The aim of this survey is to establish the state-of-art in the existing storage methods in general, specifically in LHS.

2.1   Thermal energy storage methods

Thermal Energy Storage (TES) refers to a number of technologies which store energy in a thermal accumulator for later re-use. TES systems have a potential to increase effective use of thermal energy equipment and to facilitate large scale switching (Antoni *et al.,* 2009). They are normally useful for correcting the mismatch between the supply (sun) and demand of energy (such as the generator of the AAAR).

Three different approaches or techniques are considered for storing thermal energy from solar energy. These are: Sensible Heat Storage (where a change of temperature occurs), Latent Heat Storage (where a change of phase occurs) and thermo-chemical heat storage (where a reversible chemical reaction takes place).

2.1.1 Sensible Heat Storage systems

Sensible heat water storages are the most common TES used today for domestic purposes. In Sensible Heat Storage systems (SHS), energy is stored or extracted by heating or cooling a liquid or a solid which does not change phase during the process. SHS consists of a storage medium, a container (usually a tank) and inlet and outlet devices.

The amount of energy input required to heat a TES with a sensible heat device is proportional to the difference between the final and initial temperatures of storage, the mass of the storage medium and its heat capacity. As Figure 2.1 shows, heat transferred to a storage medium leads to a linear temperature increase of that medium. From the figure, it can be observed that if the temperature of storage medium increases, its energy content (internal energy) also increases.
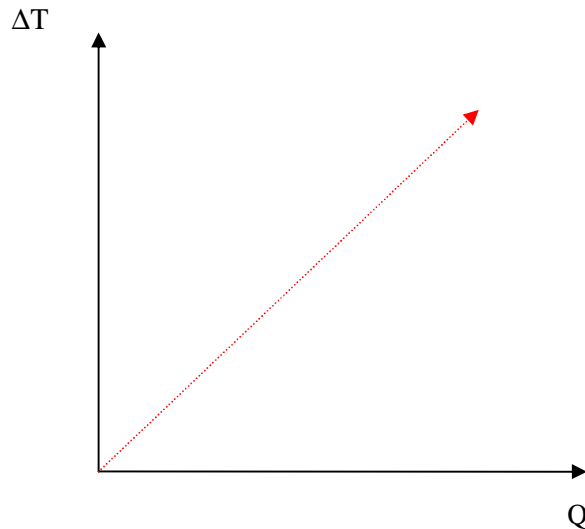
Figure 2.1: Linear relationship between energy stored and increased temperature

From first principles, the quantity of heat stored as sensible heat for solid or liquid storage is given by the following equation:

$$Q = mC_p\Delta T = \rho C_p V\Delta T \qquad \textbf{(2.1)}$$

where　Q　=　quantity of heat stored;

m　=　mass of heat storage medium;

C_p　=　specific heat capacity of the storage material;

ΔT　=　temperature change between the maximum and minimum temperatures of the storage material;

ρ　=　density of the material;

V　=　volume of storage material.

Equation 2.1 provides a means to calculate the storage capacity of a SHS. The performance of a SHS is characterised by the storage capacity, heat input levels while charging and discharging and storage efficiency.

In solar air heating systems, the usual energy storage material is a packed bed of small rocks or crushed gravel (Duffie & Beckman, 2006). The porosity of the bed or the void fraction ε has to be taken into consideration (Adeyanju and Manohar, 2009); the heat stored is given by:

$$Q = \rho(1-\varepsilon)V\Delta T \qquad \textbf{(2.2)}$$

where Q　=　quantity of heat stored;

ε　=　porosity of the packed bed;

6

ΔT =   temperature change between the maximum and minimum temperature of the
storage material;

ρ =   density of the material;

V =   volume of storage material.

SHS is possible in a variety of materials, both liquid and solid. Table 2.1 presents some common thermal energy storage materials and their properties. From the data given in this table, it is evident that water has a high value of heat capacity per unit volume.

Table 2.1: Thermal capacities at 20°C of some storage materials (Dincer, 2004)

Material	Density [kg/m^3]	Specific heat Capacity [J/kgK]	Volumetric heat capacity [10^6 J/m^{3}K]
Brick	1800	837	1.51
Wood	700	2390	1.67
Aluminium	2710	896	2.43
Steel	7840	465	3.68
Water	988	4182	4.17

SHS is the simplest form of storing thermal energy compared to latent heat or thermo-chemical heat storage systems. However, it has the disadvantage of being larger in size compared to the latent and thermo-chemical heat storage systems. For this reason, an important criterion in selecting a storage material for a SHS is its heat capacity per unit volume (ρCp) value, which characterises its ability to store the sensible heat for a given material. Another important factor related to the SHS is its inability to store or deliver thermal energy at constant temperature. The stratification processes in tanks are currently employed to improve the performance of a SHS.

Apart from the specific heat and the density of the storage material, other properties are important for SHS: Operational temperatures, thermal conductivity and diffusivity, vapour pressure, compatibility among materials stability, heat loss coefficient as a function of the surface areas to volume ratio and cost.

SHS had been analysed and described by many researchers (Van Berkel, 2000; Dincer, 2004; Mehing & Cabeza, 2008; and others).

Most solar domestic heating and space heating systems use hot water storage tanks located either inside or outside buildings or are underground. The containments used for water are tanks, pits, caverns, aquifers and lakes (Berkel, 1997).

The storage of hot water experiences two main disadvantages: Significant heat losses and the limitation of thermal storage capacity because of temperature range of non-pressurised water (0-100°C). Examples of short-term water stores are residential electrically or gas-fired domestic hot water boilers.

Thermocline energy storage systems have received much attention as they have potential for low costs resulting from minimised tankage volume (Duffie & Beckham, 2006).

In some special industrial cases water storage capacity is enlarged by pressurisation in a steam accumulator. In general, SHS consists of a cylindrical tank with either a horizontal or vertical axis (Figure 2.2b and Figure 2.2c). Sometimes, the shape is box-like as shown in Figure 2.2a.
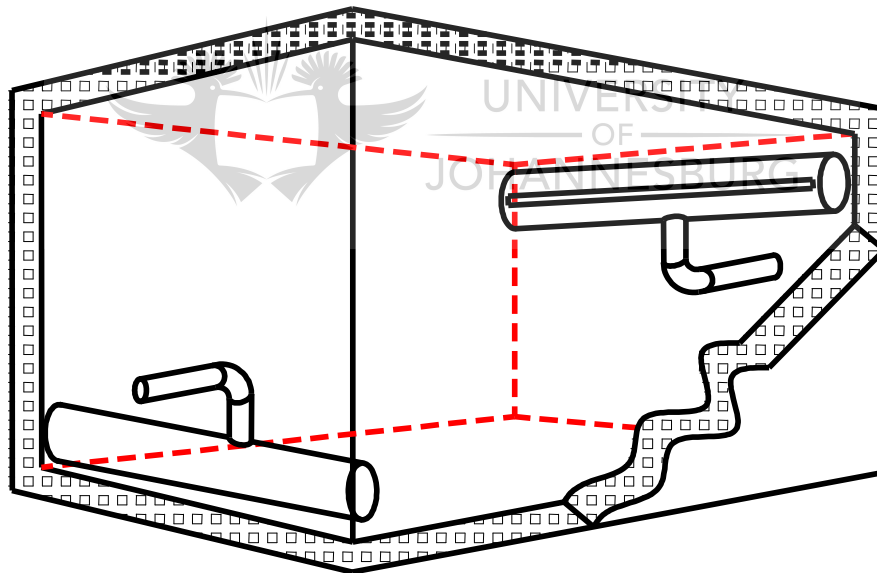
Figure 2.2a: Concrete box-like chilled water tank (modified after Van Berkel, 1997)
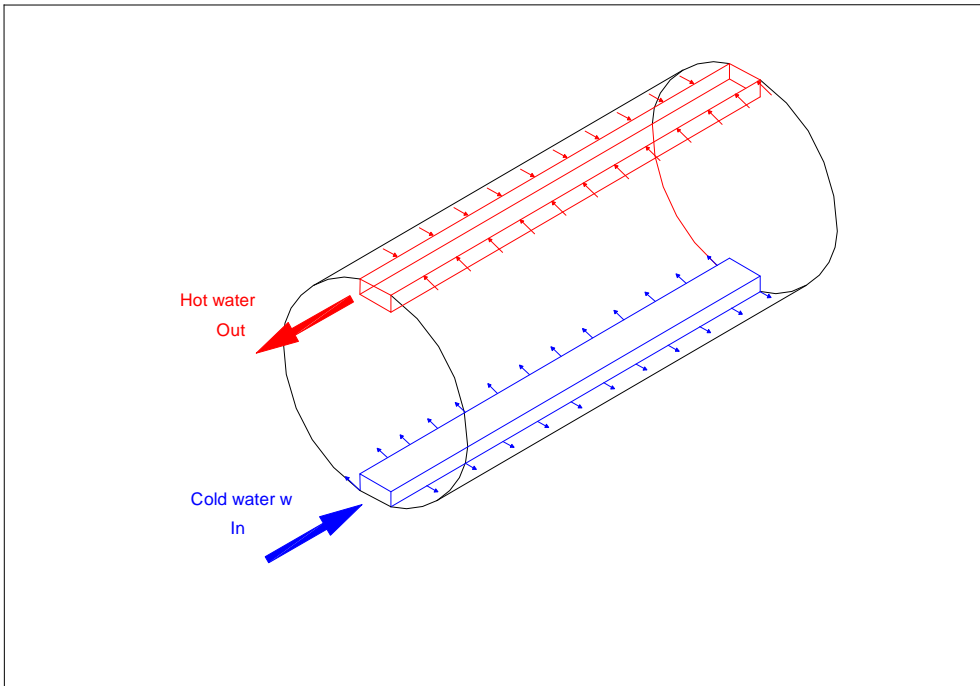
Figure 2.2b: Horizontal cylindrical tank (modified after Van Berkel, 1997)
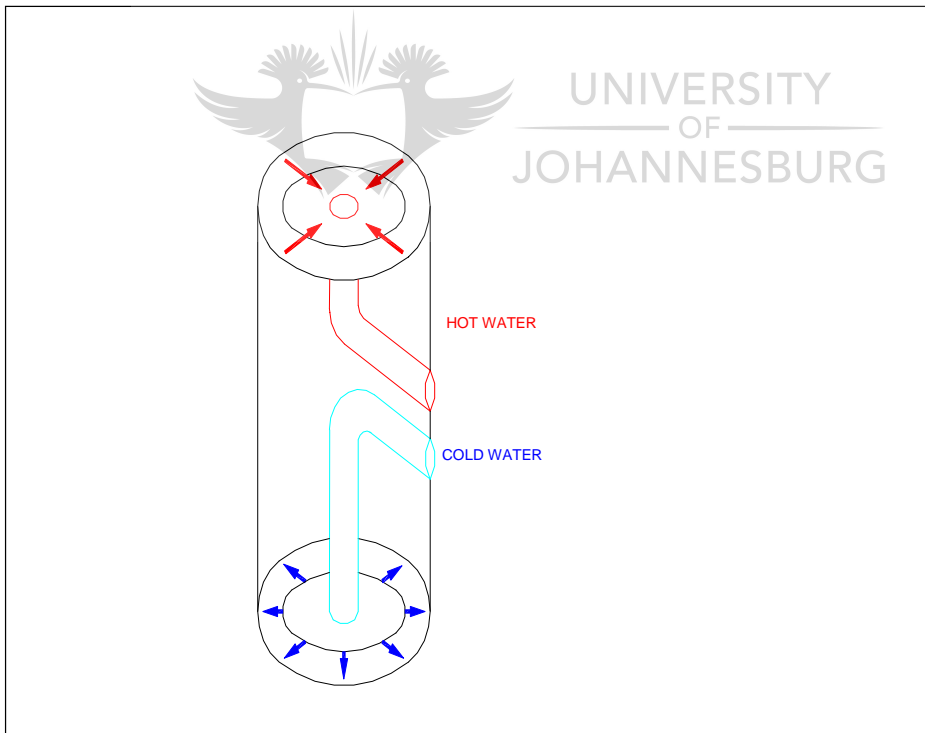
Figure 2.2c: Vertical cylindrical tank (modified after Van Berkel, 1997)

A well known storage category comprises underground thermal energy storage (Figure 2.3). A development is to use foundation piles under residential or utility buildings as ground heat exchangers (Koene, 2000).

9
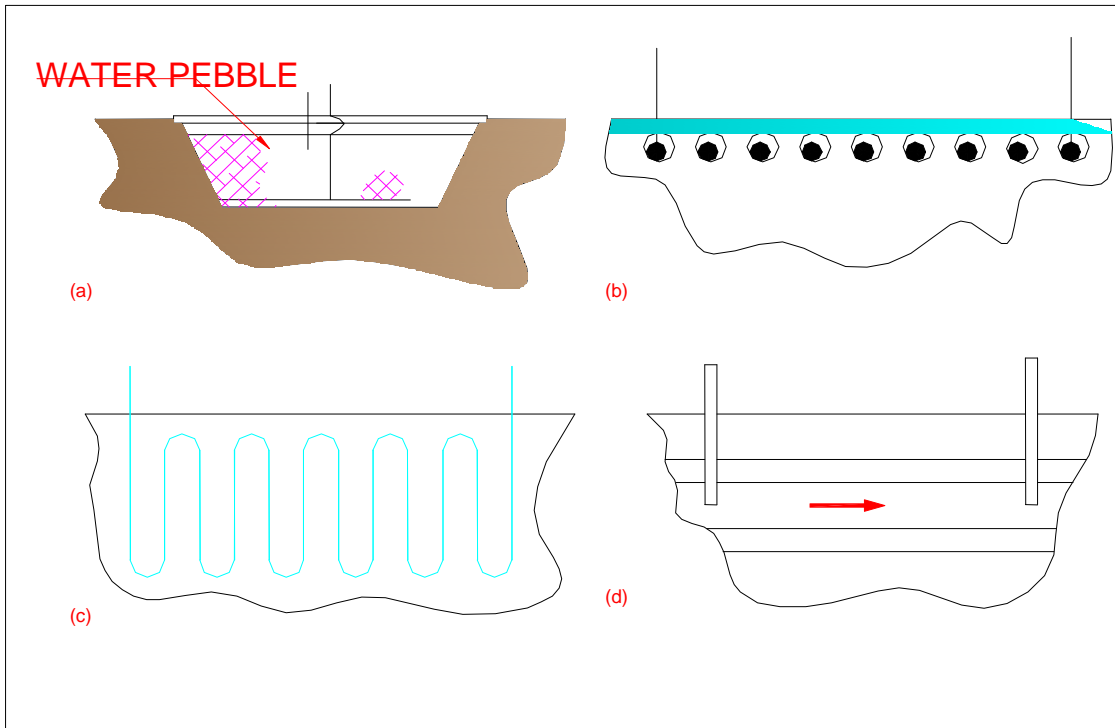
Figure 2.3: Underground thermal energy storage options: a) water pit; b) Close to earth ground store; c) Deep ground store or boreholes; d) aquifer storage (modified after Hahne, 1986)

The advantage of water tank pits is that heat is stored in the transport medium. Storage accomplished by heat capacity and volume of earth makes heat transfer effective. However, water tank pits are relatively expensive, which is a disadvantage.

Generally, underground thermal energy storage is efficient only for big storage systems (e.g. store volumes > 1000 m^3) (Van Berkel, 2000). Consequently, they are used primarily for district heating systems.

For high temperature storage (120°C-600°C) in solar electricity power plants, molten salts (e.g. sodium-nitrate salt) have been considered as the medium of storage. Molten salts, mineral oils and synthetic oils used as storage media for SHS maintain natural thermal stratification because of density differences between hot and cold fluid. The existence of a thermal gradient across storage is desirable.

2.1.2 Latent Heat Thermal Energy Storage systems

Latent Heat Thermal Energy Storage (LHS) is based on the heat absorption or release when a storage material undergoes a phase change from solid to liquid or liquid to gas or vice-versa. Figure 2.4 summarises the classification of LHS materials.

LHS can be accomplished through solid-liquid, liquid-gas, solid-gas, and solid-solid phase transformations, but only two are of practical interest, solid-liquid and solid-solid (Wang *et al.*, 2000). Solid-gas and liquid-gas transition have a higher latent heat of fusion, but their large volume changes on phase transition are associated with containment problems and rule out their potential utility in thermal storage systems. Solid - liquid PCMs present the advantages of smaller volume change during the phase change process and longer lifespan (Gao *et al.,* 2007).
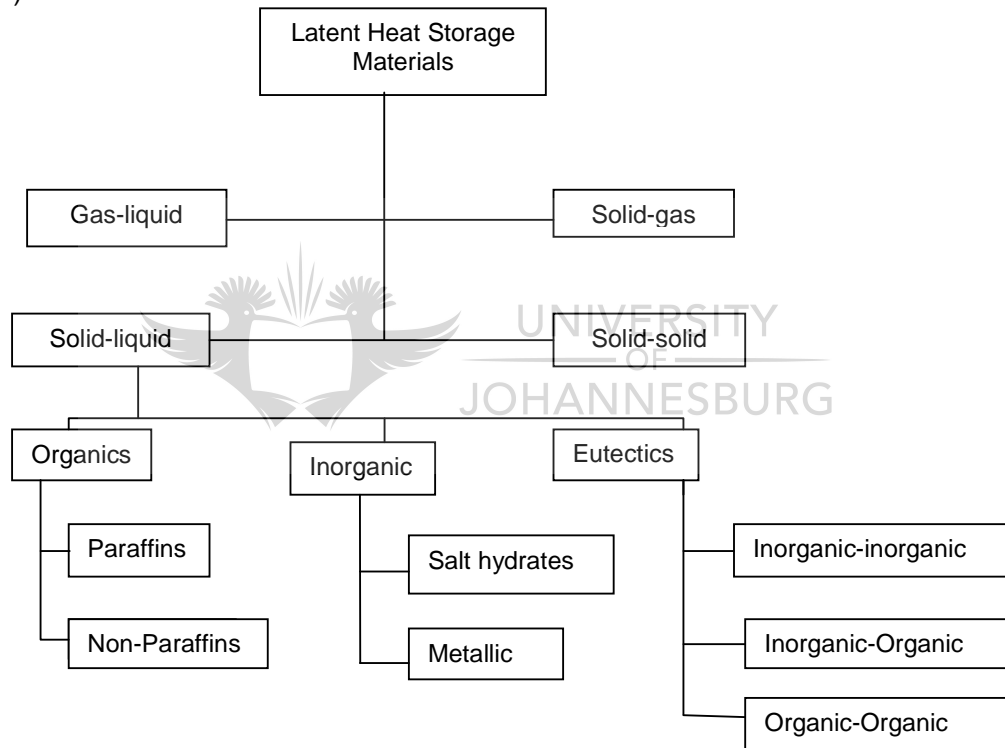
Figure 2.4: Classification of the LHS materials (modified after Sharma *et al.*, 2004)

The storage capacity of a LHS system with a PCM is given by:

$$Q = m[a_m H + C_{sp}(T_m - T_i) + C_{lp}(T_f - T_m)] \tag{2.3}$$

where Q = quantity of heat stored;

m = mass of heat storage medium;

a_m = fraction melted;

H = heat of fusion or phase change enthalpy or melting enthalpy;

C_{sp} = average specific heat between T_i and T_m;

C_{lp} = average specific heat between T_m and T_f;

T_i = initial temperature;

T_f = final temperature;

T_m = melting temperature.

Figure 2.5 illustrates the change in stored energy as a function of temperature. At the beginning of the heating process the material is in a solid state. Before it reaches the melting point T_m, the heat absorbed is sensible heat. Starting at melting point, the material undergoes a change of state from a solid to a liquid. During this process, the material absorbs heat known as enthalpy melting. The temperature remains constant. If the material is heated up further after this process, there will be sensible heat added on completion of melting.
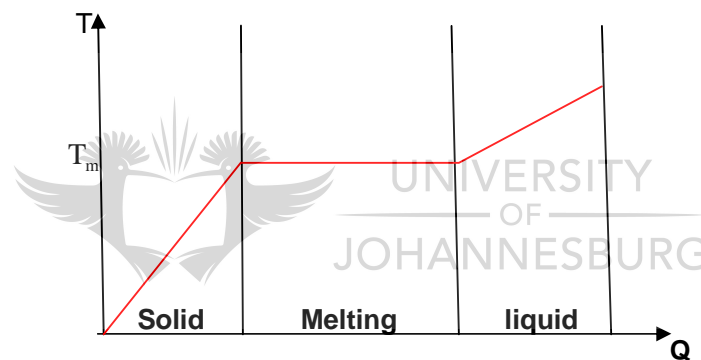
Figure 2.5: Thermal energy stored in a PCM as a function of temperature T (modified after Rubitherm, 2008)

At molecular level, latent heat of fusion associated with solid-liquid phase change is estimated according to Richardson's rule (Mehling & Cabeza, 2008). The molar heat stored is proportional to the melting temperature. The Richardson rule is given by:

1. For metals, $\qquad\qquad 1 \cdot R \cdot T_m < \Delta Q_{mol} < 1.5 \cdot R \cdot T_m$ **(2.4)**

2. For salts, $\qquad\qquad \Delta Q_{mol} < 4.5 \cdot R \cdot T_m$ **(2.5)**

Where T_m is the melting point of the PCM, ΔQ_{mol} is the molar heat stored and R the universal gas constant with R=8.3 kJ/kmol.K.

A PCM is selected depending on the application.
It has to possess desirable thermo-physical, kinetic and chemical properties.
The thermo-physical properties desirable for a PCM are: Melting temperature in the desired operating temperature range, a high latent heat of fusion per unit volume, high specific heat

and high thermal conductivity, small volume changes on phase transformation and congruent melting for a constant storage capacity.

Among kinetic properties to be considered are: High nucleation rate and high rate of crystal growth.

Chemical properties are also required for a good PCM: Chemical stability, complete reversible freeze/melt cycle, no-degradation after a larger number of freeze/melt cycles, non-corrosiveness to the construction materials, non-toxic, non-flammable and non-explosive for safety.

PCMs should be cheap and be available on a large scale.

Table 2.2 presents some commercial PCMs available on the market. A conclusion to be drawn from Table 2.2 is that only few companies are involved in characterisation and marketing of the PCM.

Although there are many applications for high, medium and low temperature, the commercial PCMs available, are only in the temperature range of 22°C and 89°C (Zalba *et al.,* 2003)

Table 2.2: Some commercial PCMs available on the market (Zalba *et al*., 2003)

Commercial Name	Type of product	Melting point (^{o}C)	Heat of fusion (kJ/kg)	Source (Producer)
RT 20	Paraffin	22	125	Rubitherm
RT27	Paraffin	28	189	Rubitherm
RT 31	Paraffin	31	168	Rubitherm
SP 22 A4	Eutectic	22	165	Rubitherm
SP 25 A8	Eutectic	25	180	Rubitherm
ClimSEL C22	Salt hydrate	22	144	Climator
ClimSEL C24	Salt hydrate	24	108	Climator
ClimSEL C28	Salt hydrate	28	126	Climator
ClimSEL C32	Salt hydrate	32	194.4	Climator
TH89	Salt hydrate	89	149	TEAP
S27	Salt hydrate	27	207	Cristopia
STL27	Salt hydrate	27	213	Mitsubishi Chemical

In Table 2.3, the advantages and disadvantages of organic and inorganic materials are presented. From the behaviour of the PCM shown in Table 2.3, an appropriate PCM can be selected for a given application.

Table 2.3: Comparisons of organic and inorganic PCMs (Zalba *et al.,* 2003)

ORGANIC	INORGANIC
ADVANTAGES	
non-corrosive	great change enthalpy
non-toxic	good thermal conductivity
little or no supercooling	cheap and non-flammable
chemically and thermally stable	
DISADVANTAGES	
lower phase change enthalpy	undercooling
low thermal conductivity	corrosion to most metals
	phase separation
	phase segregation
	lack of thermal stability

Overview of latent heat exchangers

Many papers on LHS have been written over the past decade on the advantages of various heat exchanger configurations containing PCM as storage material. A major problem in the design of LHS was the investigation of the methods of improving heat transfer rate from the LHS. Different types of heat exchangers have been developed to overcome the poor performance of heat exchangers and other problems related to the heat transfer rate in the LHS.

The double-pipe heat exchanger for LHS was studied by Fath (1999). That research suggested heat transfer rate could be enhanced by increasing the air inlet temperature, air mass flow rate and heat exchanger length. A single full length heat exchanger exhibited better thermal effectiveness than two half length and equal capacity parallel heat exchangers.

A direct contact heat exchanger with an immiscible Heat Transfer Fluid (HTF) moving through the PCM had eliminated the permanent heat exchanger surface and had been confirmed as preventing phase separation of the PCM (Fath, 1999).

Lecomte *et al.* (1985) presented a design method for sizing a shell-and-tube latent heat exchanger for a thermal system under thermodynamic conditions. It was concluded that high flow rates could not deliver significant heat from PCM to the load. Discharging of heat from the PCM to the load depended on the performance of the heat exchanger and the thermo-physical properties of the PCM.

Hasan (1994) developed a simple tube-in-tube heat exchanger for thermal energy storage with stearic acid as a PCM. He found the melting front moved in two directions: radial direction inward and axial direction from the top toward the bottom of the PCM. Melting front speed was enhanced by a convection heat transfer mechanism in the melted PCM.

Regin *et al.* (2007) described various schematics of containment used in LHS. Figure 2.6 shows the flat plate (A), shell-and-tube with internal flow (B), shell-and-tube with parallel flow (C), shell-and-tube with cross flow (D) and sphere packed bed (E).
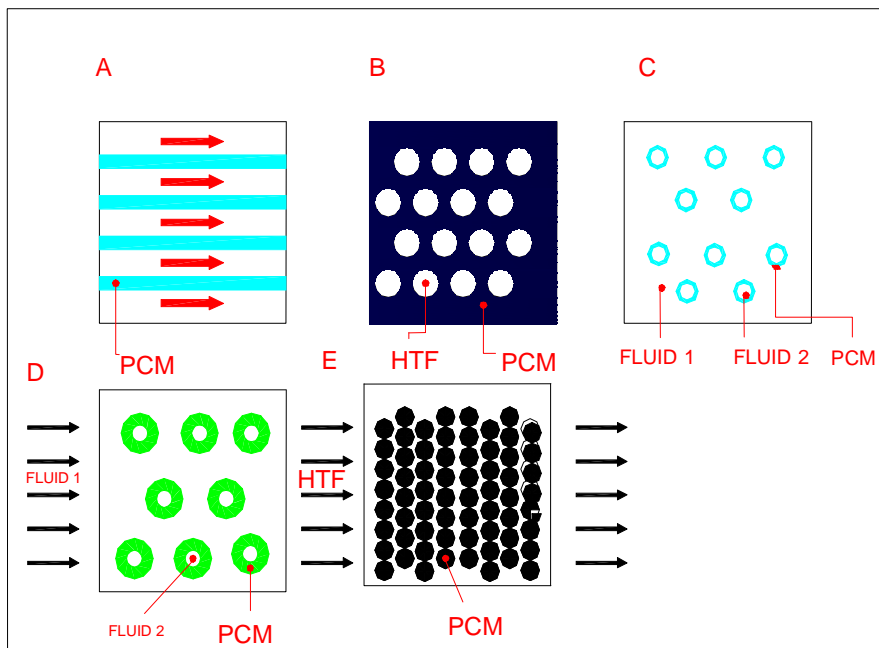
Figure 2.6: Schematic of typical LHS (modified after Regin *et al.*, 2007)

Agyenim *et al.* (2009) examined the geometry and configurations of PCM containers. To ensure long-term thermal performance of any PCM system, the size and shape of the PCM container had to correspond to the melting time of the PCM and daily insolation at a given location if the source of energy was a solar collector.

Two geometries commonly employed as PCM containers were rectangular and cylindrical containers. The most intensely analysed LHS unit was the shell-and-tube system, accounting for more than 70% as heat loss from the shell-and-tube system was minimal. Figure 2.7 gives the schematic of the cylindrical and rectangular containers.
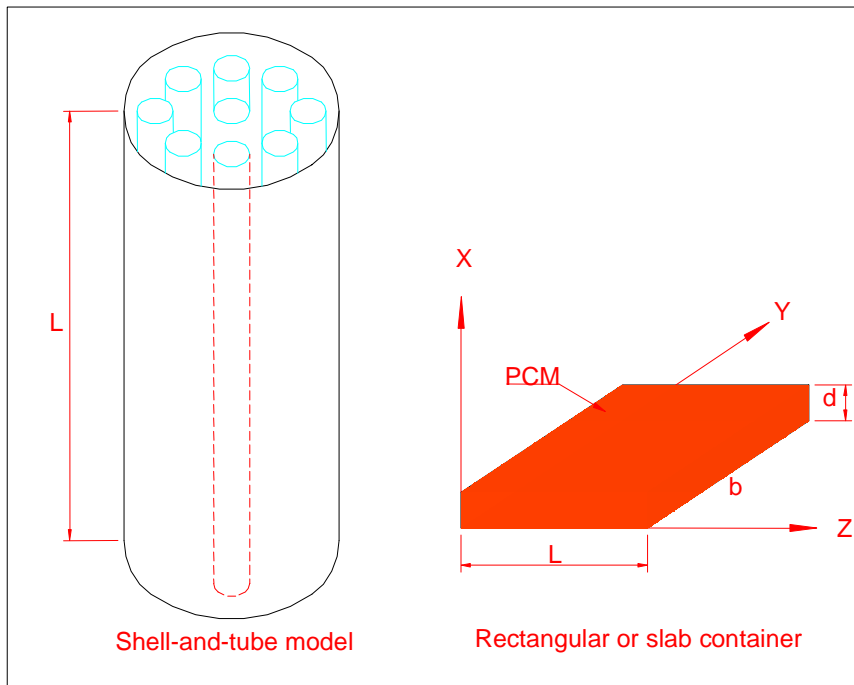
Figure 2.7: Classification of commonly used PCM containers
(modified after Agyemin *et al.,* 2009)

Gong and Mujundar (1997) investigated the effect of parallel and counter-current flow modes. Using a mixture of 80.5% LiF and 19.5% CaF as PCM and a He/Xe mixture as HTF they showed that parallel flow increased the energy charge/discharge with 5% above that of counter-current flow configurations. The penetration depth of the solid-liquid phase change interface during charge/discharge was larger because of a higher temperature difference at the fluid inlet, if hot and cold fluids entered from the same end. In addition, supercooling of the PCM did not occur in the fluid inlet region and heat transfer between the HTF and the PCM did not deteriorate. On the other hand, counter-current flow for charge and discharge processes produced significant supercooling of the PCM in the region of the cold fluid. Figure 2.8 illustrates the schematic diagram of the parallel principle in a shell-and-tube system.
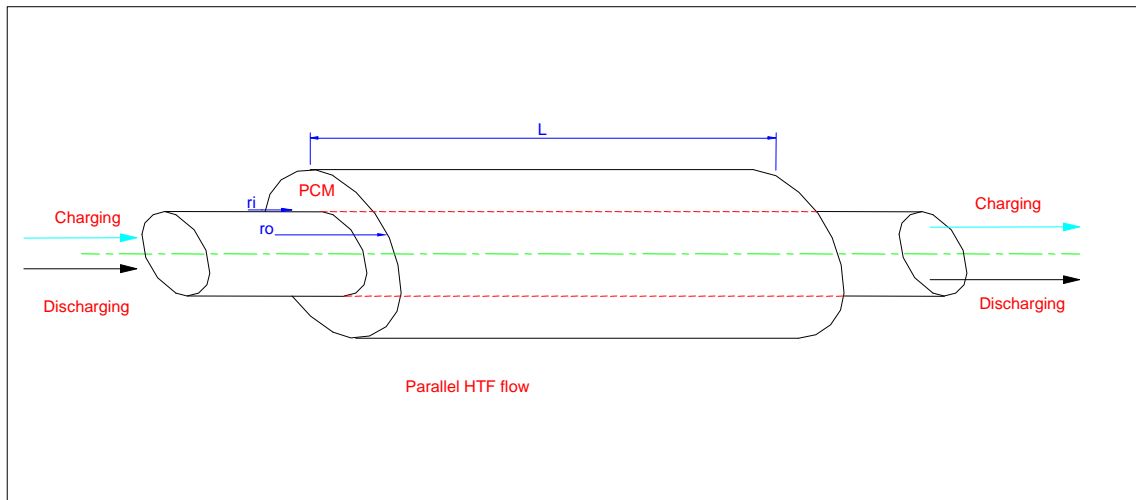
Figure 2.8: Schematic diagram of the parallel flow in a shell-and-tube system (modified after Gong and Mujundar, 1997)

A LHS promising high efficiency for a minimum volume was the shell-and-tube type of exchanger with the PCM filling the shell side while the HTF flows through the inner tubes and exchanges heat along the way (Lacroix, 1993; Esnet, 1997; Zhang, 1997).

Overview of modelling of latent storage systems

Some of the papers published on the modelling of the melting and freezing problems of LHS are reviewed.

An analysis of heat transfer problems in the phase change processes is complex as the solid-liquid boundary moves depending on the speed at which the latent heat is absorbed or lost at the boundary. The position of the boundary is unknown and forms part of the solution (Carslaw & Jaeger; 1959, Kurklu *et al.,* 1995; Agyenim *et al.,* 2010). These types of problems are referred to as a moving boundary problems or Stefan's Problem.

Solutions to phase change problems include analytical, experimental and numerical methods using one-dimensional, two-dimensional or three-dimensional models to solve energy formulated equation (Agyenim *et al.,* 2010).

A theoretical model of a shell-and-tube PCM storage unit was reported by Ismail and Alves (1986). An energy equation for the PCM was written in terms of the enthalpy. The numerical results showed the effects of the Biot number, the relative diameters of the tubes and the inlet fluid temperature on the thermal performance of the unit.

Yimmer *et al.* (1989) developed a numerical model for optimising a basic one-dimensional, shell-and-tube TES system. Lacroix (1993) developed a theoretical model to predict the

transient behaviour of a shell-and-tube storage unit with the PCM on the shell side and the HTF circulating inside the tubes. Parametric studies were performed to assess the effects of various thermal and geometric parameters on the heat transfer process and on the behaviour of the system.

Many modelling publications on the problem of phase change of a PCM remain complex and require much calculation (Jian You, 2008).

Kang *et al.* (1999) used a simple analytical model to solve a heat transfer problem of conduction of a PCM in the shell, conjugated with the convection of Heat Transfer Fluid flowing in the tube. The *conservation of energy method* is developed for an analysis of PCM solidification and melting processes. The outlet temperature of HTF from the heat exchanger is evaluated over different periods and the solidification front of the PCM in the shell determined at different positions along the tube.

This previous analytical method was applied and tested by Jian You (2008). The thermal energy storage unit involved a triplex concentric tube with PCM filling in the middle channel, with a hot HTF flowing through the outer channel during the charging process and a cold HTF flowing through the inner channel during the discharging process. To test the validity of the numerical results, an experimental apparatus was designed and built by which the effect of the inlet temperature and the flow rate of a HTF on the TES were studied. Comparison between the numerical predictions and the experimental data showed good agreement. Figure 2.9 shows the schematic diagram of the TES unit used.
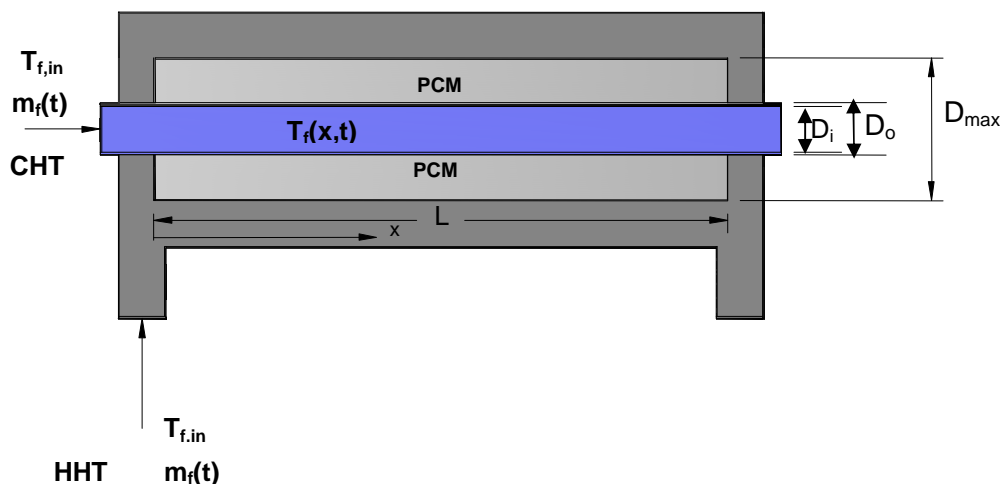
Figure 2.9: Schematic of TES unit involving a triplex concentric tube with PCM filling in the middle of the system (modified after Jian You, 2009)

In Figure 2.9, the dimensions of the middle and inner channels are given:

- D_i is the inner diameter of the tube of the middle channel. Cold Heat Transfer fluid (CHT) flows inside this tube with a mass flow rate $m_f(t)$, which is a function of time t. $T_f(x,t)$ represents the temperature of the working fluid inside of the tube as a function of the distancex and time t; D_O is the outer diameter of the tube of the middle channel;
- D_{max} is the maximum diameter of the tube that contains the PCM.

Hot Heat Transfer fluid (HHT) uses the outer channel with a mass flow rate $m_f(t)$ which is a function of time t. $T_{f,in}$ is the inlet temperature of the fluid in the middle and outer channels.

Dincer and Rosen (2002) dealt with the problems of heat transfer with PCM in simple and complex geometries and around isothermal finned cylinders. The results were presented and validated with actual existing data.

He and Zhang (2001) numerically solved a mathematical model describing the unsteady freezing problem coupled with forced convection. The method of finite difference was used to solve the equations. In their results they noted the importance of PCM thickness.

Michels and Pitz-Paal (2007) presented a numerical model to simulate different cascaded Latent Heat Storage configurations. "Dynmola/Modelica" was used to conduct the simulation using the standard library Tech-thermo. They used assumptions to simplify the heat transfer problem; the PCM was considered as a lumped mass with a uniform temperature throughout. In this work, natural convection was also considered as a type of flow regime. With their simulated results they presented experimental data to validate the model. Experimental results compared well with simulated results.

Yuksel *et al.* (2006) proposed a theoretical approach predict time and temperature during heat charge and discharge processes in the LHS, by using the average value of the mean specific heat capacities for the PCM. Analytical solutions were obtained. It was shown the decrease of the entry temperature of the working fluid had a dominant and effect on PCM solidification time.

Hsu and Sparrow (1981) provided a closed form analytical solutions based on certain assumptions after studying the freezing of a PCM outside a coolant carrying tube and on a parallel plate channel. The results proved useful in the design and analysis of thermal storage systems.

Seeniraj *et al.* (1998) developed explicit expressions for both planar and cylindrical problems upon careful study of the variables involved and subsequent analysis. By using the definition of the expression of time, they found a relation between the temperature of Heat Transfer Fluid and the melt fraction.

Alexiades and Solomon (1993) presented a review of different models to solve phase change problems. The main objective was the simulation of the processes of melting and freezing on a macroscopic scale. Among those methods, a quasi stationary approximation technique was applied to several problems of practical interest such inward and outward melting of a cylinder and inward melting of sphere. In this approximation, the sensible heat was neglected.

Shamsundar *et al.* (1992) developed an analytical model and proposed a method to size a LHS unit. From the derivation of the mathematical model, the method employed to determine dimensions of the LHS was suggested. It indicated also an efficient route to select a suitable PCM for the LHS. The design process was described then applied to a specific problem sizing the LHS unit in a NASA project able to provide sufficient hot gas to drive a propulsion unit for a space station. There was correlation between predicted and experimental results, but heat transfer analysis did not take into account the thermal conductivity of the tube and thickness of the material used.

Kurklu *et al.* (1995) proposed and applied a mathematical modelling for the calculation of the thermal performance of a PCM store cooling cycle. The model was derived from an energy balance. The amount of energy used in raising the temperature of the PCM at any time during the phase change process was predicted to be about 3.5% of total energy stored. It was also suggested that the tube thermal properties had to be taken into account during the heat transfer analysis of the PCM.

2.1.3 Thermo-chemical heat storage systems

In any chemical reaction, the enthalpy of the substances present at the end of the reaction differs from the enthalpy at the start of the reaction.

This variation is known as "heat of reaction". If the reaction is endothermic, it will absorb this heat while it takes place; if the reaction is exothermic, it will release this heat. Any chemical reaction with a high heat of reaction can be used for thermal energy storage if the products of the reaction can be stored and if the heat stored during the reaction can be released when reverse reaction occurs according to:

$$Q = a_r m \Delta h_r \tag{2.6}$$

where Q = heat stored;

  a_r = fraction reacted;

  m = mass of heat storage medium;

  Δh_r = endothermic heat of reaction.

At molecular level, the heat of a chemical reaction can be estimated (Mehling & Cabeza, 2008):

1. For a single chemical bond: $\quad 50 \cdot R \cdot T_a < \Delta Q_{mol} < 220 \cdot R \cdot T_a \tag{2.7}$

2. For a double chemical bond: $\quad 70 \cdot R \cdot T_a < \Delta Q_{mol} < 290 \cdot R \cdot T_a \tag{2.8}$

3. For a triple chemical bond: $\quad 370 \cdot R \cdot T_a < \Delta Q_{mol} < 430 \cdot R \cdot T_a \tag{2.9}$

Where T_a is the ambient temperature at about 20°C, ΔQ_{mol} is the molar heat stored and R is the universal gas constant (R=8.3kJ/kmol.K). In chemical reactions, the heat of the chemical reaction is given with respect to ambient temperature instead of melting point.

Reactions proposed for use in solar thermo-chemical storage are:

$$NH_3 \leftrightarrow \frac{1}{2}N_2 + \frac{3}{2}H_2$$

$$CH_4 + CO_2 \leftrightarrow 2CO + 3H_2$$

$$SO_3 \leftrightarrow SO_2 + \frac{1}{2}O_2$$
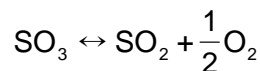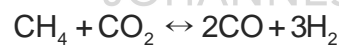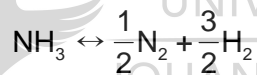
In thermo-chemical storage, thermal insulation is not necessary. A high energy density may be obtained. The stored energy may be released at high temperature. This storage method is however, complicated, expensive and it is still in its development stage (Gil *et al.*, 2009).

Selection of a suitable storage medium for the thermo-chemical TES is based on: The cost of material used, the reaction heat of a particular reaction, the speeds of both forward and reverse reactions and the temperature required for the reaction to occur (Mawire, 2010).

Thermal decomposition of metal oxides for energy storage was considered by Simmons (1976). These reactions may have an advantage that oxygen involved could be used for other purposes. Energy storage by thermal decomposition of $Ca(OH)_2$ has been extensively studied by Fujii *et al.*(1989). For the reaction $Ca(OH)_2 \leftrightarrow CaO + H_2O$, the forward reaction will proceed at temperatures above about 450°C; the rates of reaction can be enhanced with an addition of zinc or aluminum. The product CaO was stored in the absence of water.

The reverse exothermic reaction proceeds easily; in the experiments reported in Fujii *et al.*(1985). Energy was recovered at temperatures in the 100 to 200°C range; and temperatures rising to 300°C were observed.

Khanef (1999) proposed a system for storage in a solar thermal power plant (in combination with paraboloidal dishes). This application, which is an example of a medium temperature application (600°C), was less suited though for residential applications. Figure 2.10 shows a schematic of a power generation and storage system studied at the Australian National University.
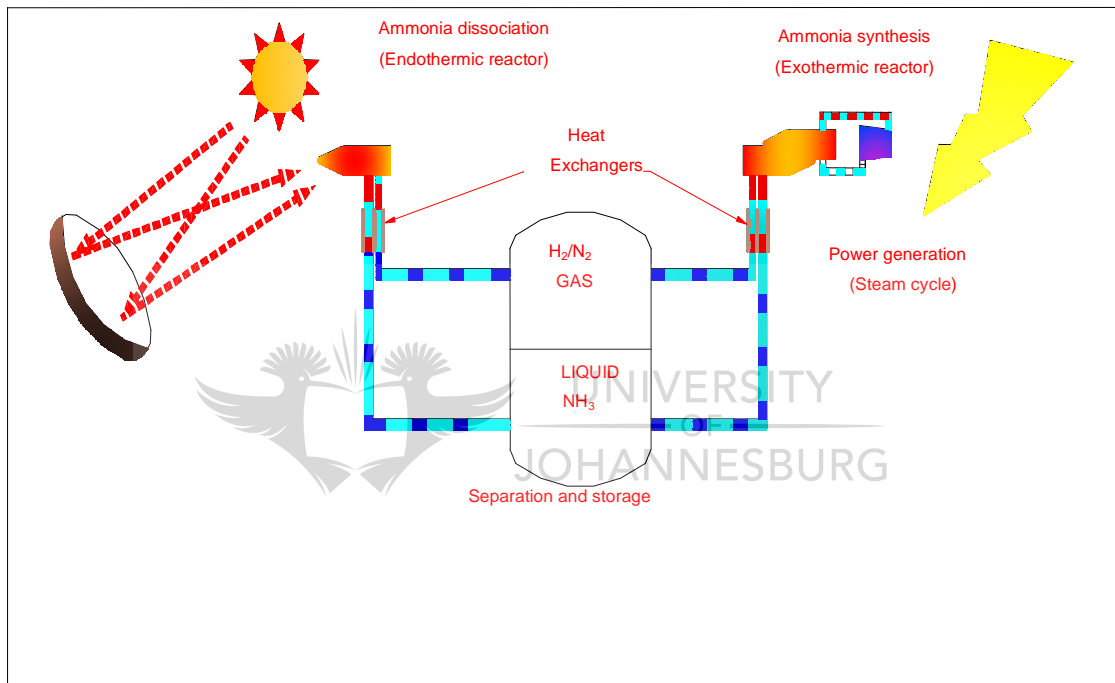
Figure 2.10: Schematic of a power generation with an integrated storage system (modified after Khanef, 1999)

2.2 Applications of thermal storage to solar absorption refrigeration

In this section, previous research on solar absorption refrigeration systems with integrated thermal storage units is presented.

Ghaddar *et al.* (1997) presented modelling and simulation of a solar absorption system for Beirut. A collector of $23.3m^2$ with an optimum water storage capacity ranging from $1000\,l$ to $1500\,l$ were required for the system to operate solely on solar energy for about seven hours a day. The monthly solar fraction of total energy for cooling was determined as a function of solar collector area and storage capacity.

23

Agyenim *et al.* (2007) investigated the possibility of integrating latent thermal energy storage to the hot side of a LiBr absorption cooling system to cover 100% of the peak cooling load for a three bedroom house on the hottest summer day in Cardiff, Wales. A 100 l of Erythritol was required to provide about 4.4 hours of cooling at peak loads based on the optimum Coefficient Of Performance (COP) of 0.7. In Figure 2.11, the schematic diagram underlying the concept depicts solar energy collection, TES and integration with the air conditioning system.
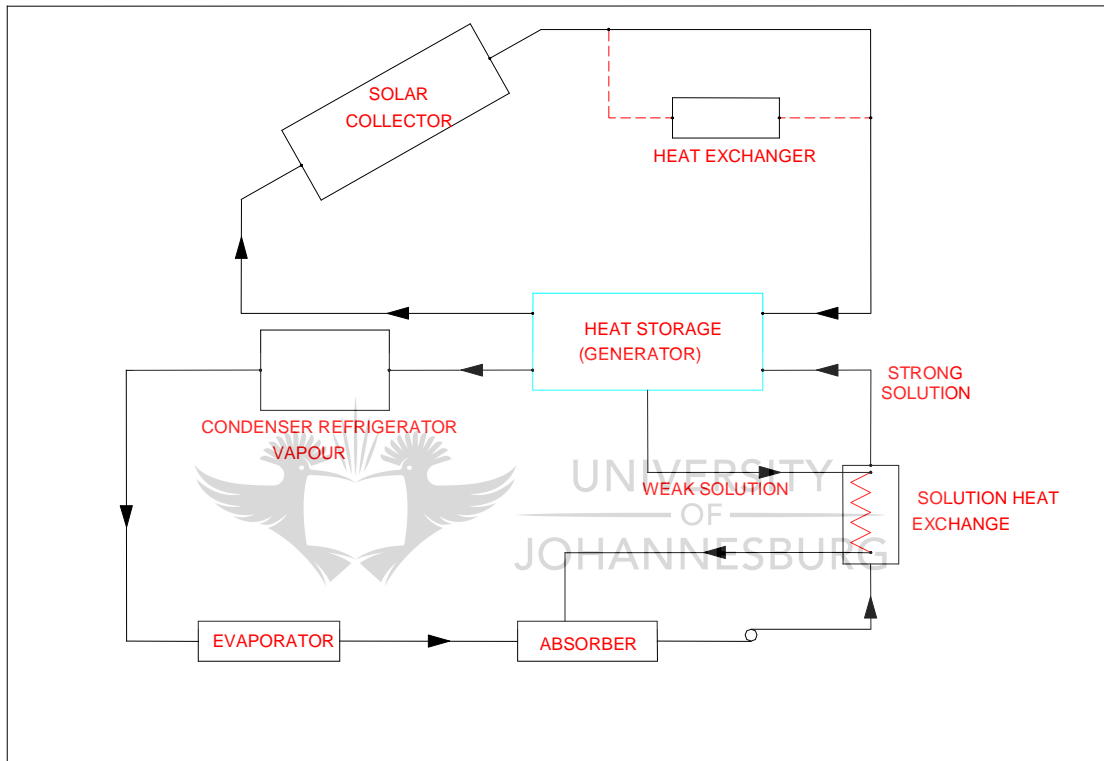
Figure 2.11: Schematic diagram of the concept showing solar energy collector, thermal storage and its integration in air conditioning system (modified after Agyemin, 2007)

Mittal *et al.* (2006) modelled and simulated a solar absorption cooling system using a water / lithium bromide solution. A computer programme was developed for the absorption system to stimulate various cycle configurations using weather data for the village of Bahal, India. The hot water from the storage unit was found to affect the surface area of some system components. It was shown high reference temperature increased the system COP.

Florides *et al.* (2002) studied the modelling and simulation of a domestic size absorption solar cooling system. It consisted of a solar collector, storage tank, a boiler and a LiBr-water absorption refrigerator. The final optimum system was comprised of a 15m^2 compound

parabolic collector tilted at 30° from horizontal and a $600\,l$ hot water storage tank. It was found a smaller tank size resulted in slightly less energy consumption by the boiler and less energy provided in solar collectors.

2.3   Summary and conclusions

Chapter 2 reviewed the three basic modes of thermal energy storage: SHS, LHS and thermo-chemical heat storage. The different applications related to these storage methods were indicated. It was observed that only a few number of papers dealt with the integration of the PCM in solar absorption refrigeration.

The LHS presents many advantages over other storage methods.

Different configurations on the latent heat exchanger were found in literature. Most efficient is the shell-and-tube heat exchanger.

From this review, different mathematical models used to solve phase change problems were identified. Some analytical approximation methods for a LHS, such as that of Shamsundar *et al.* (1992); Kang *et al.* (1999); Alexiades and Solomon (1993) and Jian Yu (2008), were found in the literature and used to validate the modified model developed in this project.

In Chapter 3, a modification of Shamsundar's model is derived and presented.
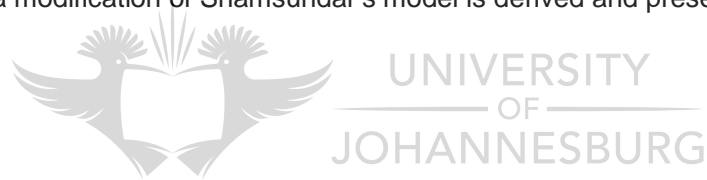
Chapter 3

MODELLING OF THE LATENT HEAT ENERGY THERMAL STORAGE UNIT

The thermal model to predict thermal performance of the LHS is presented. In Section 3.1, a short description of an AAAR is given since the LHS has to be integrated into a solar absorption system. Section 2 presents the transfer charging and discharging processes in the LHS. In Section 3 the geometry of the system is explained and the governing equations and the solution are given in Sections 4 and 5 respectively. The last section summarises Chapter 3.

3.1 Description of solar Aqua Ammonia Absorption Refrigerator

A short overview of the AAAR is presented to explain how solar energy drives an absorption refrigeration system in general. Figure 3.1 shows a block diagram of an integrated solar refrigeration system (SC, LHS and ARU) providing the cooling effect and utilising solar energy as the source of heat input. When solar radiation is insufficient, an auxiliary heat input source (waste heat) may be used to provide system backup and stability.
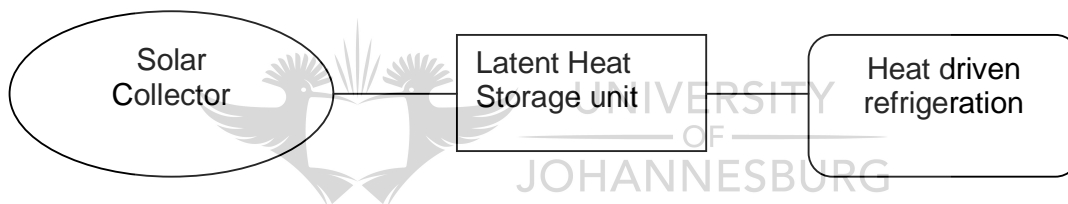
Figure 3.1: Schematic of an integrated solar Latent Heat Storage system for an absorption refrigeration machine

A schematic of the proposed AAAR machine is illustrated in Figure 3.2.

Solar energy is gathered through the solar collector and accumulated in the LHS by means of HTF. From the LHS, hot fluid is transferred to the generator of the AAAR to boil off ammonia from a solution of the ammonia and water. Ammonia vapour is produced in the generator at high pressure from a strong solution of NH_3 (ammonia). Water vapour, carried with ammonia, is removed in a rectifier and only dehydrated ammonia gas enters the condenser. High pressure NH_3 vapour condenses in the condenser. The cooled NH_3 solution then passes through a throttle valve. The pressure and the temperature of the refrigerant (ammonia) are reduced below the pressure and temperature to be maintained in the evaporator.

The cooled refrigerant enters the evaporator and absorbs heat required from the evaporator before leaving the evaporator as saturated vapour. Slightly superheated, low pressure NH_3 is

absorbed by the weak solution of NH_3 which is sprayed in the absorber, as shown in Figure 3.2.

The weak NH_3 solution (ammonia-water) entering the absorber becomes a strong solution after absorbing NH_3 vapour and is then pumped to the generator through the heat exchanger. The pump increases the pressure of the strong solution to the generator pressure. The strong NH_3 solution from the absorber absorbs heat from the high temperature weak NH_3 solution in the heat exchanger. The solution in the generator weakens as NH_3 vapour is removed. The weak high temperature ammonia solution from the generator is then passed to the heat exchanger (Ajib, 2009; Gajbert *et al.*, 2003).

Two heating mode processes are considered:

- The first mode (Mode I) is used when solar energy is sufficient to heat the ammonia temperature level required by the generator (Figure 3.2). The HTF passes through the solar collector before entering the LHS unit and then the generator.
- The second mode (Mode II) is required when there is insufficient solar energy to heat the ammonia to a required temperature. Instead of passing through the solar collector, the HTF is channelled directly into the LHS unit without passing through the solar collector, to make use of stored energy.
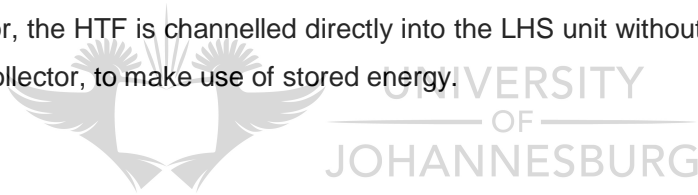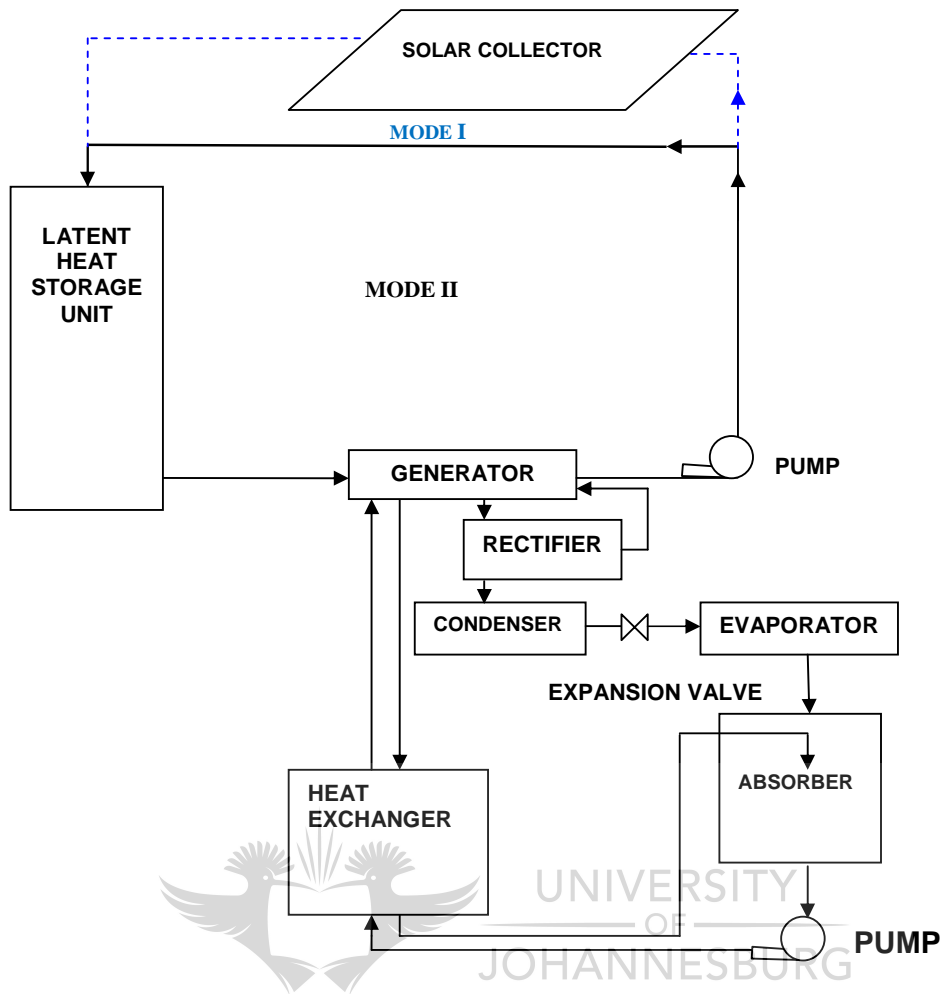
Figure 3.2: Schematic of the AAAR components

3.2   Charging and discharging processes in the latent heat storage unit

A complete storage process involves at least three cycles: Charging, storing and discharging cycles. In practical systems, some of the steps might occur simultaneously (Dincer, 2004). As shown in Figure 3.2, the LHS unit received hot HTF from the solar collector. If this fluid temperature is greater than the melting temperature of the PCM in the LHS unit, the PCM goes through a phase change from solid to liquid state. During this process the material absorbs a certain amount of thermal energy, known as the melting enthalpy. This process occurs in Mode I (see Figure 3.2). Regardless of heat input, the temperature of the material remains at a theoretically constant level, as the phase change occurs. This amount of stored thermal energy would be used during a period of low solar radiation to supply the AAAR generator (Mode II).

The discharge process occurs when a HTF, at a lower temperature than the melting point of PCM passes through a LHS unit. During this process (Mode II), the PCM in liquid state

releases the stored latent heat, also at almost constant temperature and it becomes solid. The storage material undergoes a phase change so that both solid and liquid phases are present in the storage unit at first followed by a steady increase in solid material exemplified by a moving liquid interface during heat transfer. The amount of thermal energy absorbed is directed into the AAAR generator. As heat is supplied to the ammonia-water solution in the generator at a temperature required to break up the bond of association between the refrigerant (ammonia) and the absorbent (water), there will be a change of temperature of the resulting liquid refrigerant (ammonia) to its saturation temperature. Vaporisation of ammonia will occur. Ammonia will be conveyed into the rectifier to enrich the refrigerant vapour by removing the vaporised absorbent. The cycle will continue to produce the cooling effect.

Figure 3.2 presents therefore two cycles: The solar thermal cycle and the refrigeration cycle. This study focuses only on one component of the solar thermal cycle which is the storage system.

3.3   Geometry of the latent heat exchanger unit

A schematic diagram of the latent heat exchanger storage unit is shown in Figure 3.3. This configuration is that of a shell-and-tube heat exchanger. It consists of a hollow cylinder PCM with the HTF flowing through an interior tube for the purpose of heat exchange.
The thermal model presented is primarily based on the method proposed by Shamsundar *et al*. (1992).
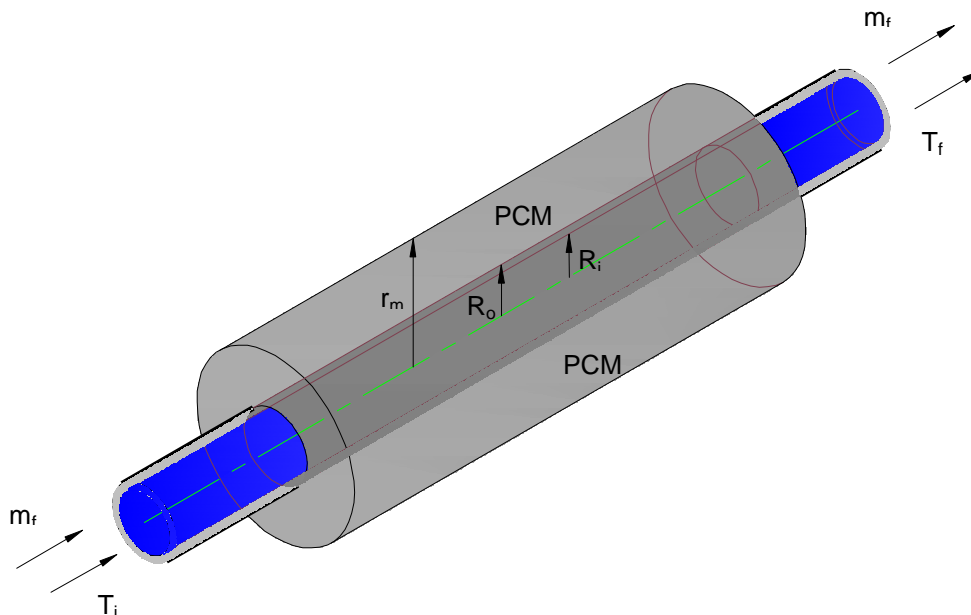
Figure 3.3: Schematic of a TES system based on a shell-and-tube configuration (modified after Shamsundar *et al*.,1992)

In Figure 3.3, m_f represents the mass flow rate, T_i and T_f are the inlet and the outlet temperatures of the HTF respectively, and L is the length of the heat exchanger, T_m is the melting point of the PCM, r_m is the radius of the frozen layer at time t since the radius of the frozen layer is a function of time. R_i is the inner radius and R_0 the outer radius of the tube exchanger .

3.4   Governing equations for the heat transfer model

Consider the HTF at inlet temperature T_i flowing inside of the tube heat exchanger of the latent heat exchanger with freezing of PCM on the outside of the tube taking place at the same time (Figure 3.3), during a discharging mode with a mass flow rate m_f . The HTF enters the tube at a temperature specified as constant and picks up heat from the Latent Heat Storage material. The heat flow inside the tube causes the freezing of some of PCM on the outside of the tube and as a result the temperature of the HTF rises.

3.4.1 Release of latent heat from the PCM

As thermal energy is extracted from the storage material (PCM), the liquid phase which is assumed to be continually in intimate contact with the solid-liquid interface, solidifies and the solid-liquid interface moves in the positive r direction (away from the inner tube) (Figure 3.3).

 An equation describing the energy released from the PCM is provided by Shamsundar *et al.* (1992), Kang *et al.* (1999) and Jian Yu (2008) as:

$$\dot{Q} = \frac{\partial \, [\pi(r_m^2 - R_0^2)\rho H]}{\partial \, t} \qquad \textbf{(3.1)}$$

where $\dot{Q}$ = heat transfer rate per unit length of the tube ;

       H   = latent heat of fusion of the PCM;

       ρ = density of the PCM;

       r_m = radius of the frozen layer of the PCM;

       R_0 = outer radius of the exchanger HTF pipe;

       t   = time.

Simultaneously as thermal energy is released from the PCM, the surface temperature of the PCM drops below the melting point, and the liquid PCM solidifies.

Shamsundar's model (**Appendix B**) considers only one single radius of the tube heat exchanger in the derivation. This model does not distinguish between the inner and outer

radius of the tube heat exchanger. As a result, the thickness and the material used for the tube wall heat exchanger are missing in the derivation. This limitation is removed in the present work by considering in the convective heat transfer Equation 3.3a the inner and outer radius of the tube heat exchanger. In Equation 3.2, it is clear specified that the radius considered, is the outer radius of the tube heat exchanger. Therefore, a general model is derived.

3.4.2 Conduction in PCM

Conduction is the transfer of thermal energy from a more energetic particles of a substance to adjacent less energetic particles as result of interaction between them (Cengel, 1997).

Consider a single one-dimensional model (Figure 3.3); the heat transfer rate per unit length of tube is given by (Shamsundar *et al.,* 1992):

$$\dot{Q} = 2\pi k_m \frac{(T_m - T_w)}{\ln(\frac{r_m}{R_0})} \qquad (3.2)$$

where $\dot{Q}$ = heat transfer rate;

T_m = melting point of PCM;

T_w = outside tube exchanger wall temperature;

r_m = PCM melt radius;

R_0 = outer radius of the tube heat exchanger;

k_m = thermal conductivity of the PCM.

The conduction in the PCM is radial (Equation 3.2). The rate of heat transfer by conduction through the PCM depends on the geometry of the medium (cylindrical for the tube), the thickness of the PCM given by the ratio $\dfrac{r_m}{R_0}$, the thermal conductivity of the PCM and the temperature difference across the PCM and the outside radius of the tube heat exchanger $(T_m - T_w)$.

3.4.3 Convective heat transfer from the tube heat exchanger to the HTF

Convection is the mode of heat transfer between a solid surface (wall tube) and adjacent liquid that is in motion, (HTF flowing inside the tube heat exchanger) (Cengel, 1997). It involves the combined effects of conduction through the wall and fluid motion.

The rate of convective heat transfer between a surface and a fluid is given by Newton's law of cooling;

$$\dot{Q} = 2\pi R_i \left[\frac{1}{\dfrac{1}{h} + \dfrac{R_i}{k_w} \ln\left[\dfrac{R_o}{R_i}\right]} \right] (T_w - T_f)$$

(3.3a)

where $\dot{Q}$ = heat transfer rate;

   h = film coefficient of the HTF;

   R_i = inner radius of the tube heat exchanger;

   R_0 = outer radius of the tube heat exchanger;

   k_w = tube wall thermal conductivity;

   T_w = tube wall temperature;

   T_f = temperature of the HTF.

The rate of heat loss from the PCM as given by Equations 3.1 and 3.2 at any section of a heat exchanger and is equal to the rate of heat gain by the HTF in that section as provided by Equation 3.3a.

From Figure 3.3, it can be noticed that the rate of convective heat transfer depends on the dimensions of the tube heat exchanger (inner radius R_i and outer radius R_o), the thermal conductivity of the wall tube heat exchanger k_w, the convection heat transfer coefficient h and temperature difference between the wall temperature tube heat exchanger and the temperature of the fluid $(T_w - T_f)$.

In Equation 3.3a, the wall tube thermal resistance is taken into account; thermal resistance in the tube is given as:

$$R_{th} = \frac{\ln\left(\dfrac{R_0}{R_i}\right)}{2\pi k_w}$$

(3.3b)

where R_{th} is the thermal resistance of the wall tube heat exchanger.

In Shamsundar's model (**Appendix B**), Equation 3.3a is given as:

$$\dot{Q} = 2\pi R_i h(T_w - T_f) \tag{3.3c}$$

The selection of tube material is vital in design calculations. The dimensions and material used in construction of the tube heat exchanger could also influence a heat exchanger's performance (Saxena *et al.,* 1982). Therefore, a general derivation of the thermal model including the ratio of outer and inner radius of the tube and the thermal conductivity of the material used for the tube wall is important to the design process.

3.4.4 Increasing of the HTF temperature

The heat transfer into the HTF causes the temperature of the fluid to rise as:

$$\dot{Q} = m_f C_p \frac{\partial T_f}{\partial x} \tag{3.4}$$

where m_f is the HTF mass flow rate, C_p the specific heat capacity of the HTF, x is the axial distance and ∂T_f is the change in temperature of the HTF over the path length.

Equation 3.4 shows the increase in the temperature of the HTF flowing on the inside of the tube heat exchanger.

3.5 Solution to the equations

The objective of a solution is to find the temperature of the HTF at different positions x along the tube heat exchanger and at the outlet of the heat exchanger where the inlet temperature fluid enters the tube at x=0. Also the PCM front radius solidification along the tube heat exchanger is determined.

From energy equations given in Sections 3.4.1, 3.4.2, 3.4.3 and 3.4.4, the next step is to find a solution. The variables of the problem are: the front radius $r_m(x,t)$ solidification of the PCM, heat transfer fluid temperature T_f and effectiveness of the heat exchanger.

The solution approach is based on the following assumptions:

- There is equilibrium solidification with a smooth interface: The freezing process takes place with a smooth interface between liquid and solid;
- Density difference between solid and liquid PCM is negligible;
- There is uniform thermal conductivity and specific heat in each phase over a narrow range of operating temperatures;
- The tube has a length greater than its diameter, axial conduction in the frozen layer (PCM) and in the HTF can be ignored;
- Convective heat transfer in the tube (HTF) is fully developed and uniform over the tube;

- Flow rate of the HTF is assumed as steady and,

- The heat storage PCM is completely liquid when the heat recovery phase begins at the freezing point; initial superheat in the liquid is therefore ignored.

Dimensionless variables are now introduced:

i. F is the frozen fraction, defined as the area of the frozen region in the radial plane divided by the area of cross section of the tube, that is (Shamsundar *et al.,* 1992),

$$F = \left(\frac{r_m^2}{R_0^2} - 1 \right)$$
(3.5)

The value of F at the inlet is represented as F_0, which is the area of solid PCM formed at inlet of the latent heat exchanger (Shamsundar *et al.,*1992).

ii.   The actual non-dimensional time variable τ is defined from Shamsundar *et al.,* 1992 as:

$$\tau = \int_0^t \left(\frac{k_m}{\rho H R_0^2} \right)(T_m - T_f)\,dt$$
(3.6a)

where k_m =   thermal conductivity of the PCM;

ρ =   density of the PCM;

T_m =   melting point of the PCM;

T_f =   bulk HTF temperature;

H =   latent heat of fusion of the PCM;

R_o =   outer radius of the exchanger HTF fluid pipe;

t =   time after which all the heat has been recovered from the heat storage.

The properties of the liquid and solid phase of the PCM remain constant with respect to temperature. This is an assumption suggested by Shamsundar *et al.* (1992) in solving the problem analytically. Therefore, Equation 3-6a may be written as:

$$\tau = \left(k_m / \rho H R_0^2 \right)\int_0^t [T_m - T_f]\,dt$$
(3.6b)

The dimensionless variable defined in Equation 3.6 is the product of the Fourier number of :

$$F = k_m t / R_0^2 C_p$$
(3.6c)

And the Stefan number:

$$Ste = C_P(T_m - T_f)/ H$$
(3.6d)

iii.   The dimensionless heat flow is given by Shamsundar *et al.* (1992):

$$\hat{Q} = \dot{Q} / 2\pi R_i h(T_m - T_f)$$

(3.7)

where $\dot{Q}$ =   heat transfer rate defined in Equations 3.1, 3.2, 3.3 and 3.4 and has the same value.

$\dot{Q}$ is the heat transfer rate lost by the PCM, which is equal to the heat transfer gained in the wall tube heat exchanger. It is the same heat transfer rate that increased the temperature of the HTF. In order words, the rate of heat transfer is conserved from the PCM through the tube wall heat exchanger to the HTF for a steady state conditions.

iv.   Another dimensionless parameter considered is expressed by Shamsundar *et al.* (1992) as:

$$\xi = \left(2\pi R_i / m_f C_{P,f}\right)\int_0^h h dx$$

(3.8)

The non-dimensional parameter defined in Equation 3.8 is the dimensionless axial distanceof the tube heat exchanger.

Boundary conditions and initial conditions

Boundary conditions for the LHS unit model are established as follows:

In the beginning of the heat recovery process, the total amount of the PCM is assumed to be in liquid phase and at freezing temperature: The inlet temperature of HTF at x=0 of the latent heat exchanger is T_i with the temperature kept constant for any time: $T_i = (T_f , x=0, t)$.

Initial conditions are:

At the beginning of the process, at time t = 0, the PCM is liquid and its melting temperature is T_m.

The solidification front radius of the PCM at the beginning of the process is equal to the outer radius of the tube heat exchanger containing the HTF: $r_m(x, t = 0) = R_0$.

Solution

A solution is sought in terms of non-dimensional variables F, τ, and ξ .

From Equation 3.2,

$$T_w = T_m - \frac{\dot{Q}\ln\left(\dfrac{r_m}{R_0}\right)}{2\pi k_m} \qquad \textbf{(3.9)}$$

Equation 3.3 may be written as:

$$\dot{Q}\left[\frac{1}{h} + \frac{R_i}{k_w}\ln\left[\frac{R_0}{R_i}\right]\right] = 2\pi R_i(T_w - T_f)$$

$$\frac{\dot{Q}}{2\pi R_i}\left[\frac{1}{h} + \frac{R_i}{k_w}\ln\left[\frac{R_0}{R_i}\right]\right] + T_f = T_w \qquad \textbf{(3.10)}$$

Because Equations 3.9 and 3.10 are equal. Therefore:

$$\frac{\dot{Q}}{2\pi R_i}\left[\frac{1}{h} + \frac{R_i}{k_w}\ln\left[\frac{R_0}{R_i}\right]\right] + T_f = T_m - \frac{\dot{Q}\ln\left[\dfrac{r_m}{R_0}\right]}{2\pi k_m} \qquad \textbf{(3.11)}$$

Rearranging Equation 3.11 gives:

$$\dot{Q}\left[\frac{\ln\left[\dfrac{R_m}{R_0}\right]}{2\pi k_m} + \frac{1}{2\pi R_i}\left[\frac{1}{h} + \frac{R_i}{k_w}\ln\left[\frac{R_0}{R_i}\right]\right]\right] = T_m - T_f \qquad \textbf{(3.12)}$$

Equation 3.12 can be written as:

$$\frac{\dot{Q}}{2\pi R_i}\left[\frac{R_i}{k_m}\ln\left[\frac{R_m}{R_0}\right] + \left[\frac{1}{h} + \frac{R_i}{k_w}\ln\left[\frac{R_0}{R_i}\right]\right]\right] = T_m - T_f \qquad \textbf{(3.13)}$$

Multiply both sides of Equation 3.13 by h and rearrange,

$$\dot{Q}\left[h\frac{R_i}{k_m}\ln\left[\frac{R_m}{R_0}\right] + \left[1 + \frac{hR_i}{k_w}\ln\left[\frac{R_0}{R_i}\right]\right]\right] = 2\pi R_i h[T_m - T_f] \qquad \textbf{(3.14)}$$

Since, $\hat{Q} = \dot{Q}/2\pi R_i h(T_m - T_f)$ from Equation 3.14 the following Equation is obtained:

$$\hat{Q} = \frac{1}{\dfrac{hR_i}{k_m}\ln\left[\dfrac{R_m}{R_0}\right] + 1 + \dfrac{hR_i}{k_w}\ln\left[\dfrac{R_0}{R_i}\right]} \qquad \textbf{(3.15)}$$

Using Equation 3.4 and 3.7, the relation becomes:

$$\hat{Q} = \frac{m_f C_{P,f}\dfrac{\partial T_f}{\partial x}}{2\pi R_i h(T_m - T_f)} \qquad \textbf{(3.16)}$$

Equation 3.16 can also be written as:

$$\hat{Q} = \frac{m_f C_{P,f}}{2\pi R_i h \partial x}\frac{\partial T_f}{T_m - T_f}$$

Because of Equation 3.8, Equation 3.16 becomes:

36

$$\hat{Q} = \frac{\partial \ln(T_m - T_f)}{\partial \xi} \tag{3.17}$$

Equation 3.1 may also be written as, by considering Equation 3.5:

$$\dot{Q} = R_0^2 \rho H \pi \frac{\partial F}{\partial t} \tag{3.18}$$

By taking Equation 3.8 divided by Equation 3.5, the following relation is obtained:

$$\hat{Q} = \frac{R_o^2 \rho H \pi \dfrac{\partial F}{\partial t}}{2\pi R_i h(T_m - T_f)} \tag{3.19}$$

$$\hat{Q} = \frac{R_o^2 \rho H}{2h R_i (T_m - T_f)} \frac{\partial F}{\partial t} \tag{3.20}$$

Taking Equation 3.6b into consideration and Equation 3.20:

$$\hat{Q} = \frac{1}{\dfrac{2\pi R_i}{k_m}} \frac{\partial F}{\partial t} \tag{3.21}$$

The group $\dfrac{hR_i}{k_m} = \beta$ is the dimensionless number, therefore, Equation 3.21 becomes:

$$\hat{Q} = \frac{1}{2\beta} \frac{\partial F}{\partial t} \tag{3.22}$$

Equations 3.15, 3.17 and 3.22 are equal since $\hat{Q}$ is the same in those Equations

$$\hat{Q} = \frac{1}{\left[\beta \ln[F+1]^{\frac{1}{2}} + \beta k \ln s + 1 \right]} = \frac{\partial}{\partial \xi} \ln(T_m \quad T_f) = \frac{1}{2\beta} \frac{\partial F}{\partial t} \tag{3.23}$$

Where $\quad k = \dfrac{k_m}{k_w} \quad$ and $\quad s = \dfrac{R_o}{R_i}$ $\tag{3.24}$

If Equation 3.23 is rearranged as:

$$2\beta \frac{\partial t}{\partial F} = 1 + \frac{\beta}{2} \ln(1+F) + \beta k \ln s \tag{3.25}$$

It shows that F is a function of τ, β, s and k.

The result obtained from the derived model (Equation 3.25) and the solution as suggested by Shamsundar's model differs. The last product $\beta k \ln s$ on the right hand side of Equation 3.25 does not appear in Shamsundar's model.

3.6   Calculation of the axial variations of F and $(T_m - T_f)$

Consider the instantaneous energy balance for the section of the tube from 0 to x (heat capacity is neglected in this derivation). The enthalpy rising in the HTF is equal to the latent heat released in the PCM (Shamsundar & Srinivasan, 1980).

$$\dot{m}_f C_p \frac{\partial T_f}{\partial x} = \frac{\partial}{\partial t}\left[\pi\left(r_m^2 - R_0^2\right)\rho H\right] = \pi R_0^2 \rho H \frac{\partial F}{\partial t} \tag{3.26}$$

The left hand side of Equation 3.26 considers the increase in the HTF temperature and the right hand side, the releasing of the latent heat in the PCM.

By multiplying Equation 3.26 by $\dfrac{k_m}{\rho R_0^2 H}$

$$m_f C_p \frac{k_m}{\rho H R_0^2} \frac{\partial T_f}{\partial x} = \pi k_m \frac{\partial F}{\partial t} \tag{3.27}$$

Integrating with respect to t,

$$m_f C_p \int_0^t k_m \left(\frac{\partial T_f}{\partial x}\right) dt / \rho R_0^2 H = \pi k_m F \tag{3.28}$$

By interchanging the order of $\dfrac{\partial}{\partial x}$ and $\int dt$ in Equation 3.28;

and by using the definition of τ (Equation 3.6b),

$$-m_f C_p \left(\frac{\partial \tau}{\partial x}\right) = \pi k_m F \tag{3.29}$$

Taking the dimensionless parameter defined in Equation 3.8, Equation 3.29 becomes:

$$\tau_0 - \tau = \frac{\pi k_m}{\dot{m}_f C_p} \int_0^x F dx = \frac{k_m}{2 R_i h} \int_0^\xi F d\xi = \frac{1}{2\beta} \int_0^\xi F d\xi \tag{3.30}$$

Differentiate Equation 3.30 with respect to ξ and combine with the last Equation 3.23 to get:

$$-d\ln(T_m - T_f) = \frac{1}{2\beta} \frac{\partial \xi}{\partial \tau} dF \tag{3.31}$$

Equation 3.31 may be written as:

$$-d\ln(T_m - T_f) = -d\ln F \tag{3.32}$$

By taking Equation 3.30 into account, Equation 3.32 is obtained.

A boundary condition, at the inlet of the tube heat exchanger the HTF temperature is T_i at time t.

Consequently, the temperature and the shape of the frozen layer vary along the axis in the same manner. That is:

$$\frac{T_m - T_f}{T_m - T_i} = \frac{F}{F_0} \qquad (3.33)$$

Using Equations 3.31 and 3.32 in Equation 3.23, the following relation for the axial variation of F is obtained:

$$\xi = \int_F^{F_0} \left[1 + \frac{\beta}{2} \ln(1 + F) + \beta k \right] d \ln F \qquad (3.34)$$

The overall frozen fraction $\overline{F}$ is obtained from the combination of Equations 3.25 and 3.30:

$$\xi \overline{F} = \int_0^\xi F d\xi = 2\beta(\tau_0 - \tau) = \int_F^{F_0} \left[1 + \frac{\beta}{2} \ln(1 + F) + \beta.k \ln s \right] dF \qquad (3.35)$$

$\overline{F}$ is the total amount of solid PCM formed from the beginning of the freezing process over the entire tube.

By integrating Equation 3.25:

$$2\beta\tau = \int_0^F \left[1 + \frac{\beta}{2} \ln(1 + F) + \beta.k \ln s \right] dF \qquad (3.36)$$

All the results are expressed in terms of F and F_0 as the primary variables.

The non-dimensional fluid temperature and the heat exchanger effectiveness ϵ are related by the result:

$$\epsilon = \frac{T_f - T_i}{T_m - T_i} = 1 - \frac{F}{F_0} \qquad (3.37)$$

where ϵ =   effectiveness of the LHS unit,

   T_f =   outlet temperature of the HTF from the heat storage unit;

   T_i =   inlet temperature of the HTF entering storage unit;

   T_m =   melting point of the PCM.

The variable ξ is the Number of Transfer Units (NTU), and is expressed as follows, if h is assumed independent of x (Shamsundar *et al.,*1992):

$$\xi = \frac{2\pi R_i hx}{m_f c_p} = NTU \qquad (3.38)$$

where NTU = Number of Transfer Units,

   R_i =   inner radius of the tube heat exchanger HTF;

   x   =   axial distance of the tube heat exchanger. For the entire tube, x is equal to the total length of the tube heat exchanger.

   m_f =   mass flow rate of the HTF in the tube heat exchanger;

C_p = specific heat capacity of the HTF at constant pressure.

For convenience in obtaining numerical results, the auxiliary functions were introduced by Shamsundar *et al.* (1992):

$$G_0(F) = \int_0^F \ln(1+F)dF = (1+F)\ln(1+F) - F \qquad \textbf{(3.39)}$$

$$G_1(F) = \int_0^F \ln(1+F)\frac{dF}{F} = \frac{1}{2}[\ln(1+F)]^2 + \int_0^F \frac{\ln(1+F)dF}{(1+F)F} \qquad \textbf{(3.40)}$$

The last integral on the right hand side of Equation 3.40 is the Debye function of order one with $\ln(1+F)$ as the argument. The evaluation of $G_1(F)$ does not provide the exact analytical solution. Shamsundar *et al.,* (1992) proposed the Padé approximation given below in order to estimate the value of F:

$$G_1(F) = \left[\frac{p\left(1 + \dfrac{17p^2}{450}\right)}{\left(1 + \dfrac{p^2}{100}\right)} + \frac{p^2}{4} \right] \qquad \textbf{(3.41)}$$

Where $\quad p = \ln(1+F) \qquad \textbf{(3.42)}$

In terms of these functions (G_0 and G_1), the results become:

$$\tau = \frac{F}{2\beta} + \frac{1}{4}G_0(F) + \frac{F.k}{2}\ln s \qquad \textbf{(3.43)}$$

The last parameter of Equation 3.43 does not appear in the derivation of Shamsundar's model. This introduces the second difference between the model as derived in the present study and Shamsundar's model.

The frozen fraction at the axial position x is given by the implicit equation:

$$\xi = NTU = \frac{2\pi R_i hx}{\dot{m}_f c_p} = \ln\left(\frac{F_0}{F}\right) + \beta.k\ln\left(\frac{F_0}{F}\right)\ln s + \frac{\beta}{2}[G_1(F_0) - G_1(F)] \qquad \textbf{(3.44)}$$

A third difference between the model derived and Shamsundar's model is now found in Equation 3.44. There is the additional term which does not appear in Shamsundar's model:

$$\beta.k\ln\left(\frac{F_0}{F}\right)\ln s$$

40

The results (Equations 3.37, 3.43, 3.44) are given in terms of the fraction of frozen layer F as the primary variable and they are used in the design and the evaluation of the performance of the LHS.

From the solution obtained in Chapter 3, the outlet temperature of the HTF, the position of the solidification front of the PCM and the heat transfer rate are calculated for a given LHS.

3.7   Summary and conclusions

The heat transfer process was analysed in the latent shell-and-tube heat exchanger with PCM on the shell side and the HTF flowing in the inner tube. To solve the complex heat transfer problem of PCM and convection heat transfer, only a heat conduction mode in the PCM was considered in the derivation of the model. The solution was obtained in terms of a non-dimensional parameter F. From the solution obtained it is now possible to evaluate the outlet temperature of HTF, the HTF distribution along the tube heat exchanger and the radius of the PCM solidified (front radius).

The thermal model of LHS is a modification of Shamsundar's model. The thermal resistance of the wall tube heat exchanger is considered in the present model. The solutions obtained are used in Chapter 4 to size the LHS and to obtain the thermal performance of the system.

The design method for LHS is presented in Chapter 4.
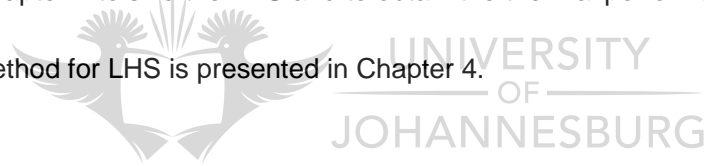
Chapter 4

DESIGN OF THE LATENT HEAT STORAGE SYSTEM

In Chapter 3, the model of the LHS was analysed and solved to predict the thermal behaviour of the thermal unit. The results of the mathematical modelling obtained from Chapter 3 provide the foundation of the LHS preliminary sizing.

In Chapter 4, a thermal design method is described and explained in Section 1, based on the method proposed by Shamsundar *et al.* (1992). LHS performance is evaluated in Section 2. In Section 3, a computer programme code, written to help obtaining the size of the LHS, is presented.

4.1 Description of the design approach

The design of a storage system involves the selection of a storage material, design of a geometrical configuration of containment and a heat exchanger type. The proposed configuration of the AAAR for this project is shown in Figure 3.2. One component of this system is the LHS unit connected to the AAAR generator from one end while another end is linked to a solar collector.

Two modes are considered to supply the thermal energy to the LHS:

- Mode I has the following loop for the working of the HTF:

  LHS $\longrightarrow$ Generator $\longrightarrow$ Collector $\longrightarrow$ LHS

- In the case of insufficient solar insolation (Mode II), the working fluid will follow the loop: LHS $\longrightarrow$ Generator $\longrightarrow$ LHS

4.1.1 Definitions of effectiveness and Number of Transfer Units

The principal design parameters for a LHS unit are: Effectiveness ε and the Number of Transfer Units (NTU). An efficient LHS is characterised by a higher effectiveness and /or a little variation of effectiveness as possible as the PCM continues to solidify.

Essentially, in defining the NTU in a LHS, only the fluid side of the heat transfer coefficient is considered, rather than the usual overall heat transfer coefficient in a conventional heat exchanger.

For a total length of tube L and n number of tubes in the heat exchanger, the equation for the NTU is given by Shamsundar *et al.* (1992) as:

$$NTU = \frac{2\pi R_i h n L}{m_f C_p}$$

(4.1)

where NTU = Number of Transfer Units;

R_i = inside radius of the tube heat exchanger;

h = convection thermal coefficient;

n = number of tubes in the heat exchanger;

L = length of tubes in the heat exchanger;

m_f = mass flow rate of the Heat Transfer Fluid inside of the tube;

C_p = specific heat capacity of the Heat Transfer Fluid.

NTU provides a measure of the size or capacity of the exchanger. It may be considered as a measure of the exchanger ability to change the temperature of the fluid and an indicator of the actual heat transfer area or physical size of the exchanger.

For a conventional heat exchanger (fluid-fluid), the effectiveness of heat exchanger is defined as the ratio of the actual heat transfer to the heat transfer when the surface area approaches infinity. Equation 4.2 gives the effectiveness of a heat exchanger fluid-fluid (Lienhard J.IV & Lienhard J. V, 2006):

$$\varepsilon = \frac{c_c(T_{CO} - T_{Ci})}{c_{min}(T_{Hi} - T_{Ci})} = \frac{c_H(T_{Hi} - T_{Ho})}{c_{min}(T_{Hi} - T_{Ci})}$$

(4.2)

where   C =   specific heat of fluid at constant pressure;

T =   temperature of HTF.

The subscripts c, H, co, ci, min, Hi, Ho stand respectively for cold, hot, cold outlet, cold inlet, minimum, hot inlet and hot outlet.

For a latent heat exchanger shell-and-tube with a PCM as storage material, the effectiveness ε is defined as the ratio of the actual heat transfer to the heat transfer corresponding to not only infinite area, but also to infinite conductance in the PCM. Therefore, the definition of the effectiveness applied to the Latent Heat Storage is given by the equation (Shamsundar *et al.*, 1992):

$$\varepsilon = \frac{T_f - T_i}{T_m - T_i}$$

(4.3)

where T_f =   outlet temperature at the heat exchanger;

T_i =   inlet temperature of HTF at the heat exchanger;

T_m =   melting point of the PCM.

The heat capacities of the HTF and PCM are neglected in Equation 4.3.

Equation 4.3 was obtained by neglecting the heat capacity of both HTF and frozen PCM.

To size the LHS unit, the following steps are applied:

4.1.2 Selection of Phase Change Material

To select an appropriate PCM for a specific application, the first criterion to be considered is the operational temperature range required by the AAAR generator. This operating temperature must match the transition temperature of the storage material. A PCM melting point had to be chosen at a temperature interval above the operating temperature. According to Lane (1983), an interval of about 5 to 10°C should be considered for many thermal systems. Assuming that a temperature difference of about 10°C is used to charge the storage unit, the melting point of the PCM should be about 10°C below charging temperature. This enables selection of a set of heat PCM storage materials with suitable melting points for a given application. In case there is more than one PCM with a suitable melting temperature, secondary comparisons is considered to select the correct PCM. Table 4.1 lists the criteria used for selecting the best PCM for this application.

Table 4.1: Secondary selective criterion for the choice of PCM (Hale *et al.,* 1971)

PROPERTY OR CHARACTERISTIC	DESIRABLE VALUE OR TENDENCY
Heat of fusion	High
Thermal conductivity	High
Specific heat	High
Density	High
Volume change during melting	Low
Vapor pressure	Low
Melting/Freezing behaviour	Dependable and reversible
Availability	Readily available
Cost	Low
Compatibility	Compatible with container
Toxic	Non toxic
Hazardous behaviour	Hazardous behaviour not exhibited
Property data	Readily available and well documented
Surface tension	Low

4.1.3 Selection of working fluid

The selection of the HTF is important to transfer thermal energy supplied from a SC to the SS and from the SS to the heat sink to cope with demand.

Criteria to be considered when selecting the HTF (Darling, 2008): Coefficient of expansion, viscosity, thermal capacity, freezing point, boiling point, flash point; it does not exhibit a high level of the toxicity behaviour.

Selecting a HTF, for example for a cold climate, solar water heating systems require a fluid with low freezing point to avoid freezing of the HTF in the pipes. On the other hand, fluids

exposed to high temperatures, as in a desert environment, should have a higher boiling point to resist boiling at operating temperature.

Darling (2008) presented the most commonly used HTF and their properties:

1. Air: It will not freeze or boil, and is non-corrosive. However, it has a low heat capacity, and tends to leak from of collectors, ducts and storage units.

2. Water: Water is non-toxic and inexpensive. With a high specific heat, and a low viscosity, it is easy to pump. Unfortunately, water has a relatively low boiling point and a high freezing point. It can also be corrosive if the pH (acidity/alkalinity level) is not maintained at a neutral level. Water with a high mineral content leads to mineral deposits forming in collector tubing and the plumbing system.

3. Glycol/water mixtures: Glycol/water mixtures have a 50/50 or 60/40 glycol-to-water ratio. Ethylene and propylene glycol are "antifreezes". Ethylene glycol is extremely toxic and should be used only in double-walled, closed-loop systems.

4. Hydrocarbon oils: Hydrocarbon oils have a higher viscosity and a lower specific heat than water. They require more energy to pump. These oils are relatively inexpensive with a low freezing point.

5. Silicones: Silicones have a very low freezing point and a high boiling point. Because silicones have high viscosity and low heat capacities they require more energy to pump. Silicones are non-corrosive and long-lasting. Silicones leak easily.

4.1.4 Determination of the latent heat exchanger effectiveness

Effectiveness of a LHS is estimated at the beginning of the process (discharging) when the storage material is in liquid form. The value of the maximum desired outlet temperature of the fluid $T_{f\,max}$ is specified. The inlet temperature of the fluid T_i at the LHS is also fixed. The maximum effectiveness ε_{max} can be estimated in the following manner:

Consider the conventional heat exchanger having the capacity ratio (CR) defined by Lienhard J. IV & Lienhard J. V, 2006, as:

$$CR = \frac{C_{min}}{C_{max}}$$

(4.4)

46

where C_{min} and C_{max} are the lower and higher capacity rates, respectively. CR has the values between 0 and 1. For parallel flow heat exchangers, the effectiveness is given as (Lienhard J. IV & Lienhard J. V, 2006):

$$\epsilon = \frac{1 - \exp(-NTU(1 + CR))}{1 + CR}$$

(4.5)

For all flow conditions if $CR = 0$, for example one side of the heat exchanger is isothermal (the PCM is assumed at melting point that means a constant temperature), the effectiveness becomes:

$$\epsilon_{max} = 1 - \exp(-NTU)$$

(4.6)

where NTU = Number of Transfers Units;

ϵ_{max} = maximum effectiveness of latent heat exchanger

The effectiveness for most of the heat exchanger configurations increases with the increasing of the NTU.

4.1.5 Determination of the parameter β

The parameter β is defined as:

$$\beta = \frac{hR_i}{k_m}$$

(4.7)

Where h = convection coefficient of heat transfer;

R_i = inner radius of the heat exchanger tube and k_m = thermal conductivity of the PCM.

This group β is determined in solving the analytical model (Chapter 3). The Biot Number is determined as a function of the outer radius R_o.

$$Bi = \frac{hR_0}{k_m}$$

(4.8)

The difference between Equations 4.7 and 4.8 is: Bi is a function of the outer radius of the tube heat exchanger R_o and β depends on the inner radius of tube heat exchanger R_i.

To estimate the parameter β, the Nusselt number Nu is estimated first depending on the type of flow regime in the tube being either laminar or turbulent.

The Nusselt number Nu is the ratio of convective to conductive heat transfer across (normal to) the boundary.

47

$$Nu = \frac{hR_0}{k_f} \qquad \textbf{(4.9)}$$

where Nu = Nusselt number;

h = convective heat transfer coefficient of the HTF;

R_0 = outer radius of the tube heat exchanger;

k_f = thermal conductivity of the HTF.

For liquid coolants, higher viscosities lead to laminar flow. If the fluid is laminar and a fully developed pipe flow considered, the uniform wall temperature boundary condition is given as (Duffie & Beckman, 2006; Shamsundar *et al.,* 1992):

$$Nu_R = 1.835 \qquad \textbf{(4.10)}$$

The Nusselt number given in Equation 4.10 refers to the radius of the tube.

If the value of thermal resistance between the HTF and the constant temperature environment (shell side filled with PCM) is low, the thermal boundary condition approaches constant temperature. Since a constant wall temperature assumption yields somewhat lower heat transfer coefficients, Equation 4.10 is the recommended assumption for conservative design (Duffie & Beckman, 2006).

The local Nu for laminar flow, in the fully developed region, is therefore independent of the distancealong axial direction x, the Reynolds number Re and the Prandtl Number Pr (Cengal, 1997; Lienhard J. IV & Lienhard J. V, 2006).

For turbulent flow, the Reynolds number Re of the flow and the Prandtl number Pr have to be estimated first and use a correlation for a fully developed heat transfer such as the Dittus-Boelter correlation to estimate the Nusselt number Nu.
The Dittus-Boelter Equation is given by:

$$Nu_R = 0.015 \, Re^{0.8} \, Pr^{0.4} \qquad \textbf{(4.11)}$$

where: Re = Reynold number;

Pr = Prandtl number.

After obtaining Nu in this way, β is calculated as follows by combining (4.7) and (4.9):

$$\beta = Nu \, \left(\frac{k_f}{k_m}\right) \frac{R_i}{R_0} \qquad \textbf{(4.12)}$$

where Nu = Nusselt number;

k_f = thermal conductivity of the HTF;

k_m = thermal conductivity of the PCM;

R_0 = outer radius of the tube containing HTF;

R_i = inner radius of the tube containing HTF.

4.1.6 Calculation of the fraction of PCM solidified at the tube inlet F_o

The value of F_o which is the fraction of PCM solidified at the tube inlet at the end of the discharge period is obtained from:

$$\xi = NTU = \frac{2\pi R_i hx}{m_f c_p} = \ln\left(\frac{F_o}{F}\right) + \beta.k \ln\left(\frac{F_o}{F}\right) \ln s + \frac{\beta}{2}[G_1(F_o) - G_1(F)] \qquad \textbf{(4.13)}$$

where

x = distance along the tube heat exchanger;

NTU = Number of Transfer Units;

h = convection coefficient film of the HTF;

m_f = mass flow rate of the HTF;

β = parameter defined in Equation 4.7;

k = ratio of thermal conductivity of PCM and thermal conductivity of wall tube heat exchanger;

C_P = specific heat capacity at constant pressure of the HTF;

F_0 ; F = fraction of PCM solidified at the tube inlet of heat exchanger and at a given position of the axial distance x along the tube respectively.

s = ratio of the outer and inner radius of the tube heat exchanger;

$G_1(F_0)$ and $G_1(F_1)$ are auxiliary functions defined in Section 3.5.

Equation 4.13 is derived in Chapter 3. It is a transcendent equation that is solved by means of different numerical methods such as Newton-Raphson and Secant methods.

4.1.7 Calculation of the non-dimensional time variable τ_o

In order to determine the radius of the tube heat exchanger, the non dimensional time variable is determined.

The non-dimensional time variable at inlet τ_o is evaluated as:

$$\tau_o = \frac{F_o}{2\beta} + \frac{1}{4}G_o(F_o) + \frac{F_o}{2}k \ln s \qquad \textbf{(4.14)}$$

where

F_0 = fraction of PCM solidified at the inlet tube heat exchanger;

s = ratio of the outer and inner radius of the heat exchanger tube;

k = ratio of thermal conductivity of PCM and thermal conductivity of wall tube heat exchanger;

$G_0(F_0)$ = auxiliary function defined in Section 3.5.

Equation 4.14 establishes the relationship between the dimensionless time τ and the fraction of solidified PCM at the inlet tube F_0. It is an important parameter in determining the dimension of the tube for the heat exchanger.

From the estimation of the dimensionless time τ, the radius of the tube heat exchanger is calculated.

4.1.8 Calculation of the outside radius of tube R_o

From the definition of the non-dimensional time variable (3.6b), the outside radius R_0 of the tube heat exchanger is determined as:

$$R_0 = \left(\frac{k_m(T_m - T_i) \cdot t}{\tau_0 \rho H} \right)^{\frac{1}{2}} \tag{4.15}$$

where t   = storage period;

ρ   = density of the PCM;

H   = heat of fusion of the PCM;

τ_0 = non-dimensional time;

k_m = thermal conductivity of the PCM;

T_m = melting point of the PCM;

T_i = inlet temperature of HTF.

4.1.9 Evaluation of others parameters of shell-and- tube latent heat exchanger

- **Tube pitch diameter D_{tp}**

The tube pitch is defined as the shortest distance between two adjacent tubes.
The formula used to estimate the tube pitch diameter is given:

$$D_{tp} = 2R_0(1 + F_0)^{\frac{1}{2}} \tag{4.16}$$

where D_{tp} = tube pitch;

R_0 = outer radius of the tube;

F_0 = fraction of PCM that has solidified at the tube inlet at the end of the discharge period.

- **Estimation of the length L and the number n of the tubes**

The number of tubes in heat exchanger depends on mass flow rate. The product Ln is obtained from:

$$Ln = (NTU m_f C_p)/(2\pi h R_i) \tag{4.17}$$

where L = length of the tube;

    n = number of the tubes in the heat exchanger;

    m_f = mass flow rate of the HTF in the tube heat exchanger;

    C_P = specific heat capacity of the HTF at constant pressure;

    h = heat transfer coefficient of the HTF flowing in the tube heat exchanger.

This condition (4.17) provides a maximum length of the tubes for a laminar flow regime in the tube. The length of the tubes was chosen below this value and all remaining design parameters calculated.

For turbulent flow, the length of the tube is simply chosen to obtain the value of Re assumed in calculation of Nusselt number Nu.
Reynolds number Re is determined from:

$$Re = \frac{2m_f L}{(\pi R_i Ln \mu)} \tag{4.18}$$

where m_f = mass flow rate of HTF;

    L = length of the tubes;

    R_i = inner radius of the tubes;

    μ = dynamic viscosity of the HTF.

- **Computation of the tank diameter** D_T

Lecomte *et al.* (1985) suggested the best arrangement of the heat exchanger tubes are hexagonal centres; the total TES unit tank diameter can be estimated from the total cross sectional area A per tube as :

$$A = \pi r_T^2 \tag{4.19}$$

Where A = cross sectional area per tube;

    r_T= tank or shell radius .

Or

$$r_T = \sqrt{\frac{A}{\pi}}$$

(4.20)

For hexagonal centres,

$$A = n\sin 60^\circ (r_m^2)$$

(4.21)

Where n is the number of the heat exchanger tubes and r_m is the PCM radius.

Therefore,

$$r_T = \sqrt{\frac{n2r_m^2\sqrt{3}}{\pi}}$$

(4.22)

Since $D_{tp} = 2\, r_m,$

The tank diameter D_T is given by the expression:

$$D_T = D_{tp}(2n\sqrt{3}/\pi)^{1/2}$$

(4.23)

where D_T =   tank diameter;

     D_{tp} =   tube pitch;

     n =   number of the heat exchanger tubes.

The determination of other related dimensions of the latent heat exchanger shell-and-tube are obtained from:

- **Tank volume** V_T

The tank volume is calculated from:

$$V_T = \pi \frac{D_T^2}{4} L$$

(4.24)

where V_T =   tank volume ;

     D_T =   tank diameter;

     L   =   length tube.

- **Liquid volume** V_L

The liquid volume in the tube heat exchanger is estimated from :

$$V_L = \pi L n R_i^2$$

(4.25)

where V_L =   liquid volume ;

     L =   tube length;

     n =   number of tubes;

     R_i =   inner radius of the tube heat exchanger.

- **Tube volume** V_{tube}

The tube volume is calculated from:

$$V_{tube} = \pi(R_0 + R_i)nL(R_0 - R_i)$$ **(4.26)**

where V_{tube} = tube volume;

R_0 = outer radius of the tube heat exchanger;

R_i = inner radius of the tube heat exchanger;

n = number of the heat exchanger tubes;

L = length of the heat exchanger tube.

- **Volume PCM** V_{PCM}

The volume of PCM required to store thermal energy for a given storage period is evaluated from:

$$V_{PCM} = V_T - V_L - V_{tube}$$ **(4.27)**

where V_{PCM} = volume of PCM;

V_T = tank volume;

V_L = liquid volume;

V_{tube} = tube volume.

- **Mass PCM** M_{PCM}

The final step is the evaluation of the amount of the PCM. With the volume of PCM calculated in the previous step, the mass of PCM is calculated as:

$$M_{PCM} = \rho_s V_{PCM}$$ **(4.28)**

where M_{PCM} = the mass of the PCM;

V_{PCM} = the volume of the PCM;

ρ_S = the density of the PCM.

4.2 Performance of the Latent Heat Storage unit

After obtaining the dimensions of the shell-and-tube LHS unit, several steps were employed to evaluate the thermal performance of the designed unit following Shamsundar *et al.* (1992):

1. Select the various instants of time during the discharge period.

2. Calculate the corresponding values of the time variable by using its definition (3.6b).

3. Solve Equation 4.14 for F_0.

4. By using the value of F_0 obtained in step 3, and then solving Equation 4.13 for the instantaneous value of the effectiveness.

5. Calculate the instantaneous fluid outlet temperature from the definition of the effectiveness given by Equation 4.3.

6. Having the value of F_0, the instantaneous value of the front solidification of the PCM was estimated by using Equation 3.5.

4.3   Computer programme code to size the Latent Heat Storage unit

A flowchart (Figure 4.1) representing an algorithm or process shows the different steps to follow in the determination of the LHS shell-and-tube heat exchanger problem.
The flow chart helps to identify problem variables and the results required.

The computer programme code was written by using SCILAB software (**Appendix F.3**). This programme allows for calculation of different parameters of the shell-and-tube heat exchanger, when given the properties of the PCM (melting point, heat of fusion, thermal conductivity, and density), the desired maximum outlet temperature, minimum outlet temperature at the heat exchanger, properties of the selected HTF and the discharge period. The dimensions of the latent heat exchanger shell–and-tube were determined in terms of the shell diameter, the inner and outer radius of the heat exchanger, length of the tube heat exchanger, number of the tube and volume of PCM.

In this project, the computer programme code (**Appendix F.3**) was written for a laminar flow regime in the tube heat exchangers.

4.3.1 Input parameters

To assist in solving the sizing problem of the LHS, the following parameters are specified:

- Properties of the PCM such as: melting point, thermal conductivity, density and latent heat of fusion;
- Properties of the HTF including thermal conductivity and specific heat capacity;
- Mass flow rate of the HTF is fixed and the type of the flow regime: laminar or turbulent;
- Inlet temperature of the HTF specified; maximum and minimum outlet temperature of the HTF from the heat exchanger are fixed, and
- Storage period of the PCM.
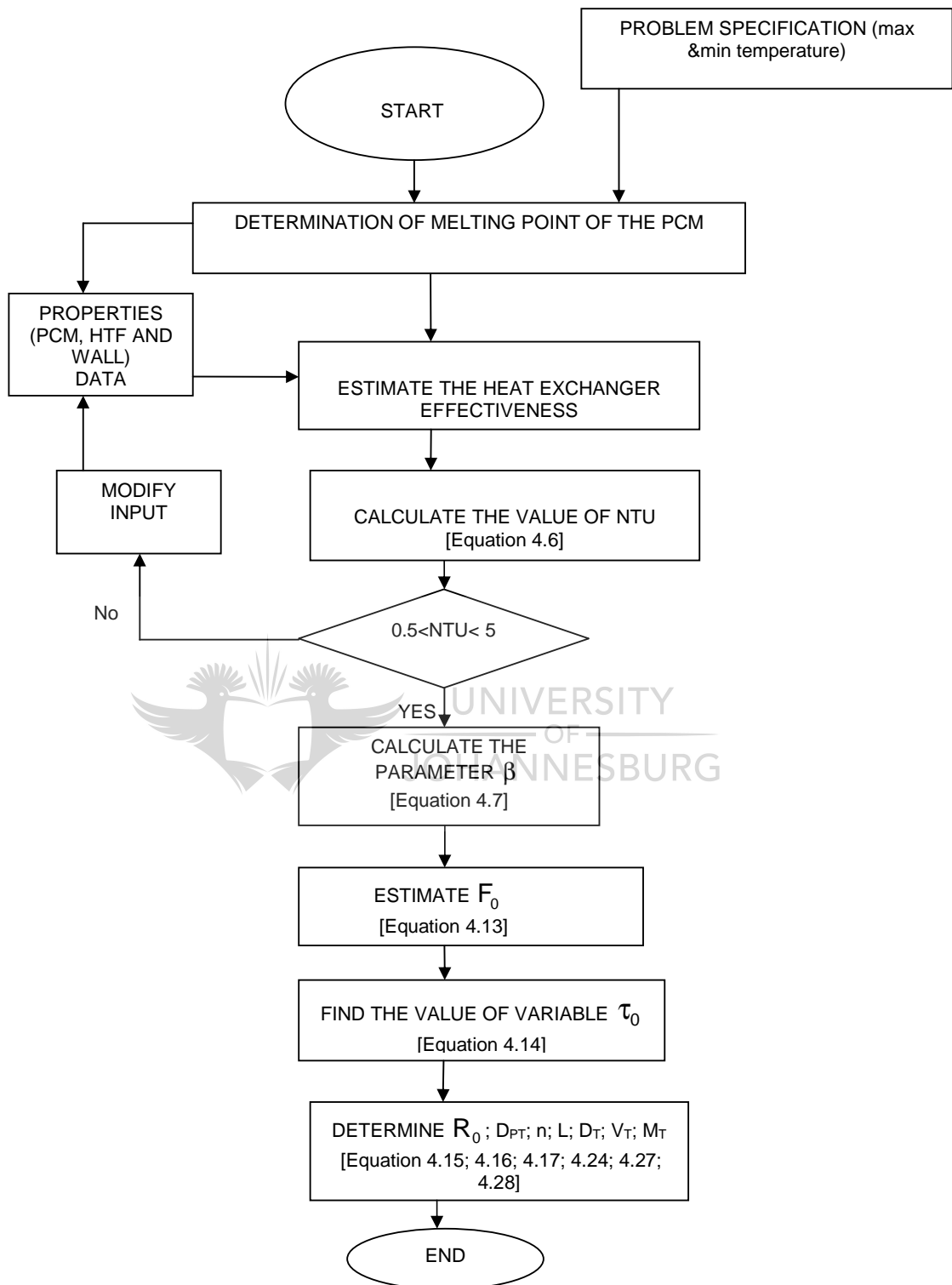
Figure 4.1: Flow chart for sizing the LHS

4.3.2 Output parameters

The following output variables will be obtained in this manner:

- Pitch tube;
- Volume of tank;
- Diameter of the shell;
- Number of tubes and the length;
- Inner and outer radius of the heat exchanger tube;
- Volume of tube, the volume of heat transfer and the volume of PCM;
- Mass of PCM.

4.4　Summary and conclusions

Chapter 4 focuses on the description of the design method for LHS. The criteria for selecting the best candidates of PCM and the HTF were indicated. The design method based on Shamsundar's work. The difference is mainly the integration of thermal conductivity and the thickness of the tube used in the proposed design method.　The different steps to follow were indicated to size the LHS.

Chapter 5 is a case study applied to the design approach given in Chapter 4.　It is used to size the LHS and to evaluate the unit's performance for a given design requirements.

Chapter 5

SIZING OF THE LATENT HEAT STORAGE

5.0   Introduction

In Chapter 5, a case study of the design method described in Chapter 4 is applied to sizing the LHS with reference to the AAAR.

Consider an absorption refrigerator machine that requires 2.35 kW as heat input to the bubble pump and the generator. The load of this machine is 1.175 kW at a temperature level of -5°C (evaporator). The solar collector supplies heat to the LHS.

With those requirements, the Coefficient Of Performance (COP) of the refrigerator approached 0.5 obtained from:

$$COP \quad = \frac{Q_{ev}}{Q_G + W_P} \tag{5.1}$$

where Q_{ev} is the refrigeration capacity, Q_G the input heat to the generator and W_P is the work done by the pump.

The problem consists to size the LHS using solar energy to drive the AAAR.

To apply the calculation procedure using the method described in Chapter 4, a case study is conducted for a given design requirement.

The main goal is to determine the dimension of the LHS in terms of the inner and outer radius of tube heat exchanger, number of tube heat exchangers, volume of the PCM, mass of the PCM, type of PCM and the appropriate HTF.

The design requirements of the LHS to be achieved are:

- Provide 100% solar heat to the domestic AAAR;
- Heat source temperature of the fluid during the charging process (from the solar collector) to the storage is fixed and equal to 130°C;
- The minimum and maximum temperatures entering the generator of the AAAR required are fixed at 82°C and 97°C respectively;
- The storage system needs to be able to supply continuously the minimum thermal energy of 2.35 kW to the generator for a period of 12 hours;
- The storage system needs to be safe and non-toxic;
- Selected PCM has to have high latent heat of fusion since there is a constraint of space and,

57

The solar collector and the AAAR are not part of the report and are designed elsewhere.

The different steps to determine the dimension of LHS for the AAAR are applied in the following sections:

5.1 Selection of the PCM for the latent heat storage

A suitable PCM with a melting point within the range of the temperature generator (82^oC) is identified. Since the temperature of the heat source (solar collector) is estimated to be 130^oC and allowing a temperature difference of 10^oC, the candidate PCM had a temperature of 120^oC as a melting point for the application.

Numerous candidate PCMs are considered for the LHS in the range of 99^oC and 120^oC (Hale *et al.,* 1971; Lane, 1983; Sharma *et al.*, 2005; Zalba, 2003). Table 5.1 provides some of the PCMs identified in the literature for the required temperature range.

Table 5.1: Thermal and physical properties of selected PCMs

PCM NAME	TYPE	MELTING POINT [^{o}C]	HEAT OF FUSION [kJ/kg]	THERMAL CONDUCTIVITY [W/m.K]	DENSITY [kg/m^3]	HEAT CAPACITY [kJ/kg.K]
E117	SALT HYDRATE	117	169	0.7	145	2.6
RT 100	PARAFFIN	99	168	0.2/0.2	940/770	1.8/2.4
CATECHOL		104.3	207	n.a	1370	n.a
ERYTHRITOL	SUGAR ALCOHOL	118	339.8	0.733/0.326	1480/1300	1.383/2.765
METHYL FUMARATE		102	242	n.a	1046	n.a
PARAFFIN WAX 106	PARAFFIN	106	80	0.63	1200	n.a
$MgCl_2.6H_2O$	SALT HYDRATE	116.7	168.9	0.704/0.57	1570/1450	2.25/2.61

From Table 5.1 PCMs identified have the required melting point; they are not all well documented for some of relevant properties needed for the sizing of the LHS. One example is Methyl fumarate in Table 5.1 that has a melting point of 102^oC, information regarding its thermal conductivity and heat capacity were not available.

If more than one PCM is identified based on the melting point, secondary comparisons (Table 4.1) are considered to select the best candidate PCM.

After screening all properties of the different candidate PCMs in Table 5.1, Erythritol deserved to be selected as PCM for this application. **Appendix C** shows a DSC curve of Erythritol obtained during the accelerated thermal test.

5.2   Selection of the working fluid for the heating application

A HTF selected in the case study was Duratherm XLT-50 (**Appendix D**). It is engineered for long-term operation in heat transfer applications requiring precise temperature control ranging from -45°C to 160°C.   It is ideal for heating and cooling and user-friendly in environmental applications.   Duratherm XLT-50 presents a low odour and has a high flash point; it is a hydrocarbon blend.

5.3   Tube material

The selection of a material for the tube heat exchanger depends on several criteria. Among them are thermal conductivity, corrosion and cost. Some common heat exchanger materials are indicated in **Appendix E.1**. Copper has a thermal conductivity of 386 W/m^{o}C at room temperature (20°C).

For the case study, the material selected for tube was the copper.

The thermo-physical properties of Erythritol (PCM), Duratherm XLT-50 (HTF) and copper (tube material) are summarised in Table 5.2.

Table 5.2: Thermal physical properties of Erythritol, Duratherm XLT-50 and copper

1. PCM: Erythritol	
Melting point, $T_m(^oC)$	118
Density of Erythritol (liquid phase), $\rho_l(kg.m^{-3})$	1300(140°C)
Density of Erythritol (solid phase), $\rho_s(kg.m^{-3})$	1480(20°C)
Latent heat , $\Delta H(kJ.kg^{-1})$	339
Specific heat of Erythritol (liquid), $C_{Pl}(J.kg^{-1}.K^{-1})$	2.765
Specific heat of Erythritol (solid), $C_{ps}(J.kg^{-1}.K^{-1})$	1.383
Thermal conductivity of Erythritol(solid), $k_s(W.m^{-1}.K^{-1})$	0.733(20°C)
Thermal conductivity of Erythritol(liquid) $k_l(W.m^{-1}.K^{-1})$	0.326(140°C)
2. HEAT TRANSFER FLUID: Duratherm XLT-50 (60°C)	
Density of Duratherm XLT-50, $\rho_f(kg.m^{-3})$	817
Thermal conductivity of Duratherm XLT-50, $k_f(W.m^{-1}.K^{-1})$	0.131
Specific heat of Duratherm-XLT-50, $C_{pf}(J.kg^{-1}.K^{-1})$	2.160
3. TUBE MATERIAL: COPPER	
Thermal conductivity of copper, $k_w(W.m^{-1}.K^{-1})$	386
Density of copper, $\rho_w(kg.m^{-3})$	8795

5.4   Determination of the LHS shell-and-tube parameters

The maximum desired outlet temperature of the HTF, T_{max} was fixed at 97°C. The minimum outlet of the HTF was T_{min}=89°C at the heat exchanger and the inlet temperature of the HTF a constant, Ti=25°C. The properties of the Duratherm XLT-50 were taken at the bulk mean fluid temperature T_b :

$$T_b = \frac{T_{f\,max} + T_0}{2} = 60^{\circ}C$$

60

From Equation 3.37, the maximum effectiveness of the heat exchanger ε_{max} = 0.77 and the minimum effectiveness of the heat exchanger expected is $\varepsilon_{min} = 0.69$. The number of transfer units NTU was determined from the Equation 4.4 and estimated at 1.49

The higher viscosity of the HTF was expected to lead to the laminar flow. The Nusselt number Nu_R =1.84 for a fully developed heat transfer.

Having Nu, the parameter β was estimated from Equation 4.10 and found to be equal to 0.376.

The transcendental Equation 4.14 evaluated the fraction of the PCM solidified F_0 at the tube inlet at the end of the discharge period.

From the values obtained for $\varepsilon_{min} = 0.69$, NTU=1.49, the consideration of copper as tube heat exchanger material , $k_w = 386 W/m.K$, $\beta = 0.376$ and the ratio of radius outer and inner of the tube heat exchanger fixed to s =1.15, the estimation of the F_0 is evaluated by analytical or numerical method.

For solving the transcendental Equation 4.14, Deadline 2.36 is used. DeadLine 2.36 is a programme used for solving equations, plotting graphs and obtaining an analysis of a function (http:// www.deadline.3x.ro).

By using the software DeadLine 2.36 to obtain the root of the Equation 4.13, F_0 = 5.94 was found as the amount of the PCM solidified at the end of the discharge period and for x= 0 m on the axial distancealong the tube (**Appendix F.1** and **Appendix F.2**).

The value of the non-dimensional time variable calculated from Equation 4.14 was $\tau_o = 9.78$

The outer radius of tube heat exchanger R_0 was calculated according to Equation 4.12.

$\tau_0 = 9.78$, $H = 339.8 \times 10^3 J/kg$; $\rho_s = 1480 kg/m^3$, $k_m = 0.733$ W$/m.K$, $T_m = 118°C$,

$T_i = 25°C$ and the discharge period fixed at t =12 h.

$R_0 = 24mm$. With the ratio outer radius and inner radius fixed and equal to 1.15, the inner radius of $R_i = 21mm$ was estimated for the tube heat exchanger.

The tube pitch was calculated from the following parameters: $F_0 = 5.94$, and the outer radius R_0 = 24 mm, Equation (4.13) provided the value of the tube pitch Dpt=0.13m.

With m_f = 0.017kg/s, NTU= 1.488, $C_{P,f} = 2.16 \times 10^3 \, J/kgK$, $R_i = 21\,mm$, $h = 11.27 W/m^2K$, the product nL was obtained and equal to 36.56 from the Equation 4.14.

With the length of the tube selected at 3 m, the number of tubes was n=13.

The tank diameter or shell diameter D_T was equal to 0.4 7m. This value was obtained by considering the Equation 4.24 with n=13, tube pitch D_{pt}=0.13 m.

The tank volume was calculated from the Equation 4.21. V_t=0.53 m³.

The PCM volume was obtained as $V_{PCM} = 0.47m^3$. Taking 10 % change in Erythritol volume during solid liquid transition, the PCM volume total was $V_{PCMt} = 0.5m^3$.

Having the volume of PCM, the mass of Erythritol was estimated from the density $\rho_s = 1480 \, kg/m^3$ as M_{PCM}=745 kg.

The programme code written in SCILAB 5.3 to size the LHS is provided in **Appendix F.3** and **Appendix F.4** for the design requirements. In Figure 5.2, a schematic of the LHS unit designed is shown and Table 5.3 sum ups the results of the LHS. The programme code was written from the design method provided in Chapter 4.
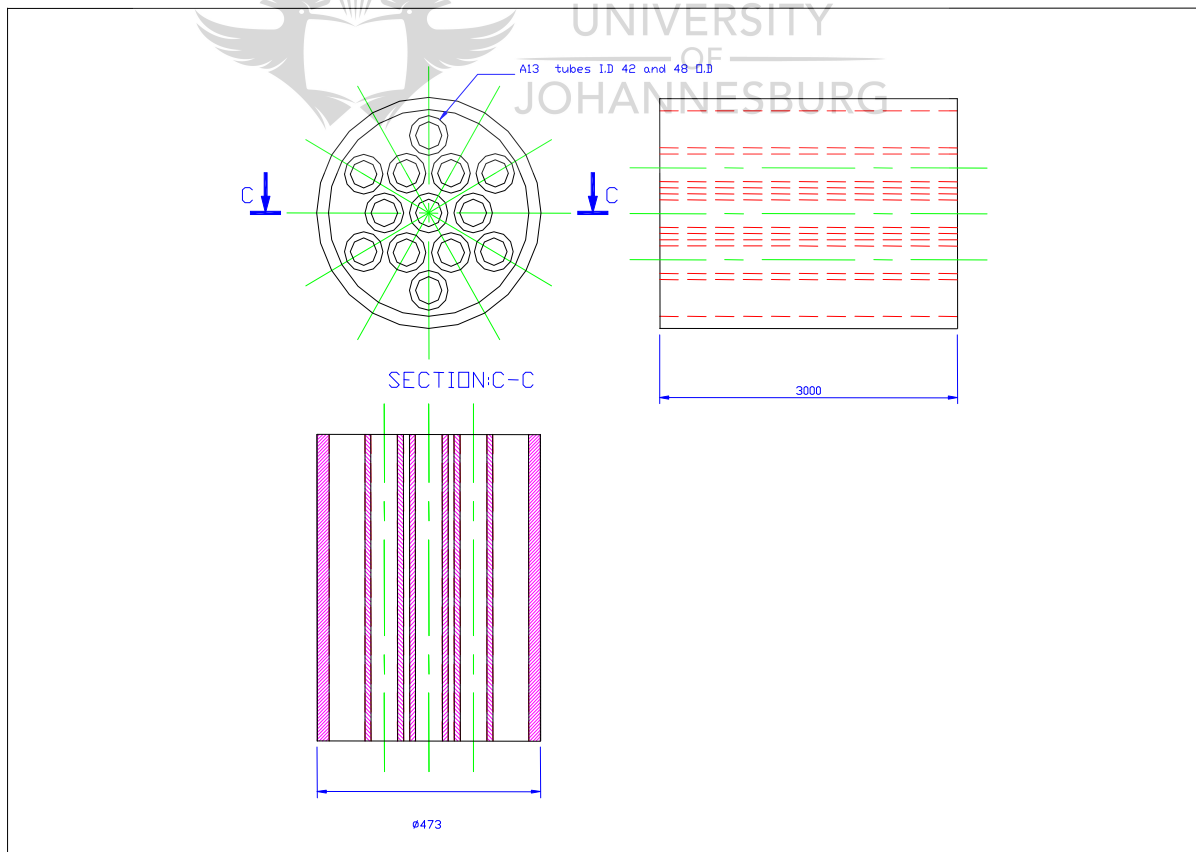
Figure 5.1: Schematic diagram of the designed Latent Heat Storage shell-and-tube

Table 5.3: Specifications of the designed Latent Heat Storage unit

PCM SELECTED	ERYTHRITOL
MELTING POINT	118°C
LATENT HEAT OF FUSION	339.8kJ/kg
HEAT TRANSFER FLUID	DURATHERM XLT-50
TUBE MATERIAL	COPPER
INLET TEMPERATURE FLUID	25°C
MASS FLOW RATE	0.017 kg/s
FLUID MAXIMUM OUTLET TEMPERATURE	97°C
FLUID MINIMUM OUTLET TEMPERATURE	89°C
OUTSIDE RADIUS OF TUBE	24mm
INSIDE RADIUS OF TUBE	21mm
LENGTH OF TUBE	3 m
NUMBER OF TUBES	13
TANK DIAMETER	0.47m
TANK VOLUME	0.53m^3
VOLUME OF PCM	0.5m^3
STORAGE PERIOD	12 h
MASS OF THE PCM	745 kg

5.5   Determination of the thermal parameters of the LHS

After sizing the shell-and-tube latent heat exchanger storage, the instantaneous outlet temperature of the HTF during the discharge period, front solidification and heat transfer were then evaluated, based on the steps explained in Section 4.2. As a result, Table 5.4 is obtained:

Table 5.4: Thermal parameters and front radius of the PCM at the inlet of the tube in the LHS at various time interval

t[h]	τ	F_0	ε	T [℃]	Q[W]	r_m [mm]
0	0	0	0.77	97	2630	24.4
2	1.63	1.13	0.74	94	2527	35.65
4	3.26	2.17	0.73	93	2493	43.46
6	4.89	3.16	0.71	91	2425	49.75
8	6.52	4.11	0.70	90	2390	55.16
10	8.15	5.04	0.69	89	2356	59.95
12	9.78	5.94	0.69	89	2349	64.29

In Table 5.4, t= the time; τ= the non-dimensional variable time; F_0 = the fraction of the solid PCM formed at the inlet of the tube heat exchanger for various instants;

ε= the effectiveness; T=the outlet temperature of HTF; Q= the heat transfer rate of Duratherm-XLT 50, and r_m= the solidification front radius of Erythritol.

From Table 5.3, it is clear that the maximum outlet temperature from the heat exchanger is $97^{o}C$ and the minimum outlet temperature $89^{o}C$.

5.5.1 The outlet temperature of Duratherm XLT-50 at the exit of the LHS unit

In Figure 5.2, the variation of the outlet temperature in the heat exchanger is given as a function of time. The storage period was 12 hrs.

The discharge process began at time t=0, the inlet HTF fixed at $25^{o}C$ then entered the heat exchanger. It caused the melting of the PCM. The temperature of the HTF (Duratherm XLT-50) decreased in time because of the increasing of the solidification front radius and of the conductive thermal resistance of PCM. The expected HTF outlet temperature varied in the range of $97^{o}C$ at the beginning of the process (at 3 m from the inlet) and $89^{o}C$ at the end of the process at 3 m and 12 hrs from the beginning of the discharge cycle.
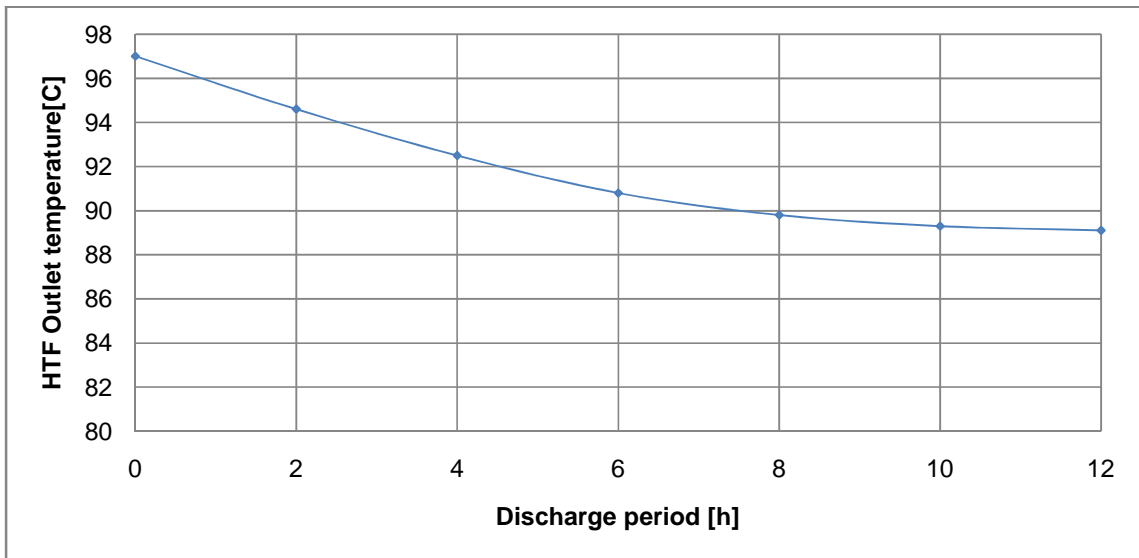
Figure 5.2: HTF outlet temperature at the exit of the LHS against the discharge period

In Figure 5.3, the variation of the HTF temperature is given as a function of the axial distance along the tube heat exchangers and for different time interval (0 to 12 h). At the inlet, the HTF temperature was 25°C and the outlet HTF temperature varied from 97°C and 89°C over this time interval. It can be observed the HTF temperature decreased in time because of the augmentation of solidification front radius of the PCM and thermal resistance in the PCM.
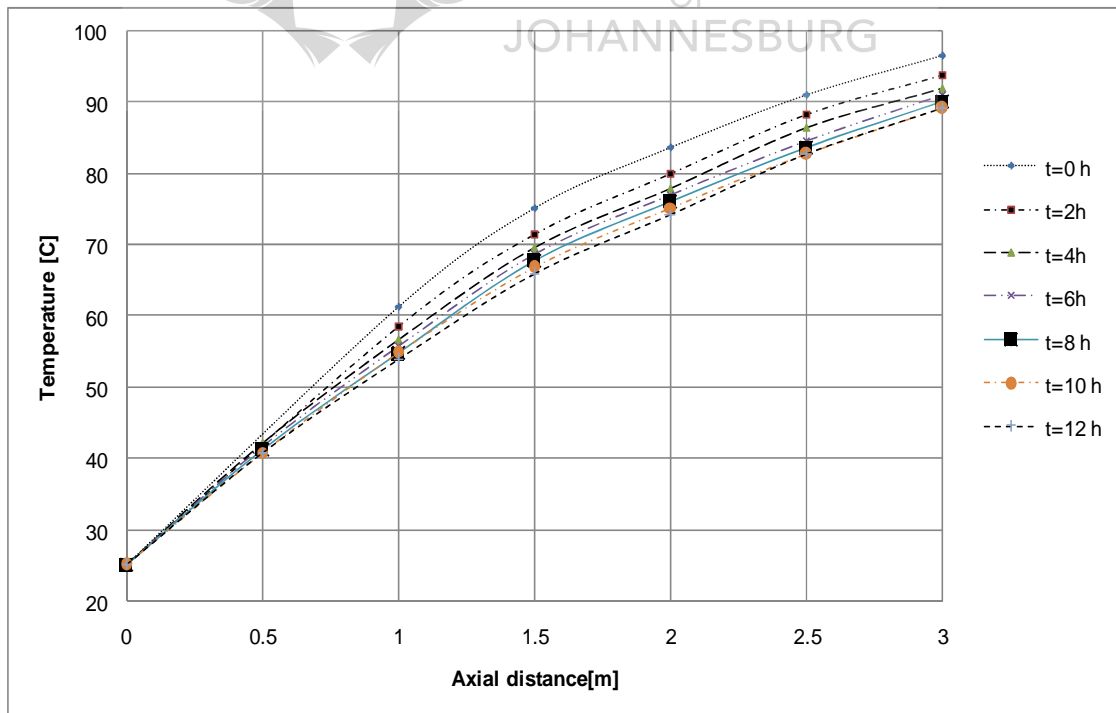
Figure 5.3: Temperature distribution of HTF against the axial distance along the tube heat exchanger and for different instants

5.5.2 The front radius solidification of Erythritol

Erythritol was considered at liquid state at the beginning of the discharge process. At time t=0h, the temperature of the PCM was assumed to be equal to the melting point. The working fluid Duratherm XLT-50 was supplied at 25°C as inlet temperature and entered the tube at this temperature and picked up heat from the Latent Heat Storage material. The rate of heat transfer from the PCM to the HTF caused the PCM to freeze on the outside of the tube simultaneously causing a rise in the fluid temperature. Figure 5.4a shows the front radius distribution of the PCM at inlet as a function of time. The minimum front radius coincided with the outer radius of the heat exchanger tube at time t = 0 since it was measured from the centre of the tube heat exchanger. The maximum front radius was equal to 64.29 mm. The solidification front radius of PCM at the tube inlet increased with time and it had a maximum value at the inlet of the heat exchanger and for maximum discharge period.
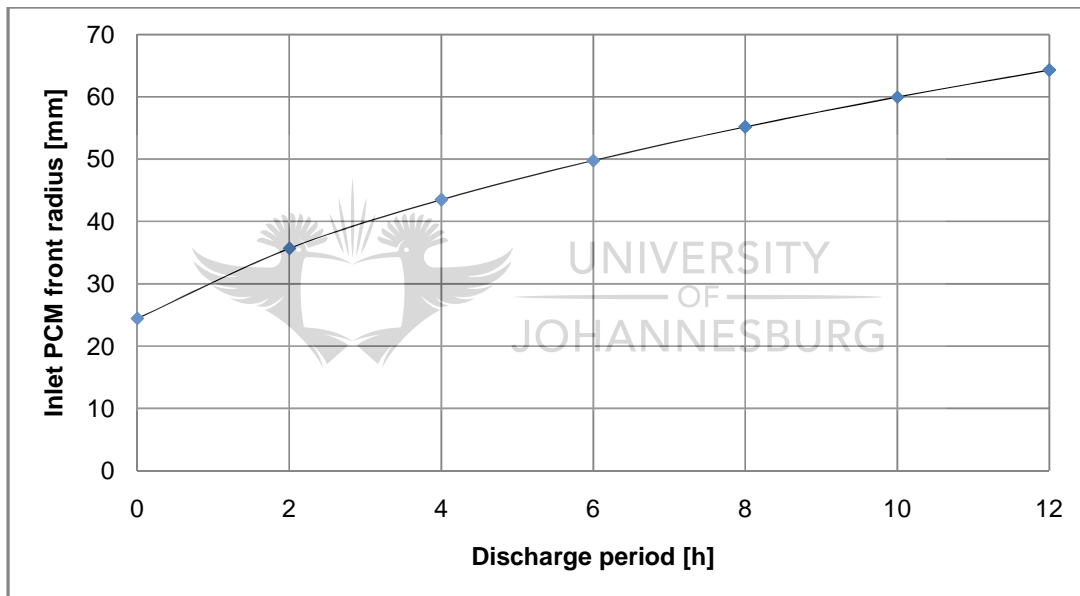
Figure 5.4a: Front solidification of PCM at the inlet tube exchanger against the discharge period

Figure 5.4b provides the variation of the fraction of PCM solidified at the tube heat exchanger inlet for different instants and positions along the tube heat exchanger.

At time t = 0 h, the solidification front radius at inlet was 24 mm, equal to 64 mm at the end of the discharge process.
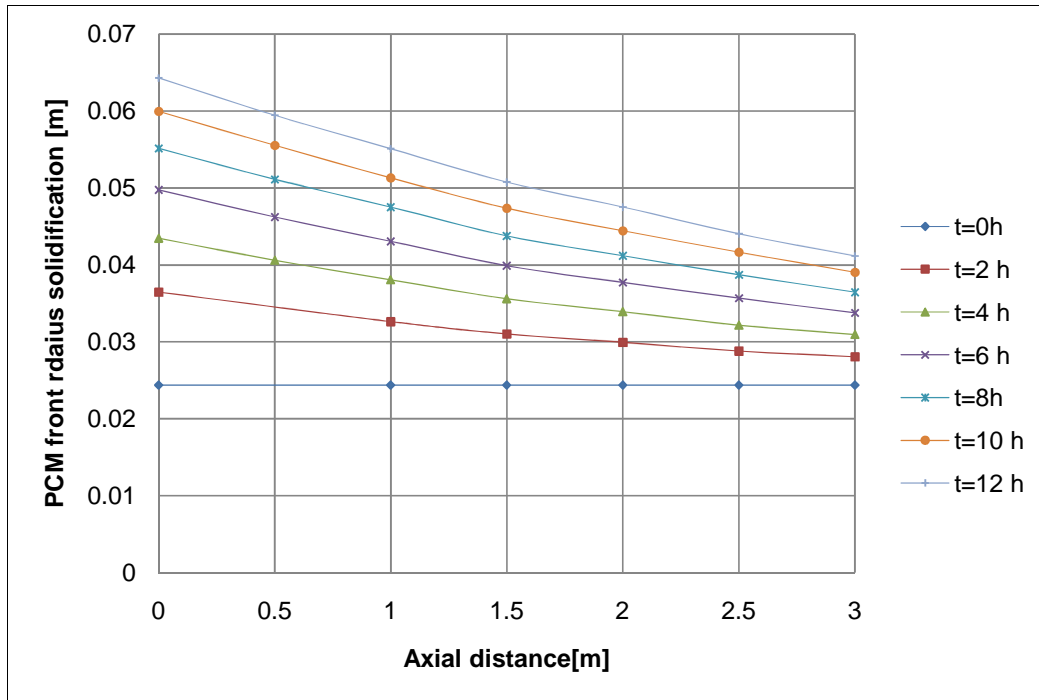
Figure 5.4b: Front solidification of the PCM as a function of the axial distance along the tube heat exchanger and the discharge period

5.5.3 Heat transfer rate

The maximum possible temperature rise of the cold fluid was from T_i to T_f.

Heat transfer rate ($\dot{Q}$) of the HTF was calculated using:

$$\dot{Q} = m_f C_p (T_f - T_i) \tag{5.2}$$

Where $\dot{m}_f$, C_p, T_f and T_i denoted the mass flow rate, specific heat capacity, the outlet and inlet temperature of fluid respectively.

The curve of heat release during the solidification process is shown in Figure 5.5. With the inlet temperature of fluid of 25°C, the heat transfer rate during solidification decreased firstly rapidly, then slowly in time. The maximum heat transfer rate was 2.63 kW and the minimum 2.35 kW, as expected from design requirements. The curve of heat transfer rate was similar to the curve of the HTF outlet temperature since the the heat transfer rate is a function of a temperature difference at the outlet and inlet of the tube heat exchanger.

67
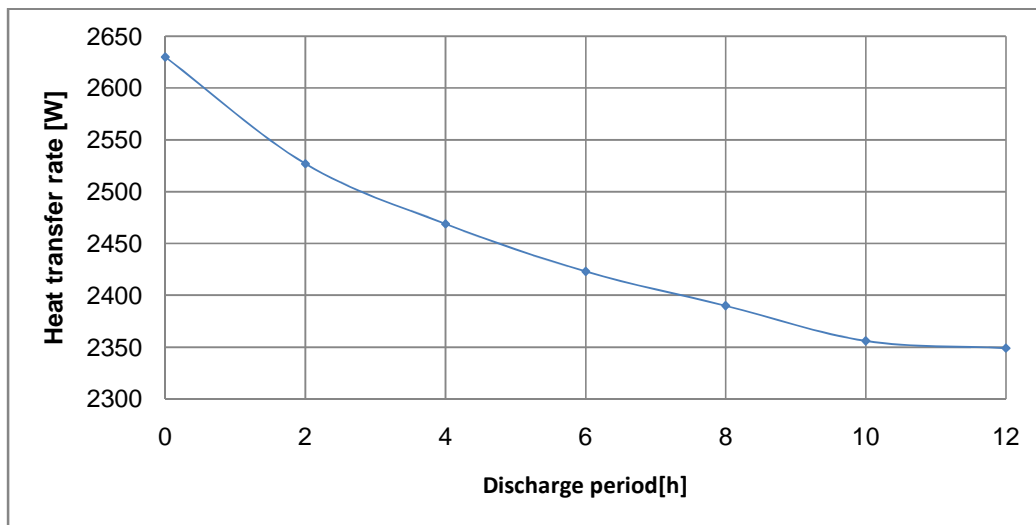
Figure 5.5: Heat transfer rate during the solidification process as a function of the discharge period

It can be seen from Figure 5.5 that the rate of heat transfer decreased rapidly to 2.5 kW. After this, the heat transfer rate showed a small decreasing slope.

5.6   Summary and conclusions

The design method explained in Chapter 4 was applied in Chapter 5. For a case study, the appropriate PCM was selected, Erythritol. The dimensions of the LHS were determined and the mass and volume of PCM estimated to supply thermal energy to the AAAR generator for the period of 12 hrs without relying on any other source than solar energy. It is to be noticed that a small variation of heat transfer rate during the discharge process from the storage unit takes place.

For 12 hrs of storing the thermal energy, the volume of PCM evaluated was 0.5 m^3. The total mass of PCM was 745 kg. The performance of the designed unit was given in terms of the outlet temperature, the front solidification of PCM and the heat transfer rate.

In Chapter 6, simulation results of the designed LHS are evaluated from Shamsundar's model and two other analytical approximations models.

Chapter 6

EVALUATION OF THE LATENT HEAT STORAGE UNIT BY OTHER ANALYTICAL MODELS

6.0   Introduction

The sizing of the LHS is presented in Chapter 4. In Chapter 5, a case study is applied to illustrate the application of the method. In Chapter 6, first the size of the LHS is determined as suggested by Shamsundar *et al.* (1992).   The simulation of the outlet temperature of the HTF, fraction of solidified PCM formed at the tube heat exchanger and heat transfer rate at the outlet of the heat exchanger are presented from Shamsundar's model and other two analytical methods.

The results obtained in Chapter 6 are compared in Chapter 7 against the results provided by the method derived in Chapter 4.

Two analytical methods used to compare the results in addition to the method suggested by Shamsundar *et al.* (1992) are:

- The first method applied by Kang *et al.* (1999) and Long Jian Yu (2008) described in **Appendix J.1**. This method is referred to as "Yu's method". The phase change problem of the PCM filling the annular of the shell side and a flowing HTF inside an inner tube was solved by means of "Yu method". Test experimental results done by Long Jian Yu (2008) showed a good agreement between the numerical and the experimental results.

    The method takes into account the tube thermal resistance. Efficiency of the LHS was considered 100%.

- The second method is briefly described in **Appendix J.2** and it is referred to as "Solomon's' method" (Alexiades and Solomon, 1993). This method did not consider the thermal resistance in the PCM, tube and HTF. It may be considered as the extreme worst scenario where the heat transfer analysis during the melting process was over simplified.

6.1   Sizing of the Latent Heat Storage unit

Results in sizing the LHS from Shamsundar's method are provided in (**APPENDIX I.1** and **Appendix I.2**) for the same design requirements as provided in Chapter 5. Dimensions were obtained from the design model provided in **Appendix I.2.**

Table 6.1: Specifications of the LHS

PCM SELECTED	ERYTHRITOL
MELTING POINT	118^oC
LATENT HEAT OF FUSION	339.8kJ/kg
HEAT TRANSFER FLUID	DURATHERM XLT-50
TUBE MATERIAL	COPPER
INLET TEMPERATURE FLUID	25^oC
MASS FLOW RATE	0.017 kg/s
FLUID MAXIMUM OUTLET TEMPERATURE	97^oC
FLUID MINIMUM INLET TEMPERATURE	89^oC
OUTSIDE RADIUS OF TUBE	20mm
INSIDE RADIUS OF TUBE	18mm
LENGTH OF TUBE	3 m
NUMBER OF TUBES	14
TANK DIAMETER	0.475 m
TANK VOLUME	$0.53 \, m^3$
VOLUME OF PCM	$0.51 \, m^3$
STORAGE PERIOD	12 h
MASS OF THE PCM	741 kg

6.2   Determination of thermal parameters of Latent Heat Storage unit

Simulations of the LHS are given in terms of the HTF temperature distribution, HTF outlet temperature at the inlet shell-and-tube heat exchanger, front solidification of the PCM and heat transfer rate during the solidification phase. Results were obtained for three analytical models: Shamsundar, Yu and Solomon.

As it was considered in Chapter 5, the inlet temperature of the HTF (Duratherm-XLT 50) was considered constant and equal to 25^oC.

6.2.1 HTF temperature distribution

Figure 6.1 shows the temperature distribution of Erythritol using Shamsundar's model during the discharge period (12hrs). The inlet temperature of Duratherm XLT-50 was 25°C and at the outlet heat exchanger the temperature fluid varied between a maximum of 97°C and a minimum of 87°C. The results are related to the discharge process when the PCM released thermal energy and there was a change in the phase from liquid to solid.
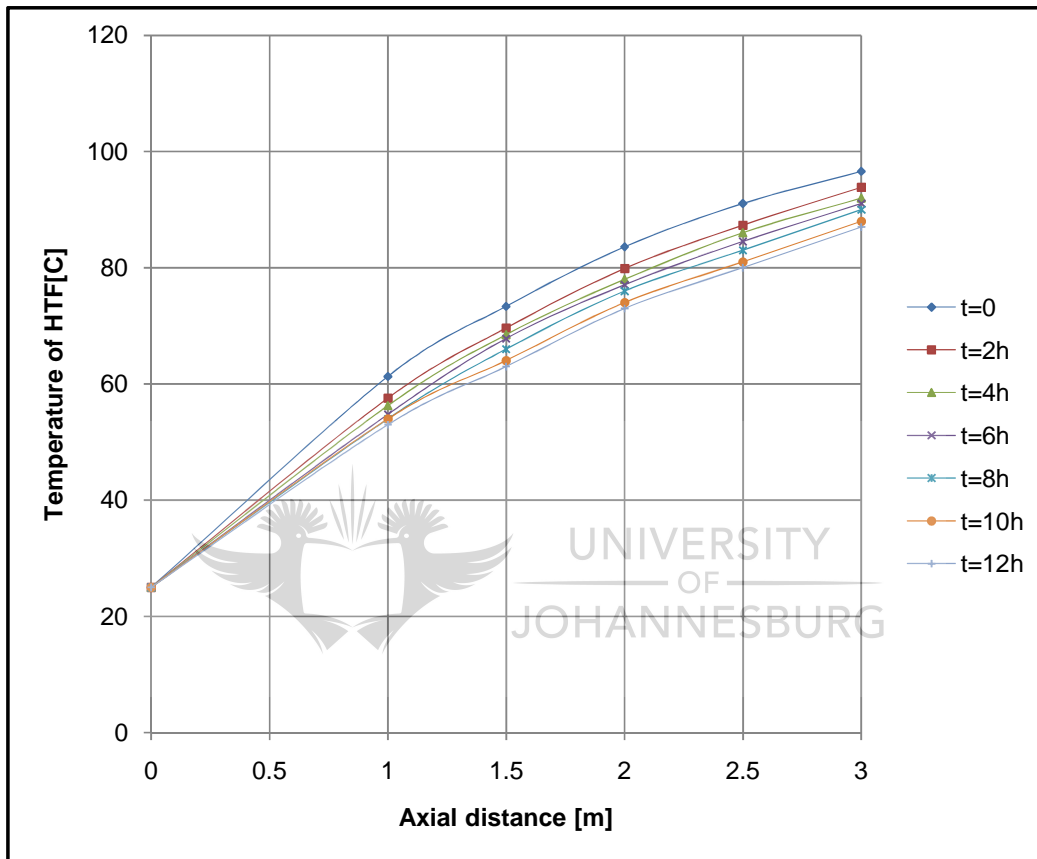
Figure 6.1: Temperature distribution of Duratherm XLT-50 versus the axial distance along the tube heat exchanger for different periods

In Figure 6.2 the temperature distribution of HTF was obtained from Yu's model. The temperature increased from 25°C at inlet up to the maximum 98°C at the outlet. The minimum temperature, calculated by means of this model at 12 hrs was 94°C.

Equations leading to this graph are given in Yu's model (**Appendix J.1**).
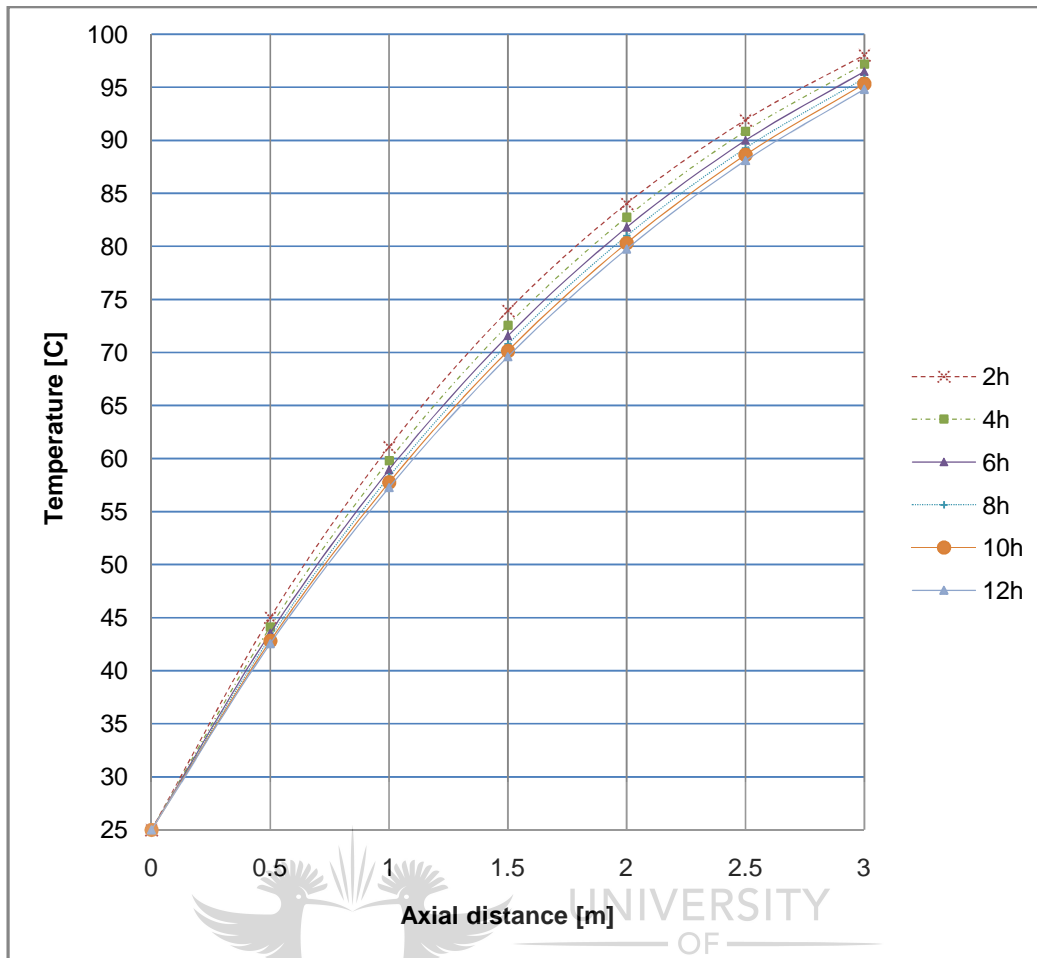
Figure 6.2: Temperature distribution of Duratherm XL-50 versus the axial distance of the heat exchanger (Yu's model)

The variations in HTF flowing inside the tube exchanger were plotted using different positions along the tube heat exchanger and for different periods (Figure 6.2). The inlet HTF was assumed to be constant and equal to $25^{o}C$. HTF outlet temperatures at different instants were obtained. The maximum outlet temperature HTF according to this model was $98^{o}C$; the minimum was $95^{o}C$.

In Figure 6.2, the HTF variation temperature was given as a function of the discharge period and axial distance along the tube heat exchanger.

The length of the tube heat exchanger was 3 m. The inlet temperature of HTF was a constant and equal to $25^{o}C$, for x = 0 m and at the outlet of heat exchanger the temperature varies for different periods of time from $98^{o}C$ to $94^{o}C$.

HTF temperature distribution (Duratherm XLT-50) according to Solomon model given in **Appendix J.2** provides one curve only (Figure 6.3). The inlet temperature entered the tube at $25^{o}C$ and exited the tube heat exchanger at $99^{o}C$. Figure 6.3 showed the variation of the HTF in the LHS as a function of the axial distance along the tube heat exchanger.
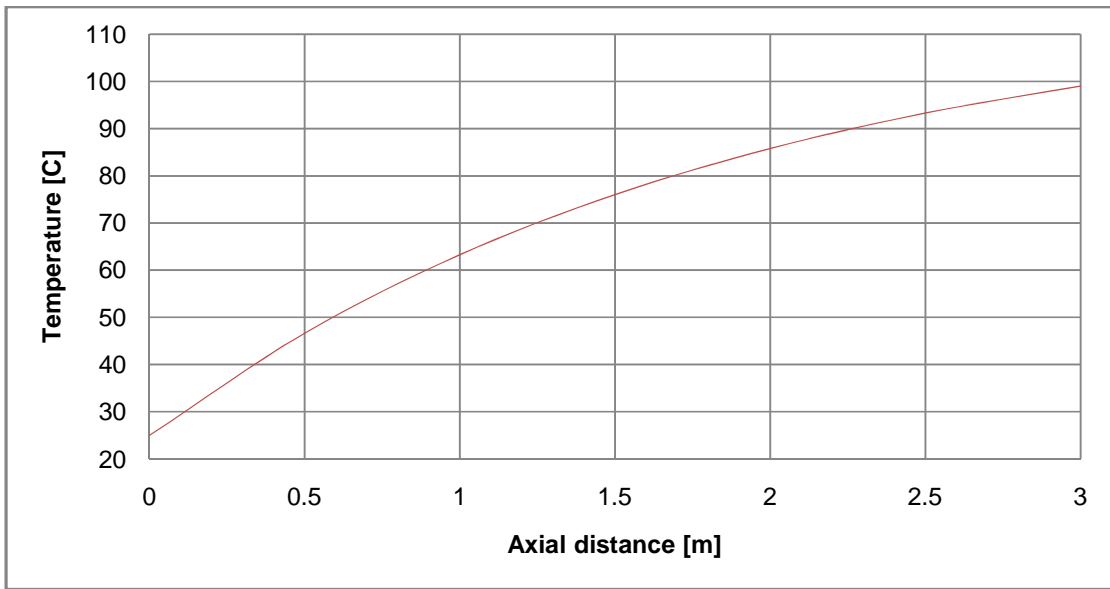
Figure 6.3: Heat transfer temperature distribution versus axial distance of the latent heat exchanger (Solomon's model)

In Figure 6.3, the quasi approximation analytical method was applied. According to, "Solomon's method", the temperature distribution of HTF was only a function of the axial distance x. It was observed that the HTF at the inlet was 25°C and the outlet temperature was equal to 97°C at the exit 3 m of the heat exchanger.

6.2.2 HTF outlet temperature

Different curves were plotted for the HTF outlet temperature from the heat exchanger. They were obtained from Shamsundar's model (Figure 6.4) and Yu's model (Figure 6.5).
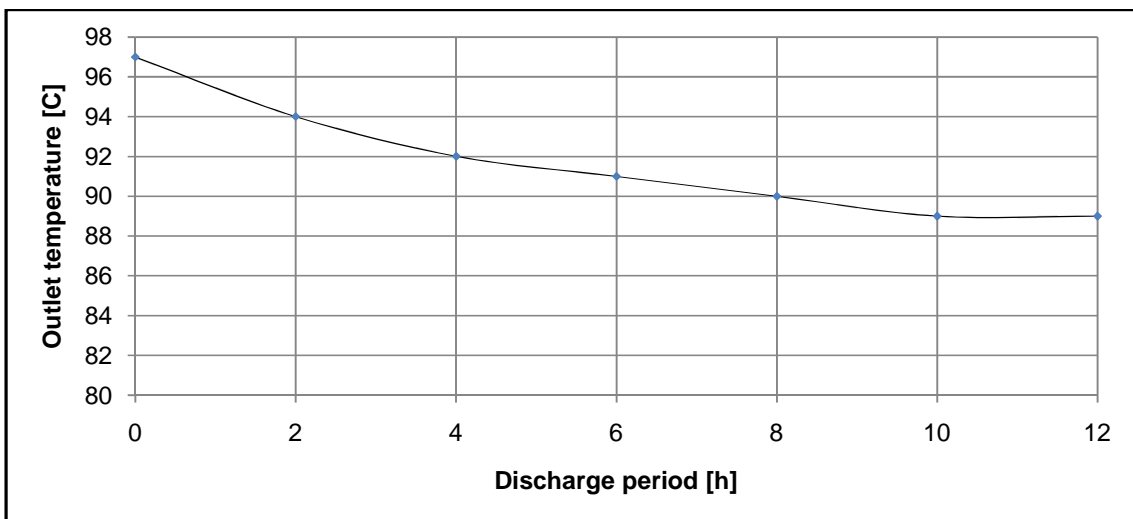
Figure 6.4: HTF outlet temperature versus the discharge period (Shamsundar's model)
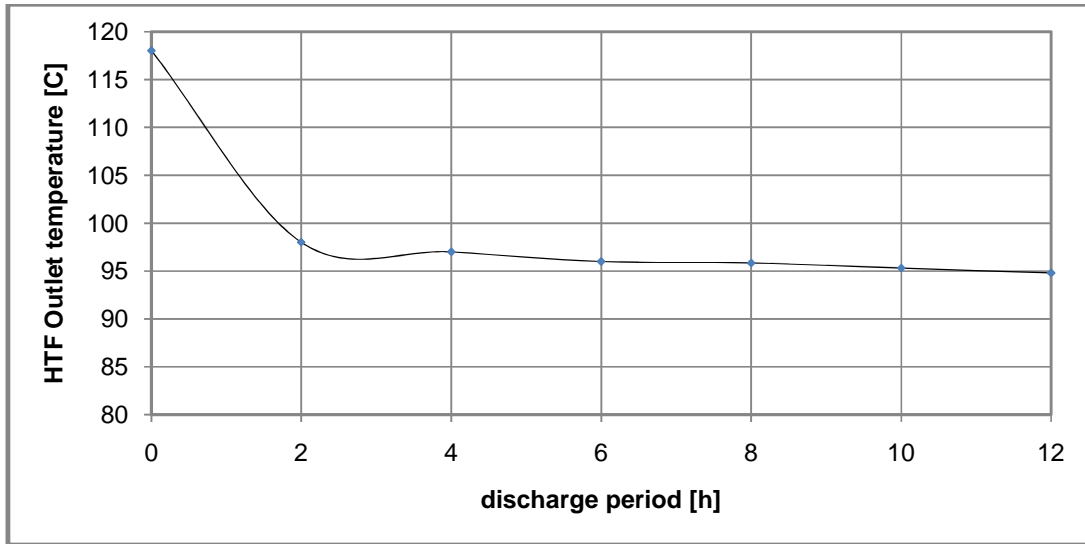
Figure 6.5: HTF outlet temperature versus the discharge period (Yu's model)

6.2.3 The front radius solidification of the PCM in the heat exchanger

The front radius solidification of the PCM was determined from the Equation 6.2. In Figure 6.6, the front radius solidification was given as a function of time and varied between the minimum of 20 mm and the maximum of 59 mm.   Results were calculated from the model given in **Appendix I.2** and for the dimensions provided in Table 6.1. It can be observed the front radius started exactly at the outer radius of the tube which is 20 mm.

The amount of fraction of PCM formed at the inlet and for the maximum period of 12 hrs was 59 mm according to Yu's method (Figure 6.6). The outer radius of the tube was 24 mm which corresponded to the minimum front radius at the inlet and for the time t = 0 h.
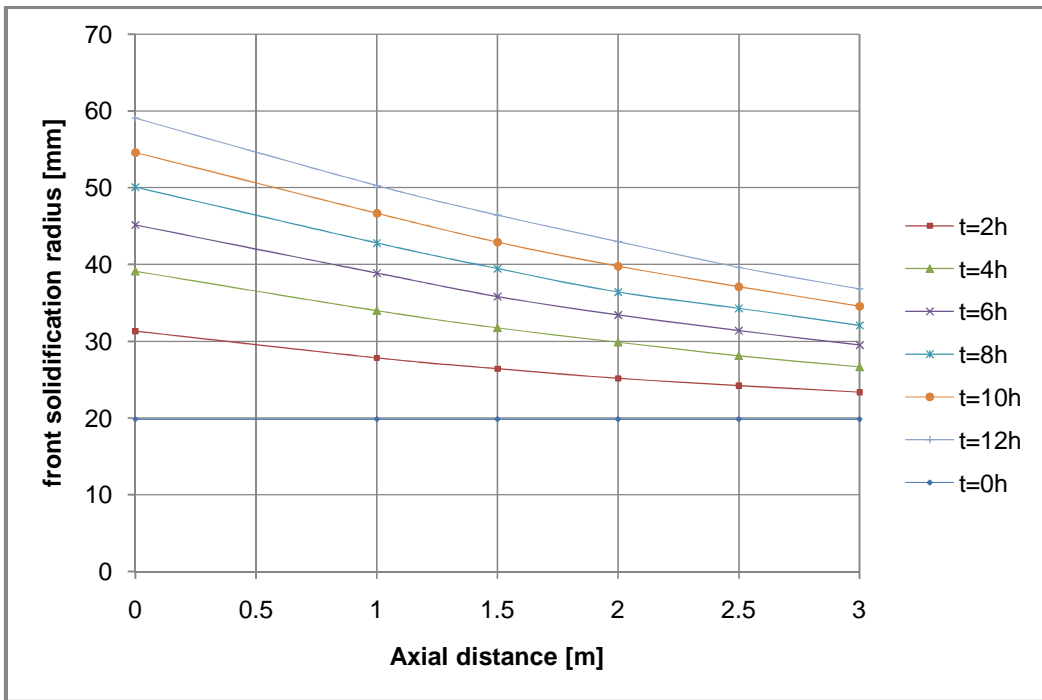
Figure 6.6: Front solidification versus axial distance of the tube heat exchanger and the discharge period (Shamsundar's model)
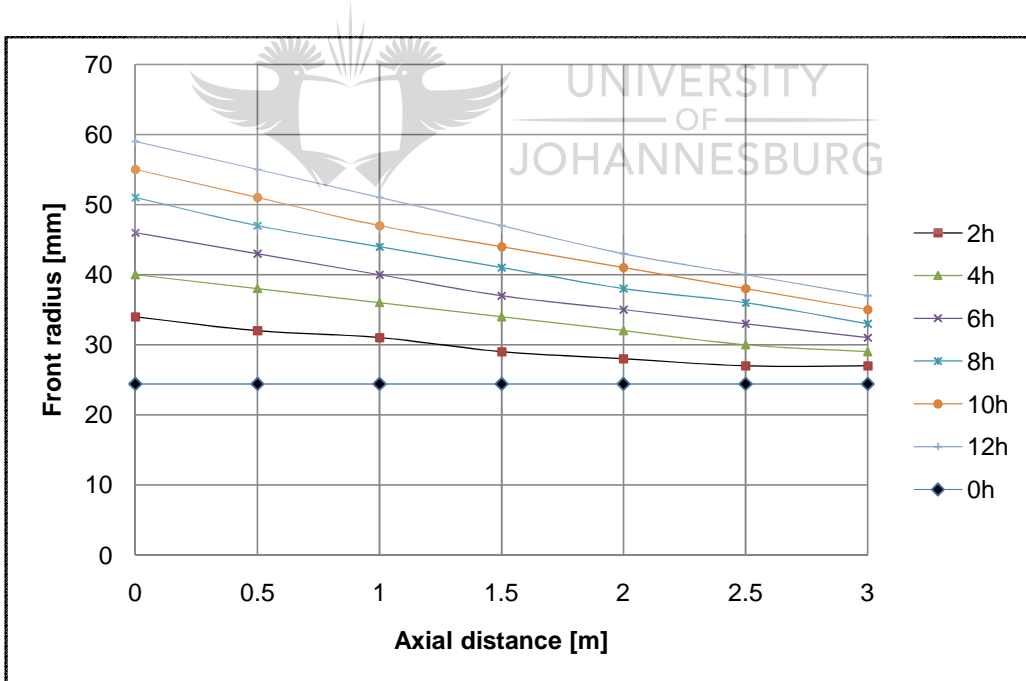
Figure 6.7: Front solidification of the PCM against the discharge period and for different axial position along the tube heat exchanger (Yu's model)

In Figure 6.7, the solidification front was plotted according to "Yu's method". The front solidification of the PCM given as a function of the axial distanceand for different periods during the discharge process showed at the inlet of the LHS had a greater amount of PCM solidified compared to the heat exchanger outlet. At the beginning of the process, the

solidifcation front radius was constant along the tube heat exchanger and was equal to 24 mm, which corresponds to the outer radius size of the tube wall. It increased with the factor time at inlet, but decreased along the tube heat exchanger for different instants. The maximum front solidification obtained using Yu's model was 59 mm.

The front radius solification of the PCM estimated from Solomon's model was provided in Figure 6.8. The minimum front radius was 24 mm, the maximum 66 mm at the inlet of the tube heat exchanger.
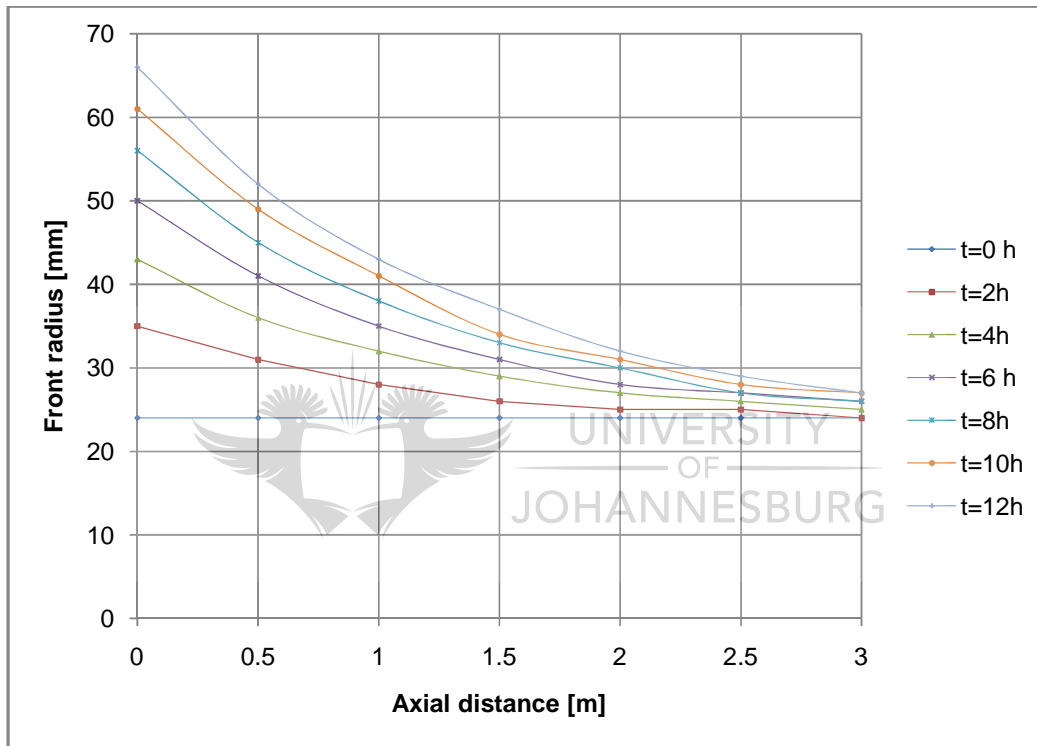
Figure 6.8: Front solidification of the PCM versus axial distance of the tube heat exchanger (Solomon's model)

Result of solidification front radius at the inlet of the latent heat exchanger according to "Solomon's method" was plotted in Figure 6.8. The inlet radius of the front solidification at the beginning of the discharge process corresponds to the value of 24 mm. It coincided exactly with the outer radius of the tube. The front solidification increased with time. At the end of the discharge period (12hrs), the maximum solidification front radius reached the magnitude of 66 mm at the inlet of the tube heat exchanger.

Figure 6.9 shows the front radius solidification at the inlet of the tube heat exchanger as a function of the discharge period. The result was obtained from Shamsundar's model.
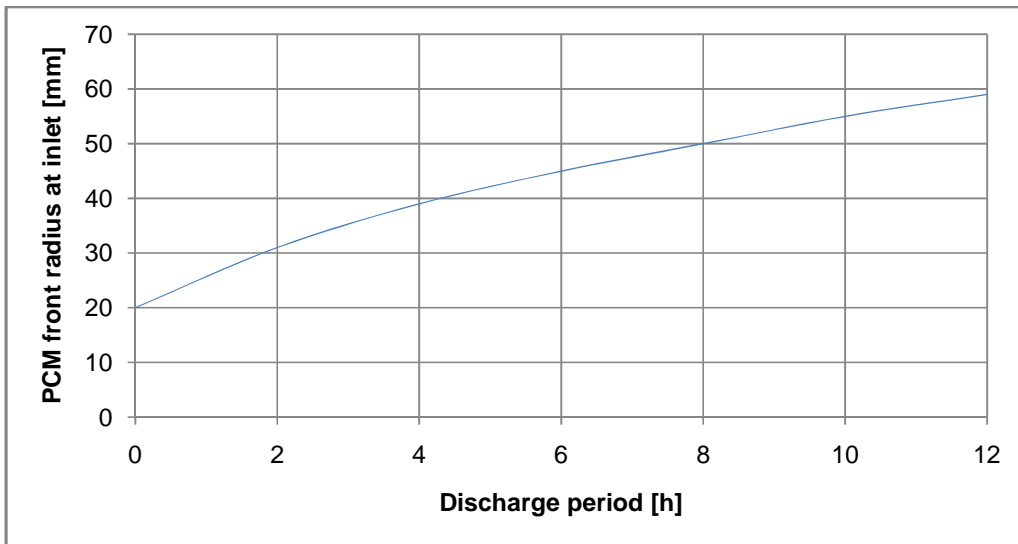
Figure 6.9: Fraction of PCM solidified at the tube inlet as function of the discharge period

Figure 6.9 shows the fraction of solidified PCM at the inlet tube heat exchanger versus the discharge period as estimated from Yu's model.
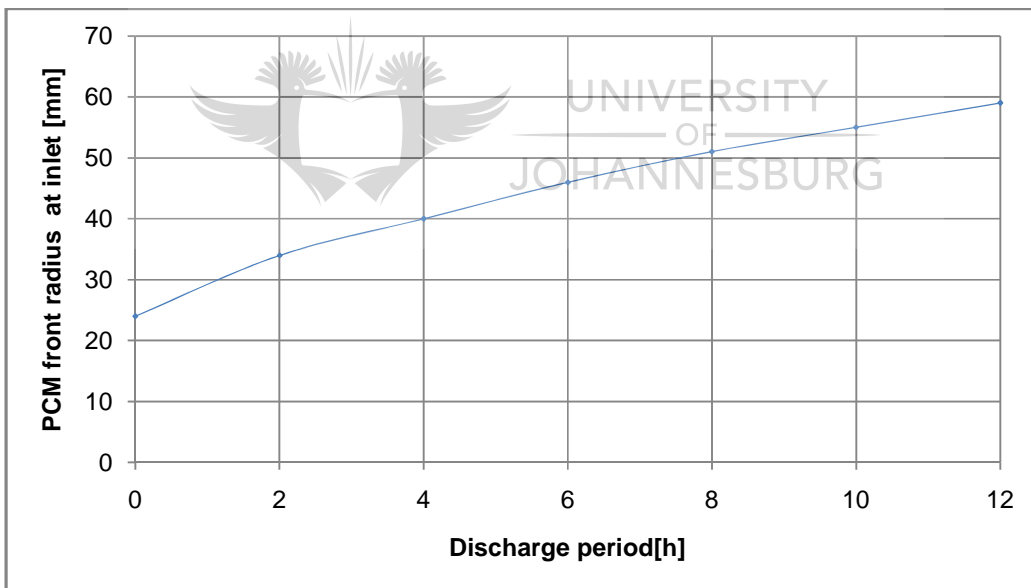
Figure 6.10: Fraction of the solidified PCM at the inlet tube heat exchanger versus the discharge period (Yu's model)

6.3 Heat transfer rate during the solidification process

Using Equation 4.27, the heat transfer rate was represented in Figure 6.11 by a curve that began at 2.65 kW and at the end of the discharge period the heat transfer rate period coincided with the value 2.35 kW, which was expected from the outlet heat exchanger as required from the design conditions.

Figure 6.11 was obtained for Shamsundar's model; the heat transfer rate was given as a function of the discharge period.
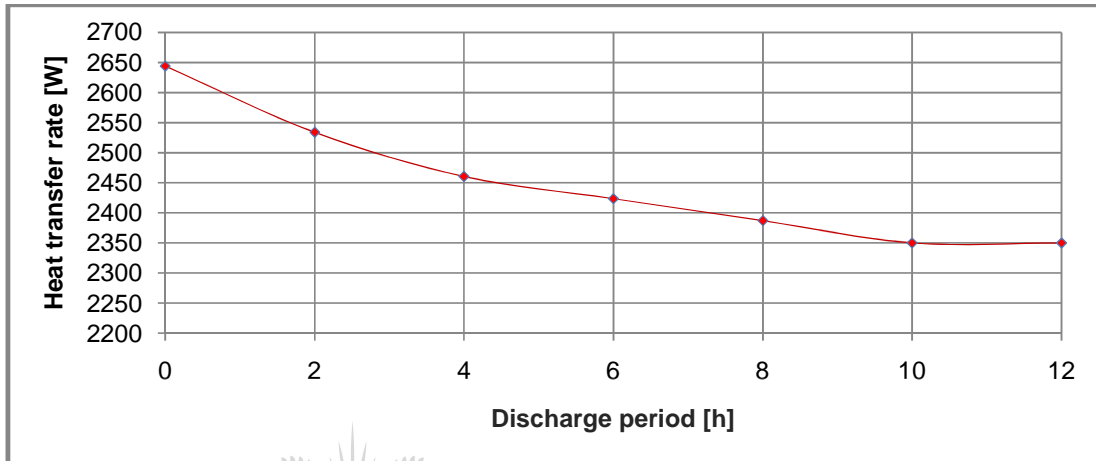
Figure 6.11: Heat transfer rate during the solidification against the discharge period (Shamsundar's model)

Figure 6.12 shows the heat transfer rate using Yu's model. The maximum heat transfer rate obtained from this model is 3.5 kW; minimum 2.56 kW.
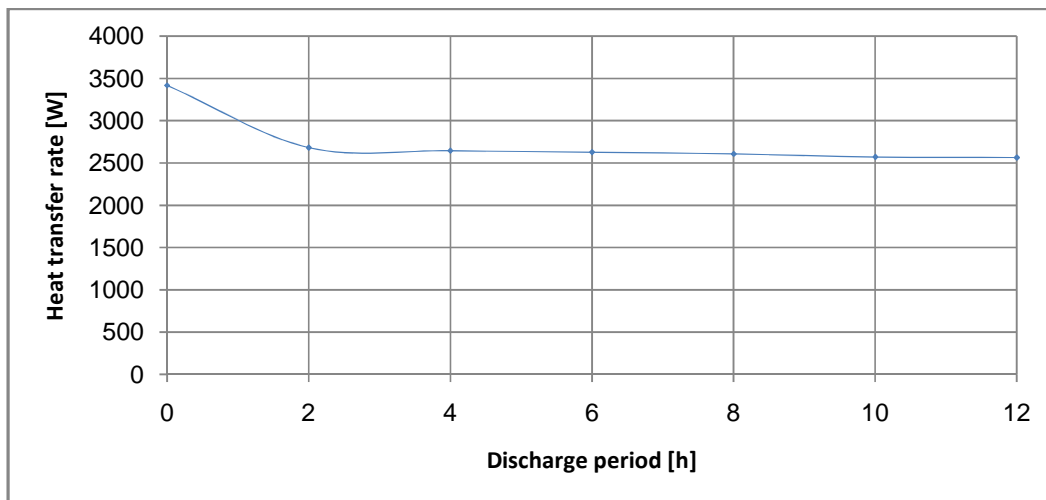
Figure 6.12: Heat transfer rate during the solidification versus the discharge period (Yu's model)

6.4   Summary and conclusions

Chapter 6 essentially focuses first on the results of the sizing of the LHS using method suggested by Shamsundar. The dimensions were obtained assuming the same design requirements in the case study in Chapter 5 for the model as suggested by Shamsundar *et al.* (1992). Simulations were carried out using the models of Yu and Salomon.

Simulation results were given for:

- HTF distribution against the time and the axial distance of the tube heat exchanger;
- HTF outlet temperature versus the discharge period;
- Fraction of the PCM solidified along the tube heat exchanger and at the inlet of the heat exchanger; and
- Heat transfer rate during solidification.

The maximum of the fraction PCM solidified at the inlet is found to be greater compared to the results at the outlet of the heat exchanger for all the models. Shamsundar's model was applied for the sizing of the LHS and simulation of the thermal parameters, other two models were used namely Yu's model and Solomon's model to obtain simulation of the thermal parameters. Results indicate identical trends.

Those results are compared in the next chapter against those obtained from the model proposed in Chapter 4 for the case study applied in Chapter 5.
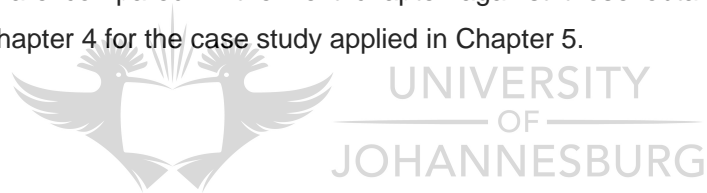
Chapter 7

DISCUSSIONS OF RESULTS

7.1   Introduction

In Chapter 7, the results of the model developed and solved in Chapters 3 and 4 are compared against results from other models in order to validate the results obtained in Chapter 5.

7.2   Comparison of results

7.2.1 Sizing of the LHS

Table 5.3 and Table 6.1 summarised the sizing by the two methods: Shamsundar (**Appendix I.1**) and the model derived in Chapter 4 (modification of Shamsundar's model). For the same requirements of design, the outer radius was 20 mm and the inner radius 18 mm of the tube heat exchanger. The number of heat exchanger tubes in the LHS was found equal to 14 and the mass of the PCM was calculated and found equal to 741 kg by using the design method suggested by Shamsundar *et al.* (1992). It was found that results obtained by using the modified method suggested in Chapter 4 differed slightly: The outer and inner radius were respectively 24 mm and 21 mm. The number of tubes heat exchanger in the LHS required was 13 and the mass of the PCM obtained became 745 kg.

The main reason for the difference in sizing from the two design approaches was that both design methods depend on the value of the fraction of the PCM solidified at the inlet of the tube heat exchanger for the entire discharge period F_0.

It was noticed the two transcendental equations for the two models differed slightly as indicated in Chapters 3 and 4. From Shamsundar's model, the value of $F_0 = 7.9$ and by using the modification Shamsundar's model as obtained in Chapter 4, $F_0 = 5.9$. The dimensionless time τ was determined from the value of F_0. Having the value of τ, the outer radius R_0 of the tube heat exchanger could be evaluated from Equation 4.15.

The volume and the mass of the PCM in the LHS were a function of the outer radius R_o. The greater the value of the fraction of the PCM solidified at the inlet of the tube heat exchanger (Shamsundar's model), the greater the value of the dimensionless time τ. As a result, the outer radius has a lower value. Therefore the volume and the mass of the PCM were also lower compared with the modification Shamsundar's model. That is the reason why the mass of PCM obtained from the modification method as suggested in Chapter 4 is greater than the mass of PCM calculated from Shamsundar's model.

The ratio of the tube radius was fixed and had the value of 1.15. The thermal conductivity of the tube material was considered in the modification Shamsundar's method and the thermal resistance for the tube material taken into account. It was found that the choice of tube material had an effect on the size of the LHS: The size of the LHS increased if thermal resistance for the tube was considered. **Appendix E.1** gives the thermal conductivity of the material used in the design of heat exchanger.

For instance, by taking a material such as cupro-nickel for the tube material heat exchanger with thermal conductivity equal to 29 W/m.K, the sizing of the LHS, using the modified method, provided the outer radius equal to 26 mm, the inner radius equal to 22 mm ; the mass of the PCM obtained was 751 kg.

It was concluded using thermal resistance of the tube material in the design affected the sizing of the LHS.

7.2.2 HTF Temperature distribution

The HTF temperature distribution obtained from the modified Shamsundar's model and other analytical models were compared.

Figure 5.4, Figure 6.1, Figure 6.2 and Figure 6.3 showed HTF temperature distribution as obtained from respectively the modified, Shamsundar, Yu and Solomon models. The first three indicated a similar trend. The inlet temperature of HTF began at 25°C and decreased in time. It was also noticed the temperatures along the tube heat exchanger decrease. Solomon's model provided only one curve for HTF. According to Solomon's model, the temperatures estimated were a function of time and remained constant for the same position along the tube heat exchanger.

7.2.3 HTF outlet temperature

The outlet temperature curves of the HTF from the latent heat exchanger shell-and-tube for the modified, Shamsundar's and Yu's method were plotted in Figure 5.3, Figure 6.4 and Figure 6.5.

The modified and Shamsundar's method began at 97°C as the outlet temperature from the heat exchanger at time t =0 h; Yu's method began the discharge process with an initial condition fixed at 25°C, the outlet temperature at 118°C. At the end of the process with Yu's method the outlet temperature of the HTF was 95°C; with the modified, and Shamsundar's models, 89°C. According to Yu's model, the initial condition of the temperature of HTF at t = 0 and for any position along the tube heat exchanger was equal to the melting temperature of

the PCM selected, namely Erythritol, at 118°C. The efficiency of the latent heat exchanger was taken in the calculation of both modified and Shamsundar's methods.
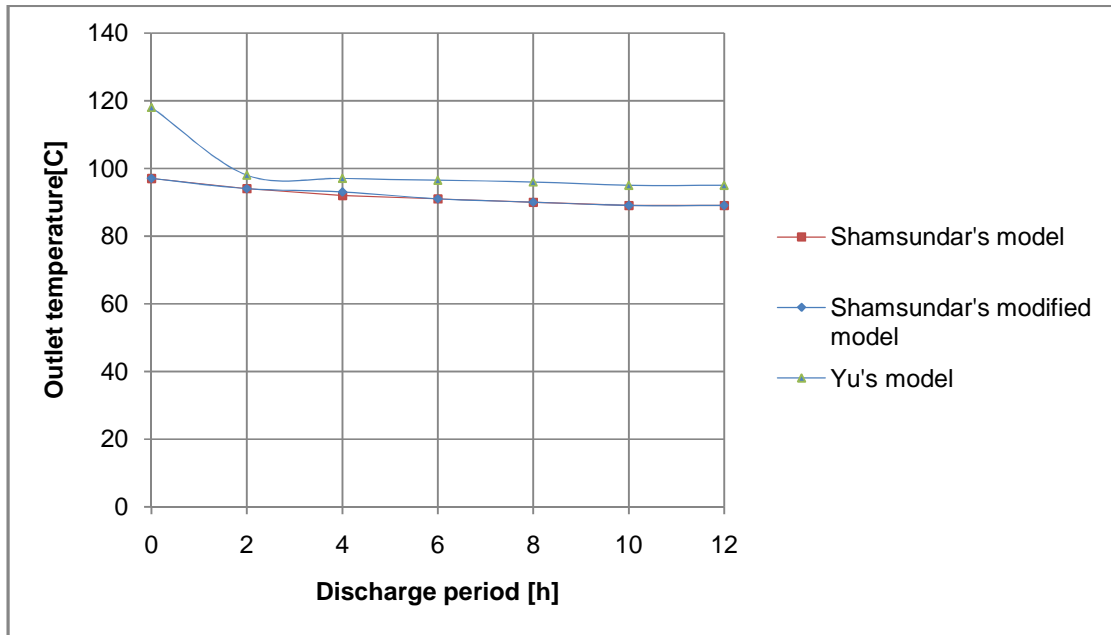
Figure 7.1: HTF outlet temperature against the discharge period for different models

Modified and Shamsundar's model gave similar results as it can be seen in Figure 7.1. Yu's model was slightly different because of the initial conditions and efficiency of the heat exchanger. Yu's model provided outlet temperature equal to the melting point at the beginning of the discharge process; Shamsundar's model provided a maximum temperature 97°C. That was the maximum temperature expected at the outlet of the heat exchanger at the beginning of the discharge process. When the discharge period was over (12 hrs) for this case study, the minimum temperature obtained was respectively 89°C and 95°C for Shamsundar's and Yu's models. The three analytical models provided a minimum temperature as estimated at the outlet heat exchanger for the discharge period 12 hrs. Solomon's model provides a fixed temperature of 99°C at the outlet of the heat exchanger, Yu's model a slightly high temperature. The reason was Yu's model did not take into account the minimum efficiency of the LHS as in Shamsundar's model. It was concluded that from the heat transfer point of view, the thermal resistance of conduction of the tube wall heat exchanger does not affect heat transfer if the tube material has a high value of thermal conductivity.

7.2.4 Front solidification of the PCM

The front solidifications obtained from different models were compared. The comparison consisted only on the amount of fraction of solid formed at the inlet of the tube heat

exchanger. At this level of the heat exchanger, a maximum amount of solidified PCM was obtained when the discharge period was reached.

Figure 7.2 indicates the variation of the front solidification of the PCM as a function of time.
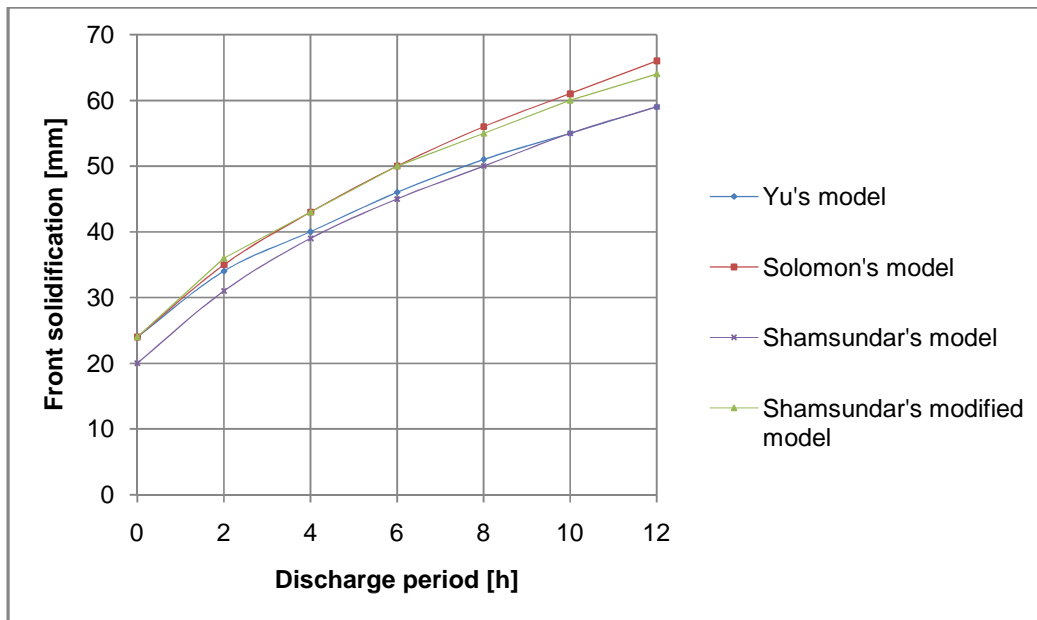
Figure 7.2: Front solidification of PCM against the discharge period for different analytical models

Shamsundar's model began with front solidification of 20 mm. Since the front radius at the beginning of the process and at the inlet of the heat exchanger coincided in the modified and Shamsundar's model to the outer radius of the tube wall heat exchanger, the values of 20 mm and for other 24 mm were obtained for modified and Shamsundar's model respectively. That was why the curves start with different values namely 20 and 24 mm.

The difference in terms of solidification front of Yu's, Solomon's and modified models was small as shown in Fig. 7.2. They all began at 24 mm; at the end of the discharge process, Shamsundar's model provided the front solidification equal to 64 mm; Solomon's method provided 66mm and Yu's value for solidification front was 59 mm.

7.2.5 Heat transfer rate during solidification of the PCM

The heat transfer rate during the solidification process depended on mass flow rate, the specific heat of the HT and the temperature difference at the outlet and inlet of HTF. The inlet temperature of Duratherm XLT-50 was fixed at 25°C, the heat transfer rate for the different analytical models followed the same path as the HTF outlet temperature.

Figure 7.3 showed the heat transfer rate for Shamsundar's, Shamsundar's modified and Yu's model.
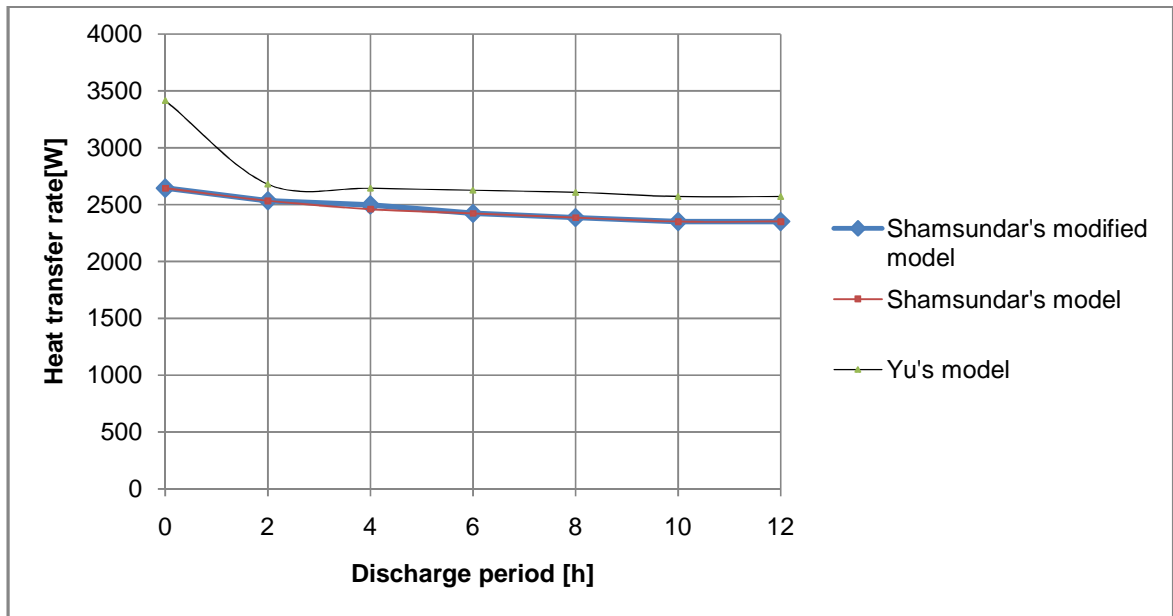
Figure 7.3: Heat transfer rate during the solidification process for different models

7.3   Summary and conclusions

In Chapter 7, the results obtained for the shell-and-tube latent heat exchanger were calculated. The results otained from the derived model were compared against other analytical models. The comparison of the model derived and other models indicated a similar trend in terms of the outlet temperature expected at the heat exchanger. Maximum temperature was 97°C, minimum 89°C. The solidification front radius varied between a minimum of 20 mm and a maximum 66 mm.

The thermal properties of the tube material heat exchanger in the LHS were found to have a slightly effect on the sizing of the LHS and the heat transfer process.

Chapter 8

CONCLUSIONS AND RECOMMENDATIONS

8.1   Conclusions

A preliminary design of the LHS for an AAAR was proposed in this project.

Shell-and-tube was selected as the best configuration heat exchanger. It stores thermal energy by means of a PCM filling the space outside the tube heat exchanger. A HTF flowing through the tube heat exchangers exchange the thermal energy with the PCM.

Criteria to select an appropriate PCM for a given heating application were indicated. HTF had to be selected according to the desired parameters.

An analytical thermal modelling of the LHS was derived based on the model suggested by Shamsundar *et al*. (1992). In this derivation, the thermal resistance and the thermal conductivity of the tube wall were taken into consideration.

The solution of the proposed model was given as a function of dimensionless parameter F, which is the fraction of solidified PCM during the discharge process along the tube heat exchanger. Shamsundar's method was modified as the thermal resistance of the tube was considered in the derivation of the model.

Analytical model was used to determine key design parameters of the latent shell-and-tube heat exchanger. The method used to size the LHS unit gave the preliminary results of the shell-and-tube heat exchanger filled with the PCM in the shell and a flowing HTF in the tube system. The performance of the LHS was also indicated.

For the case study investigated in Chapter 5, Erythritol was selected as storage material. Erythritol emerged as the most suitable for its high latent heat of fusion compared to other potential PCM candidates. Its melting point is 118°C. The maximum desired temperature at the AAAR generator was 97°C.

Kakuichi *et al*. (1998) predicted the degradation of only 10% of Erythritol even if used for about eight years for continuation heating. It is non-toxic and easily available.

HTF was also selected for its long-term operation and other relevant properties. For this study, the HTF selected was Duratherm XLT-50.

To determine the dimension of a LHS with reference to solar absorption refrigeration, two design methods were applied to size the LHS: Shamsundar and the modification method of Shamsundar. They provided a difference results in PCM mass of 2%.

The outlet temperature distribution, the solidification front radius and the heat transfer rate were calculated during the heat recovery process or the discharge cycle.

From a thermal point of view, results obtained from Shamsundar's and Shamsundar's modified were almost identical. Considering other models (Yu and Solomon), results differed essentially because of initial conditions and the efficiency of the storage system, but the trends and the results were in the range desired for the AAAR generator (the HTF outlet temperature, front solidification and heat transfer rate).

It was concluded the modification of the model and design method did not affect the thermal behaviour of the system but the dimension of the LHS, as proposed, differed slightly from the design method suggested by Shamsundar *et al.* (1992).

8.2   Proposals for Further Research

Developing an understanding in the phase change process is a complex procedure as the experiment, observation; model building and analysis are involved. Therefore, there is a need to complete this theoretical project by building a storage unit and comparing the experimental results with the theoretical results obtained in this study.

A drawback in Erythritol is its low thermal conductivity. Several means of improving this heat conductivity needs to be explored such, as the utilisation of fins into the heat exchanger surface of the tube to increase effectiveness of the latent shell-and-tube heat exchanger.

There is a need also to optimise the size of the LHS. This should include the determination of the cost-effectiveness of the design.

It is recommended that future investigation focuses on the areas of optimisation of heat transfer modelling studies, heat conduction enhancement, long term testing of the unit and integrated the storage system designed in the absorption refrigeration machine to evaluate the performance of the entire thermal system (solar collector, storage unit and cooling cycle), to improve the sizing and the performance of the latent shell-and-tube heat exchanger.

REFERENCES

Adeyanyu, A.A. and Manohar, K. (2009). Theoretical and experimental investigation of heat transfer in packed beds. Res.J.Applied Sci, 4:166-177.

Agyenim, F. (2009). Solar air conditioning and the need for energy storage for meeting domestic cooling. http://www.Hvacteachers.org/documents/Solar-Airconditioning. Accessed 12/05/2009.

Agyenim, F., Hewitt, N., Eames, P. and Smyth, M. (2010). A review of materials, heat transfer and phase change problem formulation for latent heat thermal energy storage systems (LHTESS). Renewable and Sustainable Energy Reviews, 14(2): 615-628.

Agyenim, F., Knight, I. and Rhodes,M.(2007). The use of Phase Change Material (PCM) to improve the Coefficient Of Performance of a chiller for meeting domestic cooling in Wales. Second PALENC Conference and 28th AIVC conference in building low energy cooling Advanced ventilation Technologies in the 21st century, September 2007, Crete Island , Greece.

Ajib, S. (2009). Solar thermal energy for drive absorption refrigeration machines in the range of small cold capacities, possibilities and prospective. GCREADER. Jordan.

Agyenim, F., Knight, I.and Rhodes, M. (2010). Design and experimental testing of the performance of an outdoor LiBr/H2O solar thermal absorption cooling system with a cold store. Solar Energy, 84(5): 735-744.

Alexiades, V. and Solomon A.D. (1993). Mathematical modeling of melting and freezing process. Washington,DC: Hemisphere Publishing Corporation.

Anon. (2008) PDC solar. Bringing energy home. http://www.pdcsolar.co.za. Accessed 3/01/2008.

Anon. (2008). Copper Tubes-ASTMB 88M. http:// www.EngineeringToolbox.com. Accessed 5/01/2008

Anon (2009). Duratherm extended life fluid. http://www.heat-transfer-fluid.com. Accessed 8/02/2009

Bajnoczy, G. (1999). Heat storage by two grade Phase Change Material. Periodica Polytecinica Ser Chem Eng, 43(2):137–47.

Bansal, N.K, Buddhi, D. (1992). An analytical study of a Latent Heat Storage system in a cylinder. Solar Energy, 33(4):235–242.

Bellecci, C.and Conti, M. (1993). Phase change thermal storage: transient behaviour analysis of a solar receiver/storage module using the enthalpy method. International Journal of Heat and Mass Transfer, 36(8): 2157-2163.

Buddhi, D., Sahoo, L.K. (1997). Solar cooker with Latent Heat Storage design and experimental testing.Energy Convers. Manage, 38(5):493-501.

Carslaw,H.S. and Jaeger,J.C.(1959). Conduction of heat in solids. London:Clarendon Press, Oxford.

Cengel, Y. (1997). Heat transfer: a practical approach. New York: Mc Graw-Hill.

Chikukwa, A. (2007). Modelling of a solar stove: small scale concentrating system with heat storage (potential for cooking in rural areas, Zimbabwe).Doctoral thesis. Norwegian University of Sciences and Technology.

Chwieduk, D.A. (1999). Analysis of using renewable heat source heat pumps in Poland. Abstract submitted to the ISES 99, solar world congress, Jerusalem.

Darling D., (2008). The encyclopaedia of alternative energy and sustainable living. http://www.daviddarling.info/encyclopedia/H/AE heat transfer fluid.html. Accessed 25/11/2008.

Deadline 2.36 (2003-2007). Computer Software. Available from: http:// www.deadline.3x.ro

Dincer, I., and Rosen, M.A. (2002). Thermal energy systems and applications. New York: Willey.

Duffie, J.A. and John, A. (2006). Solar engineering of thermal processes. New Jersey: John Wiley.

Esen, M., and Durum, A. (1998). Geometric design of solar–aided latent heat store depending on various parameters and Phase Change Materials. Solar Energy, 62(1): 19-28.

Farid, M.M., Khudhair, A.M., Razack, S.A.K. and Al-Hallaj, S. 2004. A review on phase change energy storage: Materials and applications. Energy Conversion and Management, 45 (9-10):1597-1615.

Fath, H.E.S. (1998). Technical assessment of solar thermal energy storage technologies. Renewable Energy, 14(1-4): 35-40.

Fatih Demirbas, M. (2006). Thermal energy storage and Phase Change Materials: An overview,Energy Sources, Part B: Economics. Planning and Policy 1(1): 85-95.

Felix Regin, A., Solanki, S.C. and Saini, J.S. (2009). An analysis of a packed bed latent heat thermal energy storage system using PCM capsules: Numerical investigation. Renewable Energy, 34(7):1765- 1777.

Florides, G.A., Kalogirou S.A, Tassou, S.A. and Wrobel, L.C. (2002): Modelling, simulation and warming impact assessment of a domestic size absorption solar cooling system. Applied Thermal Engineering, 22:1313-1325.

Fraas, A. (1998). Heat exchanger design. New York: John Wiley.

Fujii, I.,Tsuchiya, K., Higano, M., and Yamada, J. (1985). Studies of an Energy Storage System by Use of the Reversible Chemical Reaction: $CaO + H_2O \leftrightarrow Ca(OH)_2$. Solar energy, 34(5):367-375.

Fujii, I., Tsuchiya, K., Higano, M., Shikakura, Y., and Murthy M.S. (1989). Consideration on Thermal Decomposition of Calcium Hydroxide Pellets for Energy Storage. Trans.ASME J. Solar Energy Eng , 111(2):245-250.

Gajbert, H. and Fiedler, F. (2003). Solar combisystems. A state of Art Report.Ph.D. course solar heating. Department of civil engineering technical University of Denmark.

Gao W., Lin W., Liu T. And Xia C. (2007). An experiment study on the heat storage performances of polyacohols NPG, TAM, PE, and AMPD and their mixtures as solid- solid Phase Change Material   s for solar energy applications. International Journal of Green Energy, 4: 301-311.

Garg, H.P. (1987). Advances in solar energy technology. Dordrecht: D.Reidel Publishing Company.

Ghaddar, N.K., Shihab, M., Bdeir, F. (1997). Modeling and simulation of solar absorption system performance in Beirut. Renewable Energy, 10(4): 539-558.

Gil, A., Medrano, M., Martorell, I., Lázaro, A., Dolado, P., Zalba, B. and Cabeza, L.F. (2010). State of the art on high temperature thermal energy storage for power generation. Part 1- Concepts, materials and modellization. Renewable and Sustainable Energy Reviews, 14(1): 31-55.

Gong, Z. and Mujumdar, A.S. (1997). Finite-element analysis of cyclic heat transfer in a shell and tube latent heat energy storage exchanger, Applied Thermal Engineering, 17(4): 583–591.

Hahne, E. (1986).Thermal storage some view on some problems. Proceedings of the 8th International Heat Transfer Conference, San Francisco, USA.

Hale, D.V, Hoover, M.J, O'Neill, M.J. (1971). Phase Change Materials handbook. Alabama: NASA-CR-61313.Lockeed missiles and Space Company.

Hasnain, S.M. (1998). Review on sustainable thermal energy storage technologies, part I: Heat storage materials and techniques. Energy Conversion and Management, 39(11): 1127-1138.

He, Q. and Zhang, W.N.(2001). A study on Latent Heat Storage exchangers with the high temperature Phase Change Materials, Int. J. Energy Res., 25:331-341.

Hu, H. and Argyropoulos, S.A.(1996). Mathematical modelling of solidification and melting: a review. Modelling Simul.Mater.Sci.Eng, 4:371-396.

Ismail, K.A.R., Alves, C.L.F. (1986). Analysis of the shell-and-tube PCM storage system. Proceedings of the 8th International Heat Transfer Conference, 1781–1786.

Jayakumar, P. (2009). Solar energy Resource Assessment Handbook. Prepared for APCTT.

Jurinak, J.J., Adbel Khalik, S.I. (1979). On the performance of air-based solar Heating systems utilizing phase change energy storage. Solar Energy, 24 :503–522.

Kalogirou, S.A. (2004). Solar thermal collectors and applications. Progress in Energy and Combustion Science, 30(3): 231-295.

Kaneff, S.(1999). A 20 dish solar thermal array providing 2.6 MWe via an existing coal fired steam driven turbigenerator system. Abstract submitted to the ISES '99 solar world congress, Jerusalem.

Kang, Y.B., Zhang, Y.P., Zhu, Y.Q. (1999). A simple model for heat transfer analysis of tube and shell with Phase Change Material and its performance simulation. International Journal of Heat Mass Transfer, 45:230-236.

Kenisarin, M.and Mahkamov, K. (2007). Solar energy storage using Phase Change Material s, Renewable and Sustainable Energy Reviews, 11(9):1913-1965.

Koene, F.G.H, Van Helden, W.G.and Romer, L. (2000). Energy piles as cost effective ground heat exchangers. Proceedings of Terrastock 2000, 8th International Conference on thermal energy storage, Stuttgart.

Kreith, F., Kreider, J.F. (1978). Principles of solar engineering. New York: Mc Graw-Hill.

Kurklu, A., Wheldon, A, Hadley, P. (1996). Mathematical modelling of the thermal performance of a Phase Change Material (PCM) store cooling cycle. Applied Thermal Engineering, 16 (7): 613-623.

Lacroix, M. (1993). Study of the heat transfer behaviour of a latent heat thermal energy storage unit with a finned tube, International Journal of Heat and Mass Transfer, 36:2083-2092.

Lecomte, D.and Mayer, D. (1985). Design method for sizing a latent heat store/heat exchanger in a thermal system. Applied Energy, 21:55–78.

Lienhard, J. IV and Lienhard, J. V.(2006). A heat transfer textbook. Massachusetts: Phlogiston Press.

Michels, H. and Pitz-Paal, R. (2007). Cascaded Latent Heat Storage for parabolic trough solar power plants. Solar energy, 81(6):829-837.

Mawire, A. (2009). Characterisation of a Thermal Energy Storage System Developed for Indirect Solar Cooking. Doctoral dissertation. Mafikeng : North West University.

Mawire, A. and McPherson, M. (2009). Experimental and simulated temperature distribution of an oil-pebble bed thermal energy storage system with a variable heat source, Applied Thermal Engineering, 29(5-6): 1086-1095.

Mehling, H. and Cabeza, L.F. (2008). Heat and Cold storage with PCM. Berlin-Heldbergy:Springer.

Morrison, D.J., Abdel Khalik, SI. (1978). Effects of phase change energy storage on the performance of air-based and liquid-based solar heating systems. Solar Energy 20: 57–67.

Pridasawa, W. and Lundqvist, P. (2003). Feasibility and efficiency of Solar-driven Refrigeration Systems, 21 st IIR International Congress of Refrigeration, August 17-22, Washington D.C., USA.

Regin, A.F., Solanki, S.C. and Saini, J.S. (2006). Latent heat thermal energy storage using cylindrical capsule: Numerical and experimental investigations. Renewable Energy, 31(13):2025-2041.

Reuss, M., Mueller J.P., Roehle B., Weickler, M. and Schoelkopf, W. (1998). A new concept of hybrid energy storage in solar heating. Proceedings of the second Stockton International Geothermal Conference, Stockton.

Saxena, S., Subrahmaniyam, S. and Sarkar, M.K.(1982). A preliminary model for phase change thermal energy storage in a shell and tube heat exchanger. Solar Energy, 29 (3): 257-263

Scilab version 5.3 beta 5 (1989-2010). (Computer software).France:INRIA.

Seeniraj, V.R, Velraj R., and Kannan, N.P. (1998). Analytical solutions for planar and cylindrical axisymmetric melting with heat capacity effects of flowing stream and PCM.Int. comm. heat mass transfer, 25(7): 973-1041.

Shamsundar, N. (1982). Formulae for Freezing outside a Circular Tube with Axial Variation of Coolant Temperature. International Journal of Heat and Mass Transfer, 25:1614–1617.

Shamsundar, N.and Srinivasan, R. (1980). Effectiveness NTU charts for heat recovery from Latent Heat Storage units. J. Solar Energy Eng, 102:263–271.

Shamsundar, N., Stein E., Rooz E., Bascaran E., Lee T.C.(1992). Design and Simulation of Latent Heat Storage Units. Final Report. Texas :National Renewable Energy Laboratory. University of Houston.

Sharma, A., Sharma, S.D. and Buddhi, D. (2002). Accelerated thermal cycle test of acetamide, stearic acid and paraffin wax for solar thermal Latent Heat Storage applications. Energy Conversion and Management, 43(14): 1923-1930.

Sharma, A., Tyagi, V.V.,Chen, C.R. and Buddhi, D. (2009). Review on thermal energy storage with Phase Change Materials and applications. Renewable and Sustainable Energy Reviews, 13(2):318-345.

Sharma, S.D., Iwata, T., Kitano, H. and Sagara, K. (2005): Thermal performance of a solar cooker based on an evacuated tube solar collector with a PCM storage unit, Solar Energy, 78(3):416-426.

Sharma, A.,Sharma, S.D. and Buddhi, D. (2002). Accelerated thermal cycle test of acetamide, stearic acid and paraffin wax for solar thermal Latent Heat Storage applications. Energy Conversion and Management, 43 (14):1923-1930.

Sharma, S.D., Iwata, T., Kitano, H. and Sagara, K. (2005).Thermal performance of a solar cooker based on an evacuated tube solar collector with a PCM storage unit. Solar Energy, 78(3):416-426.

Sharma, S. and Kazunobu, S. (2005). Latent Heat Storage materials and Systems: a review. International Journal of Green Energy, 2:1-56.

Simmons, J.A. (1976). Reversible Oxidation of Metal Oxides for Thermal Energy Storage. Proc ISES Meeting, Winnipeg, 8, 219.

Solomon, A.D. (2006). Modeling melting and solidification Processes. Israel:Sami Shamoon Academic College of Engineering.

Sparrow, E.M. and Hsu C.F. (1981). Analysis of Two-dimensional Freezing on the outside of a Coolant carrying Tube. International Journal of Heat and Mass Transfer, 24: 1345–1357.

Stine,W. and Geyer, M., 2008. Power from the sun.http:// www.powerfromthesun.net. Accessed 14 January 2008.

Stoecker, W. F. and Jones, J. W. (1982). Refrigeration and air conditioning. 2nd edition. Singapore: McGraw Hill.

Swet, C. (1979): energy storage for solar applications. In Solar energy handbook. New York: McGraw-Hill.

Van Berkel, J. (2000). Solar thermal techniques. Research commissioned by the Netherlands Agency and the Environment NOVEM Project 143.620-935.8. Rhenen.

Venter, N. and Netshilaphala, N. (2006). Environmental impact assessment process. Proposed concentrating solar power (CSP) plant and associated infrastructure in the northern cape area. http://www.eskom.co.za .Accessed 14 January 2008.

Verma, P., Varun, R.P. and Singal, S.K. (2008). Review of mathematical modeling on latent heat thermal energy storage systems using phase-change material. Renewable and Sustainable Energy Reviews, 12 (23):999–1031.

Wang, J., Ouyang, Y. and Chen, G.(2001). Experimental study on charging processes of a cylindrical heat storage capsule employing multiple Phase Change Materials. Int. J.Energy materials, 25:439-447.

Yian –You, L. (2008). Numerical and experimental investigation for heat transfer in triplex concentric tube with Phase Change Material for thermal energy storage. Solar energy, 82(11):977-985

Yimmer,B. and Adami, M. (1989). Parametric Study and Optimization of Phase Change Thermal Energy Storage System. National Heat Transfer Conference, HTD, Multiphase Flow,Heat and Mass Transfer,109: 1-89.

Yuksel, N., Avci A., Kilic M. (2006). A model for latent heat energy storage systems. International Journal of Energy Research, 30(14): 1146–1157.

Zalba, B., Marín, J.M., Cabeza, L.F and Mehling, H. (2003). Review on thermal energy storage with phase change: materials, heat transfer analysis and applications. Applied Thermal Engineering 23(3): 251–283.

Zhang, Y.and Faghri, A. (1996). Heat transfer enhancement in latent heat thermal energy storage system by using the internally finned tube. International Journal of Heat Mass Transfer, 39(15): 3165–3173.

APPENDICES

APPENDIX A.1   : AREA OF WORLD WITH HIGH INSOLATION

APPENDIX A.2   : ANNUAL SOLAR RADIATION OF SOUTH AFRICA

APPENDIX B   : SHAMSUNDAR'S MODEL

APPENDIX C   : DSC CURVE OF ERYTHRITOL

APPENDIX D   : PROPERTIES OF DURATHERM XLT-50

APPENDIX E.1   : TYPICAL HEAT EXCHANGER MATERIALS AND THEIR
THERMAL CONDUCTIVITIES

APPENDIX E.2   : DIMENSIONS OF COPPER TUBES TYPES

APPENDIX F.1   : GRAPHICAL DETERMINATION OF F_0

APPENDIX F.2   : ANALYTICAL DETERMINATION OF F_0

APPENDIX F.3   : PROGRAMME CODE OF THE DESIGN OF THE LATENT
HEAT STORAGE UNIT (MODIFIED MODEL)

APPENDIX F.4   : RESULTS OF THE PROGRAMME CODE OF THE LATENT
HEAT STORAGE UNIT (MODIFIED MODEL)

APPENDIX G   : SIMULATION OF THE THERMAL MODEL LATENT HEAT
STORAGE UNIT (MODIFIED MODEL)

APPENDIX H   : GRAPHICAL DETERMINATION OF F_0 (SHAMSUNDAR'S
MODEL)

APPENDIX I.1   : PROGRAMME CODE (SHAMSUNDAR'S MODEL)

APPENDIX I.2   : RESULTS OF THE PROGRAMME CODE OF THE LATENT
HEAT STORAGE UNIT (SHAMSUNDAR'S MODEL)

APPENDIX J.1   : ANALYTICAL APPROXIMATION METHOD 1

APPENDIX J.2   : ANALYTICAL APPROXIMATION METHOD 2

APPENDIX A.1: AREA OF THE WORLD WITH HIGH INSOLATION

[Source: Dr. P. Jayakumar, Solar Energy Resource Assessment Handbook, 2009]
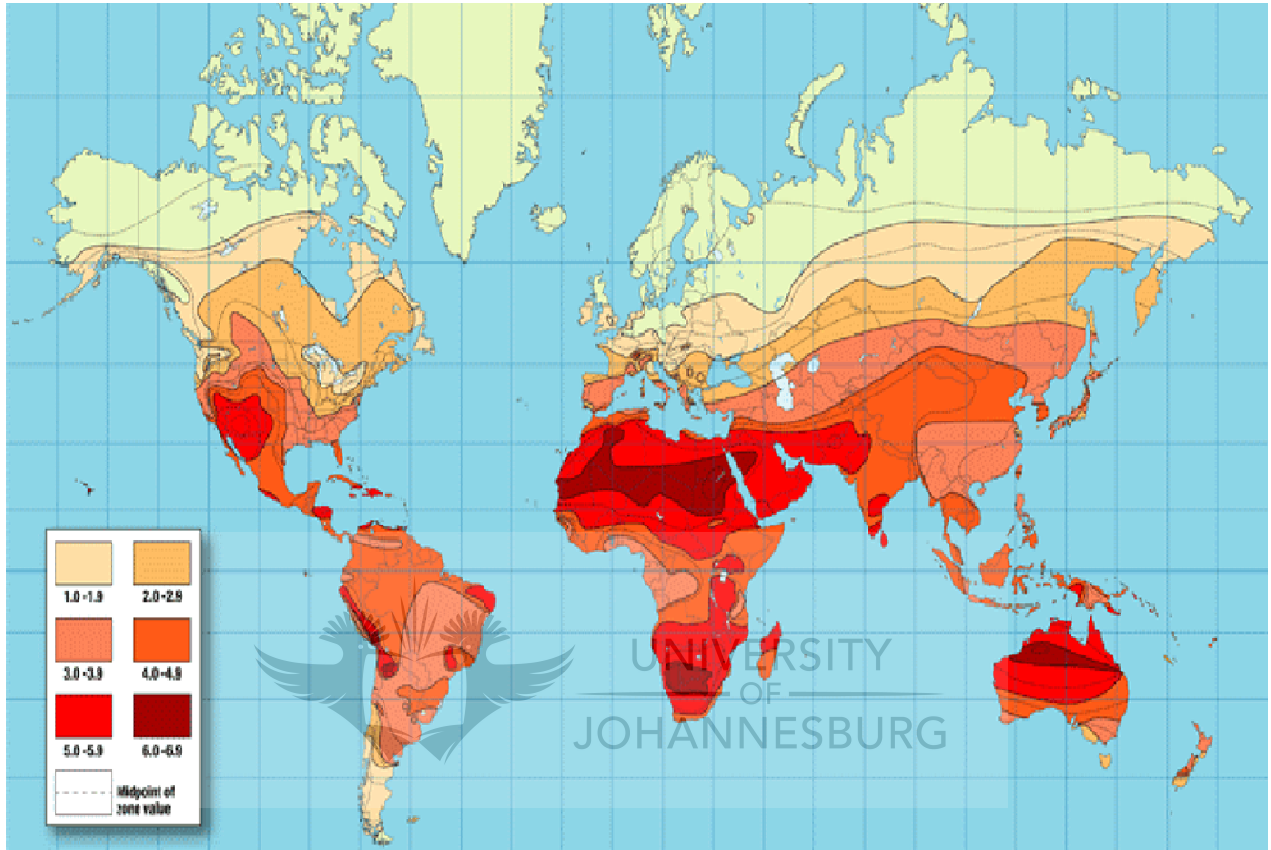
APPENDIX A.2: ANNUAL SOLAR RADIATION OF SOUTH AFRICA

[SOURCE: ESKOM, 2006]

South African Renewable Resource Database - Annual Incoming Shortwave Radiation
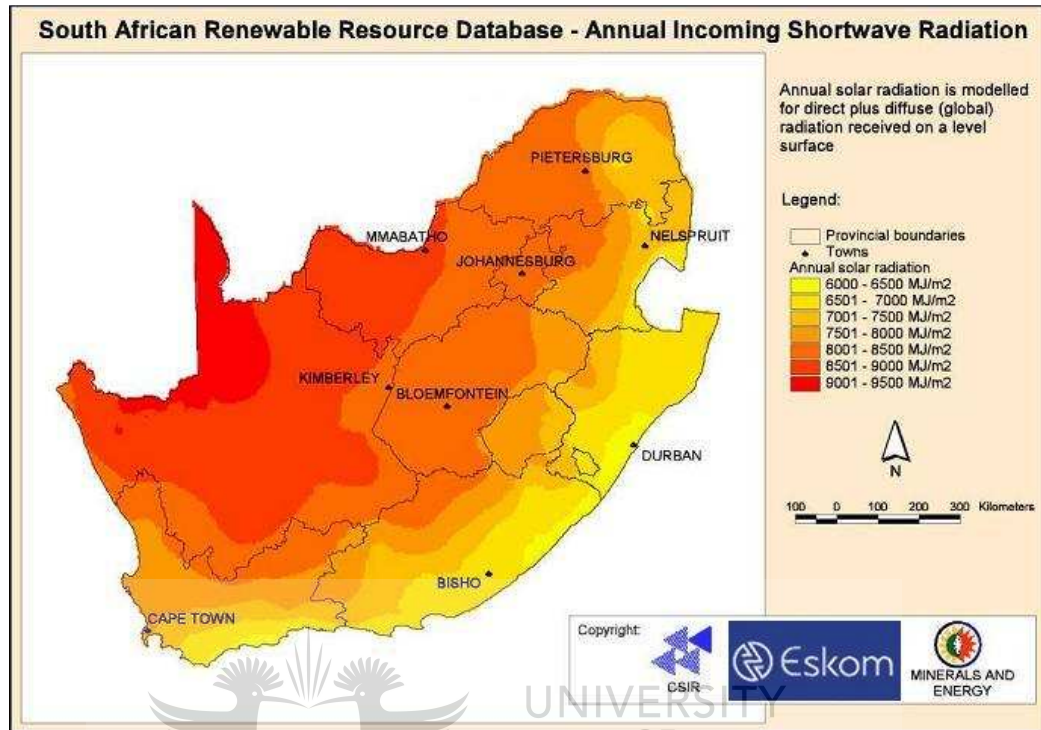
APPENDIX B: SHAMSUNDAR'S MODEL

The analytical model as suggested by Shamsundar *et al.* (1992) is given below:

1. Heat conduction in the solid PCM:

$$\dot{Q} = 2\pi k (T_m - T_w) / \ln\left(\frac{r_m}{R}\right)$$

(B.1)

where $\dot{Q}$ =   heat of conduction per unit length in the PCM;

     k =   thermal conductivity of the PCM;

     T_m =   melting point of the PCM;

     T_w =   wall temperature of the tube heat exchanger;

     r_m =   radius of the solidified PCM. It is a function of time and x;

     R =   radius of the tube exchanger.

2. The convection of the HTF in the tube heat exchanger was given by:

$$\dot{Q} = 2\pi R h (T_w - T_f)$$

(B.2)

where $\dot{Q}$ =   convection heat rate per unit length in the tube heat exchanger;

     R =   radius of the tube heat exchanger;

     h =   convection coefficient heat transfer;

     T_f =   HTF temperature in the tube heat exchanger;

     T_w =   wall temperature of the heat exchanger.

3. The temperature of the HTF rising was given by the Equation:

$$\dot{Q} = m_f \frac{\partial T_f}{\partial x}$$

(B.3)

where $\dot{Q}$ =   heat transfer rate in the HTF;

     m_f =   mass flow rate of the HTF;

$\dfrac{\partial T_f}{\partial x}$ =   change of the HTF temperature as a function of axial distancealong the tube heat exchanger.

4. The heat loss from the shell caused the PCM to freeze:

$$\dot{Q} = \frac{\partial[\pi(r_m^2 - R^2)\rho H]}{\partial t}$$

(B.4)

where $\dot{Q}$ =   heat transfer rate per unit length of the tube ;

     H =   latent heat of fusion of the PCM;

     ρ =   density of the PCM;

     r_m =   radius of the frozen layer of the PCM;

     R =   radius of the exchanger HTF tube;

     t =   time.

The solution is provided in terms of non-dimensional variables and parameters.

$$\tau = \frac{F_0}{2\,Bi} + \frac{1}{4}\left(\left(1 + F_0\right)\ln\left(1 + F_0\right) - F_0\right) \tag{B.5}$$

$$NTU_x = \frac{2\pi Rhx}{m_f C_P} = \ln\left(\frac{F_0}{F}\right) + \left(\frac{Bi}{2}\right)\left[G_1(F_0) - G_1(F)\right] \tag{B.6}$$

$$G_0(F) = (1 + F)\ln(1 + F) - F \tag{B.7}$$

$$G_1(F) = p(1 + 17p^2/450)/(1 + p^2/100) + p^2/4 \tag{B.8}$$

$$\varepsilon = \frac{T_f - T_0}{T_m - T_0} = 1 - \frac{F}{F_0} \tag{B.9}$$
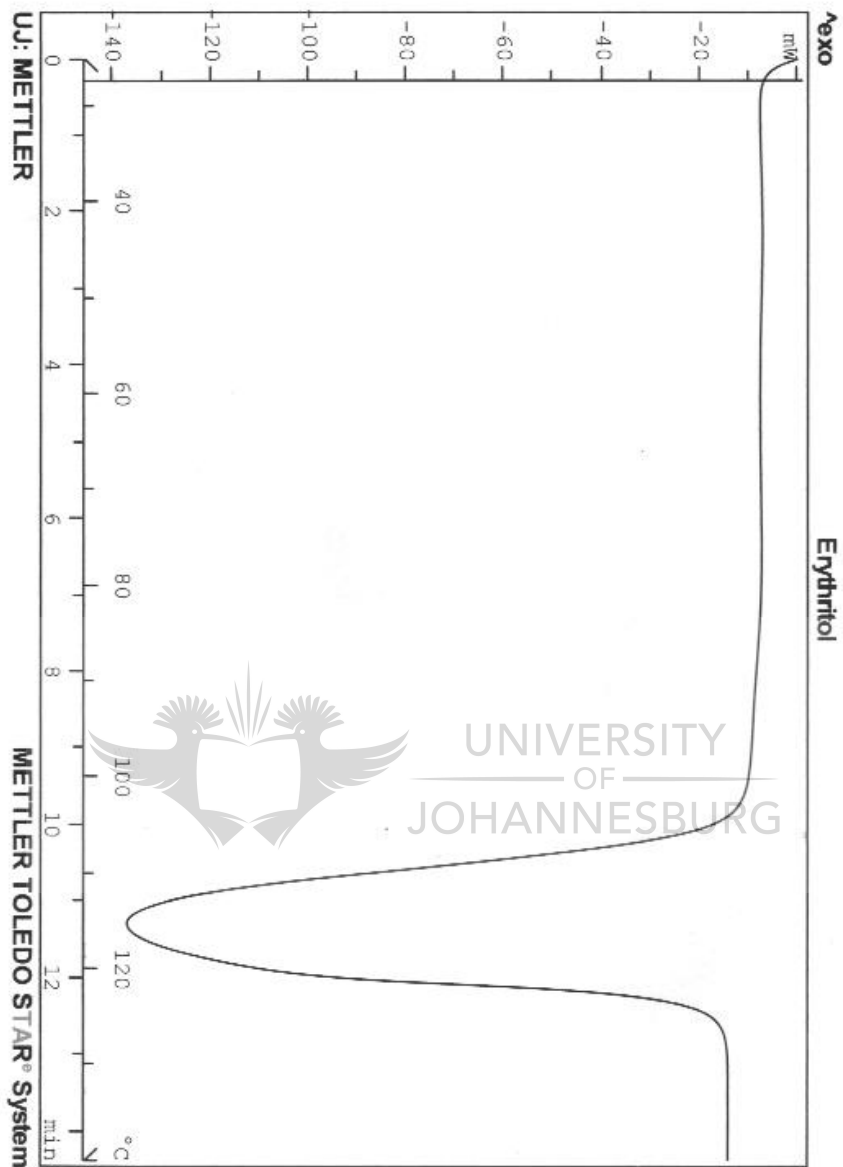
DURATHERM
EXTENDED LIFE FLUIDS

P.O. Box 563, Lewiston, NY 14092 • P 800 446 4910 • F 905 984 6684 • info@heat-transfer-fluid.c

Property Vs. Temperature
Duratherm XLT-50 - Metric Units
Temperature (Celsius)
Minimum: -46 Maximum 177

Temperature (Celsius)	Density (kg/m3)	Kinematic Viscosity (Centistoke)	Dynamic Viscosity (Centipoise)	Thermal Conductivity (W/m.K)	Heat Capacity (kJ/kgK)	Vapour Pressure (kPa)
-46	871	100.37	87.42	0.140	1.926	0.00
-40	868	68.53	59.49	0.139	1.926	0.00
-34	865	37.10	32.20	0.138	1.938	0.00
-29	863	16.02	13.91	0.138	1.950	0.00
-23	860	5.19	4.46	0.137	1.962	0.00
-18	857	4.52	3.87	0.137	1.974	0.00
-12	854	3.99	3.41	0.137	1.986	0.00
-7	852	3.56	3.03	0.136	1.998	0.00
-1	849	3.20	2.72	0.136	2.010	0.00
4	846	2.90	2.45	0.135	2.022	0.00
10	844	2.65	2.24	0.135	2.034	0.00
16	841	2.43	2.04	0.135	2.046	0.00
21	838	2.24	1.88	0.134	2.058	0.00
27	835	2.08	1.74	0.134	2.069	0.00
32	833	1.94	1.62	0.134	2.081	0.00
38	830	1.82	1.51	0.133	2.093	0.14
43	827	1.71	1.41	0.133	2.110	0.67
49	824	1.61	1.33	0.132	2.127	1.21
54	820	1.52	1.25	0.132	2.144	1.74
60	817	1.44	1.18	0.131	2.160	2.28
66	814	1.37	1.12	0.131	2.177	2.41
71	811	1.30	1.05	0.130	2.194	3.61
77	808	1.24	1.00	0.130	2.211	4.81
82	805	1.19	0.96	0.129	2.227	6.01
88	801	1.14	0.91	0.129	2.244	7.21
93	798	1.09	0.87	0.128	2.261	8.41
99	795	1.05	0.83	0.128	2.278	11.35
104	784	1.01	0.79	0.127	2.294	14.29
110	773	0.97	0.75	0.127	2.311	17.22
116	761	0.94	0.72	0.126	2.328	20.16
121	750	0.91	0.68	0.125	2.345	23.10
127	739	0.88	0.65	0.125	2.361	26.41
132	728	0.85	0.62	0.124	2.378	29.72
138	716	0.82	0.59	0.124	2.395	33.03
143	705	0.8	0.56	0.123	2.412	36.34
149	694	0.77	0.53	0.123	2.428	39.64
154	683	0.75	0.51	0.123	2.445	44.48
160	672	0.73	0.49	0.119	2.462	49.33
166	661	0.72	0.48	0.119	2.474	54.17
171	651	0.69	0.45	0.119	2.487	59.01
176	641	0.67	0.43	0.116	2.500	63.85

UNIVERSITY OF JOHANNESBURG

APPENDIX E.1: TYPICAL HEAT EXCHANGER MATERIALS AND THEIR THERMAL CONDUCTIVITIES

[SOURCE: www.engineeringtoolbox.com]

Thermal conductivities of some common heat exchanger materials are indicated below:

Material	Thermal Conductivity (W/m^{o}C)
Admiralty (71 Cu - 28 Zn - 1 Sn)	111
Aluminum	202
Aluminum brass (76 Cu - 22 Zn - 2 Al)	100
Brass (70 Cu - 30 Zn)	99
Carbon Steel	45
Chrome-moly steel (2 1/4 Cr - 0.5 Mo)	38
Chrome-moly steel (5 Cr - 0.5 Mo)	35
Copper	386
Cupro-nickel (90 Cu - 10 Ni)	71
Cupro-nickel (70 Cu - 30 Ni)	29
Monel (67 Ni - 30 Cu - 1.4 Fe)	26
Nickel	62
Red Brass (85 Cu - 15 Zn)	159
Stainless Steel, type 316 (17 Cr - 12 Ni - 2 Mo)	16
Stainless Steel, type 304 (18 Cr - 8 Ni)	16
Titanium	19

APPENDIX E.2: DIMENSIONS OF COPPER TUBES TYPE A

[Source: www.engineeringtoolbox.com]

Type A			
Nominal Size Outside Diameter (mm)	Wall Thickness (mm)	Tolerance +/- Maximum Deviation at any Point (mm)	Weight (kg/m)
6	0.9	0.08	0.12
8	0.9	0.09	0.18
10	0.9	0.09	0.23
12	1.2	0.1	0.36
15	1.2	0.1	0.47
18	1.2	0.1	0.57
22	1.6	0.15	0.92
28	1.6	0.15	1.19
35	1.6	0.15	1.50
42	1.8	0.2	2.03
54	2.1	0.2	3.06
67	2.4	0.25	4.35
79	2.8	0.3	5.99
105	3.4	0.35	9.70
130	4.0	0.4	14.2
156	4.8	0.5	20.3
206	6.8	0.7	38.0
257	8.5	0.85	59.3
308	10.3	1	86.1

APPENDIX F.1: GRAPHICAL DETERMINATION OF F_0

Deadline 2.36 was used to solve the transcendental equation: In this equation the unknown F_o was replaced by x
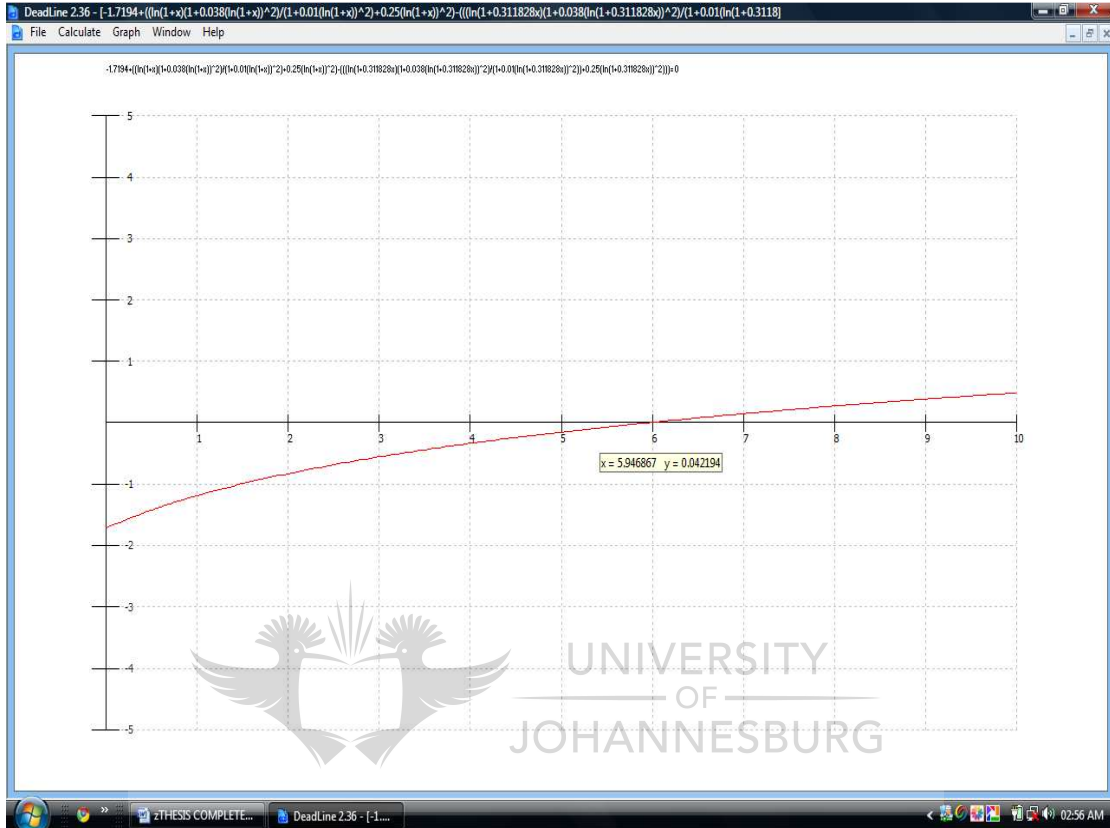
Deadline 2.36 assists in determining the root of the equation by plotting the function. Result or root of the transcendental equation is obtained where there is intersection of graph with the x-axis.

From the graph, the root is found between 5 and 6.

The numerical result provided by Deadline 2.36 software was: F_0= 5.95486139

-1.7194+((ln(1+x)(1+0.038(ln(1+x))^2)/(1+0.01(ln(1+x))^2)+0.25(ln(1+x))^2)-(((ln(1+0.311828x)(1+0.038(ln(1+0.311828x))^2)/(1+0.01(ln(1+0.311828x))^2))+0.25(ln(1+0.311828x))^2))) = 0

m=0.1

[0; 10]

1 root found.

x_1	5.95486139

The value of F was found to be equal to 5.95486139 by solving the transcendental equation (4-13).The result compared well with the result obtained from the graph and from the programme code.

APPENDIX F.3: PROGRAMME CODE OF THE DESIGN OF THE LATENT HEAT STORAGE (MODIFIED MODEL)

(SCILAB CODE)

```
//PROGRAMME DESIGN OF LATENT HEAT STORAGE UNIT
Tm=118      // Melting point of Erythritol [°C]
H=339800    // Latent heat of fusion of Erythritol [°C]
Cps=1383    // Specific heat of solid Erythritol @ 20°C [J/kg C]
Cpl=2765    // Specific heat of liquid Erythritol @ 140°C [J/kg C]
ks=0.733    // Thermal conductivity of solid Erythritol @ 20°C [ W/m K]
kl=0.326    // Thermal conductivity of liquid Erythritol @ 140°C [W/m K]
Ps= 1480    // Density of solid Erythritol @ 20°C  [kg/m^3]
Pl =1300    // Density of liquid Erythritol @ 140°C [ kg/m^3]
kw=386 // Thermal conductivity of copper
// HEAT TRANSFER FLUID SELECTED: DURATHERM XLT-50
// PROPERTIES OF DURATHERM XLT-50 AT MEAN TEMPERATURE=60°C
kf=0.131    // Thermal conductiivity of Duratherm XLT-50 [ W/m K]
Cpf=2177    // Specific heat of Duartherm XLT-50  [ J/kg C]
nuf=1.18e-3 // Dynamic viscosity of Duratherm XLT-50 [ Pa.s]
Pf=814      // Density Duratherm XLT-50 [ kg/m3]

// PARAMETER SPECIFICATIONS OF WORKING FLUID IN HEAT EXCHANGER
Ti=25
Tmax=97    // Outlet Temperature of Duratherm XLT-50 [C] from the heat exchanger
Tmin=89    // Outlet Temperature of Duratherm XLT -50 [C] from the heat exchanger [C]
mft=0.017   // Total mass flow rate [ kg/s]
td=43200    // Discharge period  of heat exchanger [s], 12 hours is the discharge period

emax=(Tmax-Ti)/(Tm-Ti) // maximum  effectiveness of heat exchanger
emin=(Tmin-Ti)/(Tm-Ti) // minimum  effectiveness of heat exchanger

Nu=1.83            // Nusselt Number for fully developed flow laminar ( Nu=h*Ri/kf).It is equal to
3.67 with reference to the diameter.
NTU=-log(1-emax)   // Number of Transfer Units ( 0.5< NTU >5
B=Nu*(kf/ks)*(1.15) // The parameter B is calculated for fully developed flow laminar, The ratio
outer radius and inner radius of the tube exchanger is fixed at 1.15

// DETERMINATION OF THE FRACTION OF THE PCM SOLIDIFIED AT THE INLET HEAT
EXCHANGER
p0=-log(1-emin);
x=(NTU-p0)*2/B;
y=exp(x);
F0=(y-1)/(1-y*(1-emin));
if F0 < 0 then y=exp(2*x/p0); F0=sqrt(y/(1-emin))// F0 is the approximate value of F0. In order to
find the value of F0, the Newton-Raphson method is applied
end;

F1=(1-emin)*F0;
p1=log(1+F0);
p2=p1*p1;
G1=(1+(17/450)*p2)*p1/(1+(1/100)*p2)+(p2/4);// F0 is determined by iteration
p3=log(1+F1);
p4=p3*p3;
G2=(1+(17/450)*p4)*p3/(1+(1/100)*p4)+(p4/4);
x=-log(1-emin)+B*(ks/kw)*(1.15)*(-log(1-emin))+B/2*(G1-G2)-NTU;
y=B/2*(p1/F0-(1-emin)*p3/(1+F1));
F2=F0-x/y
```

```
F3=(1-emin)*F2;
p5=log(1+F2);
p6=p5*p5;
G3=(1+(17/450)*p6)*p5/(1+(1/100)*p6)+(p6/4);
p7=log(1+F3);
p8=p7*p7;
G4=(1+(17/450)*p8)*p7/(1+(1/100)*p8)+(p8/4);
x1=-log(1-emin)+ B*(ks/kw)*(1.15)*(-log(1-emin))+B/2*(G3-G4)-NTU;
y1=B/2*(p5/F2-(1-emin)*p7/(1+F3));
F4=F2-x1/y1

F5=(1-emin)*F4;
p9=log(1+F4);
p10=p9*p9;
G5=(1+(17/450)*p10)*p9/(1+(1/100)*p10)+(p10/4);
p11=log(1+F5);
p12=p11*p11;
G6=(1+(17/450)*p12)*p11/(1+(1/100)*p12)+(p12/4);;
x2=-log(1-emin)+ B*(ks/kw)*(1.15)*(-log(1-emin))+B/2*(G5-G6)-NTU;
y2=B/2*(p9/F4-(1-emin)*p11/(1+F5));
F6=F4-x2/y2

F7=(1-emin)*F6;
p13=log(1+F6);
p14=p13*p13;
G7=(1+(17/450)*p14)*p13/(1+(1/100)*p14)+(p14/4);
p15=log(1+F7);
p16=p15*p15;
G8=(1+(17/450)*p16)*p15/(1+(1/100)*p16)+(p16/4);
x3=-log(1-emin)+ B*(ks/kw)*(1.15)*(-log(1-emin))+B/2*(G7-G8)-NTU;
y3=B/2*(p13/F6-(1-emin)*p15/(1+F7));
F8=F6-x3/y3

F9=(1-emin)*F8;
p17=log(1+F8);
p18=p17*p17;
G9=(1+(17/450)*p18)*p17/(1+(1/100)*p18)+(p18/4);
p19=log(1+F9);
p20=p19*p19;
G10=(1+(17/450)*p20)*p19/(1+(1/100)*p20)+(p20/4);
x4=-log(1-emin)+ B*(ks/kw)*(1.15)*(-log(1-emin))+B/2*(G9-G10)-NTU;
y4=B/2*(p17/F8-(1-emin)*p19/(1+F9));
F10=F8-x4/y4

F11=(1-emin)*F10;
p21=log(1+F10);
p22=p21*p21;
G11=(1+(17/450)*p22)*p21/(1+(1/100)*p22)+(p22/4);
p23=log(1+F11);
p24=p23*p23;
G12=(1+(17/450)*p24)*p23/(1+(1/100)*p24)+(p24/4);
x5=-log(1-emin)+ B*(ks/kw)*(1.15)*(-log(1-emin))+B/2*(G11-G12)-NTU;
y5=B/2*(p21/F10-(1-emin)*p23/(1+F11));
F12=F10-x5/y5

F13=(1-emin)*F12;
p25=log(1+F12);
p26=p25*p25;
G13=(1+(17/450)*p26)*p25/(1+(1/100)*p26)+(p26/4);
```

```
p27=log(1+F13);
p28=p27*p27;
G14=(1+(17/450)*p28)*p27/(1+(1/100)*p28)+(p28/4);
x6=-log(1-emin)+ B*(ks/kw)*(1.15)*(-log(1-emin))+B/2*(G13-G14)-NTU;
y6=B/2*(p25/F12-(1-emin)*p27/(1+F13));
F14=F12-x6/y6

F15=(1-emin)*F14;
p29=log(1+F14);
p30=p29*p29;
G15=(1+(17/450)*p30)*p29/(1+(1/100)*p30)+(p30/4);
p31=log(1+F15);
p32=p31*p31;
G16=(1+(17/450)*p32)*p31/(1+(1/100)*p32)+(p32/4);
x7=-log(1-emin)+ B*(ks/kw)*(1.15)*(-log(1-emin))+B/2*(G15-G16)-NTU;
y7=B/2*(p25/F14-(1-emin)*p31/(1+F15));
F16=F14-x7/y7

F17=(1-emin)*F16;
p33=log(1+F16);
p34=p33*p33;
G17=(1+(17/450)*p34)*p33/(1+(1/100)*p34)+(p34/4);
p35=log(1+F17);
p36=p35*p35;
G18=(1+(17/450)*p36)*p35/(1+(1/100)*p36)+(p36/4);
x8=-log(1-emin)+ B*(ks/kw)*(1.15)*(-log(1-emin))+B/2*(G17-G18)-NTU;
y8=B/2*(p33/F16-(1-emin)*p35/(1+F17));
F18=F16-x8/y8
eps=abs(F18-F16)/F18
p37=log(1+F18)      // parameter in  calculation the dimensionless time [tau]
Go=(1+F18)*p37-F18  // parameter in calculation the dimensionless time [tau]
tau=F18/(2*B)+Go/4+F18*(ks/kw)*log (1.15)/(2) // Dimensionless time, The ratio outer radius and
inner radius of the tube exchanger is fixed at 1.15

Ro=sqrt(ks*(Tm-Ti)*td/(tau*Ps*H)) // The outside radius of the tube [m]
Ri=Ro/1.15    // The inside radius of the tube [m]. The ratio outer radius and inner radius of the
tube exchanger is fixed at 1.15
h1=B*ks/Ro   // Convective heat transfer coefficient [W/m2.K]
Dp=2*Ro*sqrt(1+F18)// Tube pitch [m]
v=(NTU*mft*Cpf)/(2*%pi*Ri*h1)// product of the number of tubes and the length of tube
L=3       // length of tube fixed at 3 m
n=v/L        // number of tube
ceil(n)
mf=mft/n // mass flow rate in a tube[kg/s]
Re=(2*mf)/(%pi*Ri*nuf)  // Reynolds number in the tube( less than 2300, laminar flow rate)
Dt=Dp*sqrt(2*((3)^0.5)*n/%pi) // Tank diameter [m]
Vt=%pi*Dt^2*L/4  // Tank volume [m^3]
Vl=%pi*n*L*Ri^2  // Liquid volume [m^3]
Vtu=%pi*(Ro+Ri)*n*L*(Ro-Ri)// Tube volume [m^3]
Vpcm=Vt-Vl-Vtu // Volume of PCM [m^3]
Vpcmt=(Vpcm/10+Vpcm) // Volume of Erythritol changes about 10% during solid to liquid phase
transition[m^3]
Mpcm=Ps*Vpcmt    // mass of PCM [kg]
```

APPENDIX F.4: RESULTS OBTAINED USING THE PROGRAMME CODE OF THE LATENT HEAT STORAGE UNIT (MODIFIED MODEL)

Scilab-5.3.0-beta-5

Startup execution:
 loading initial environment

-->// PROGRAMME CODE FOR THE DESIGN OF THE LATENT HEAT STORAGE UNIT

-->Tm=118   // Melting point of Erythritol [^{o}C]
 Tm =

   118.

-->H=339800   // Latent heat of fusion of Erythritol [^{o}C]
 H =

   339800.

-->Cps=1383   // Specific heat of solid Erythritol @ 20°C [J/kg C]
 Cps =

   1383.

-->Cpl=2765   // Specific heat of liquid Erythritol @ 140°C [J/kg^{o}C]
 Cpl =

   2765.

-->ks=0.733   // Thermal conductivity of solid Erythritol @ 20°C[W/m.K]
 ks =

   0.733

-->kl=0.326   // Thermal conductivity of liquid Erythritol @ 140°C[W/m.K]
 kl =

   0.326

-->Ps= 1480   // Density of solid Erythritol @ 20°C[kg/m^3]
 Ps =

   1480.

-->Pl =1300   // Density of liquid Erythritol @ 140°C [kg/m^3]

107

```
 Pl  =

    1300.

-->

-->kw=386 // Thermal conductivity of copper
 kw  =

    386.

-->

-->// HEAT TRANSFER FLUID SELECTED: DURATHERM XLT- 50

-->// PROPERTIES OF DURATHERM XLT- 50 AT MEAN TEMPERATURE=60$^{o}$C

-->kf=0.131   // Thermal conductivity of Duratherm XLT-50 [W/m K]
 kf  =

    0.131

-->Cpf=2177   // Specific heat of Duratherm XLT-50[J/kg C]
 Cpf  =

    2177.

-->nuf=1.18e-3 // Dynamic viscosity of Duratherm XLT-50 [Pa.s]
 nuf  =

    0.00118

-->Pf=814      // Density Duratherm XLT-50 [ kg/m3]
 Pf  =

    814.

-->

-->// PARAMETER SPECIFICATIONS OF WORKING FLUID IN HEAT EXCHANGER

-->Ti=25
 Ti  =

    25.

-->Tmax=97   // Outlet Temperature of Duratherm XLT-50 [C] from the heat exchanger
 Tmax  =

    97.

-->Tmin=89    // Outlet Temperature of Duratherm XLT -50 [C] from the heat exchanger [C]
 Tmin  =

    89.

-->mft=0.017   // Total mass flow rate [kg/s]
```

```
 mft  =

    0.017

-->td=43200   // Discharge period of the heat exchanger [s], 12 hours is the discharge period
 td  =

    43200.

-->

-->emax=(Tmax-Ti)/(Tm-Ti) //  the maximum  effectiveness of heat exchanger
 emax  =

    0.7741935

-->emin=(Tmin-Ti)/(Tm-Ti) //  the minimum  effectiveness of heat exchanger is:
 emin  =

    0.6881720

-->

-->Nu=1.83           // Nusselt Number for fully developed flow laminar (Nu=h*Ri/kf). It is
equal to 3.67 with reference to the diameter.
 Nu  =

    1.83

-->NTU=-log(1-emax)   // Number of Transfer Units ( 0.5< NTU >5
 NTU  =

    1.4880771

-->B=Nu*(kf/ks)*(1.15) // the parameter B is calculated for fully developed flow laminar, the
ratio outer radius and inner radius of the tube exchanger is fixed at 1.15
 B  =

    0.3761112

-->

-->// DETERMINATION OF FRACTION OF PCM SOLIDIFIED AT THE  INLET HEAT
EXCHANGER

-->p0=-log(1-emin);

-->x=(NTU-p0)*2/B;

-->y=exp(x);

-->F0=(y-1)/(1-y*(1-emin));

-->if F0 < 0 then y=exp(2*x/p0); F0=sqrt(y/(1-emin))// F0 is the approximate value of F0. In
order to find the value of F0, the Newton-Raphson method is applied
 F0  =
```

```
    7.8111232
-->end;

-->

-->F1=(1-emin)*F0;

-->p1=log(1+F0);

-->p2=p1*p1;

-->G1=(1+(17/450)*p2)*p1/(1+(1/100)*p2)+(p2/4);// F0 is determined by iteration

-->p3=log(1+F1);

-->p4=p3*p3;

-->G2=(1+(17/450)*p4)*p3/(1+(1/100)*p4)+(p4/4);

-->x=-log(1-emin)+B*(ks/kw)*(1.15)*(-log(1-emin))+B/2*(G1-G2)-NTU;

-->y=B/2*(p1/F0-(1-emin)*p3/(1+F1));

-->F2=F0-x/y
 F2  =

   6.2785722

-->

-->F3=(1-emin)*F2;

-->p5=log(1+F2);

-->p6=p5*p5;

-->G3=(1+(17/450)*p6)*p5/(1+(1/100)*p6)+(p6/4);

-->p7=log(1+F3);

-->p8=p7*p7;

-->G4=(1+(17/450)*p8)*p7/(1+(1/100)*p8)+(p8/4);

-->x1=-log(1-emin)+ B*(ks/kw)*(1.15)*(-log(1-emin))+B/2*(G3-G4)-NTU;

-->y1=B/2*(p5/F2-(1-emin)*p7/(1+F3));

-->F4=F2-x1/y1
 F4  =

   6.0101963

-->

-->F5=(1-emin)*F4;
```

```
-->p9=log(1+F4);

-->p10=p9*p9;

-->G5=(1+(17/450)*p10)*p9/(1+(1/100)*p10)+(p10/4);

-->p11=log(1+F5);

-->p12=p11*p11;

-->G6=(1+(17/450)*p12)*p11/(1+(1/100)*p12)+(p12/4);;

-->x2=-log(1-emin)+ B*(ks/kw)*(1.15)*(-log(1-emin))+B/2*(G5-G6)-NTU;

-->y2=B/2*(p9/F4-(1-emin)*p11/(1+F5));

-->F6=F4-x2/y2
 F6  =

    5.9383822

-->

-->F7=(1-emin)*F6;

-->p13=log(1+F6);

-->p14=p13*p13;

-->G7=(1+(17/450)*p14)*p13/(1+(1/100)*p14)+(p14/4);

-->p15=log(1+F7);

-->p16=p15*p15;

-->G8=(1+(17/450)*p16)*p15/(1+(1/100)*p16)+(p16/4);

-->x3=-log(1-emin)+ B*(ks/kw)*(1.15)*(-log(1-emin))+B/2*(G7-G8)-NTU;

-->y3=B/2*(p13/F6-(1-emin)*p15/(1+F7));

-->F8=F6-x3/y3
 F8  =

    5.9178435

-->

-->F9=(1-emin)*F8;

-->p17=log(1+F8);

-->p18=p17*p17;

-->G9=(1+(17/450)*p18)*p17/(1+(1/100)*p18)+(p18/4);

-->p19=log(1+F9);
```
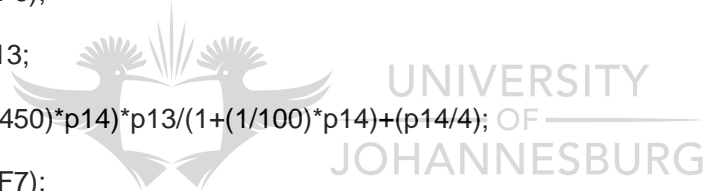
```
-->p20=p19*p19;

-->G10=(1+(17/450)*p20)*p19/(1+(1/100)*p20)+(p20/4);

-->x4=-log(1-emin)+ B*(ks/kw)*(1.15)*(-log(1-emin))+B/2*(G9-G10)-NTU;

-->y4=B/2*(p17/F8-(1-emin)*p19/(1+F9));

-->F10=F8-x4/y4
 F10 =

   5.9118658

-->

-->F11=(1-emin)*F10;

-->p21=log(1+F10);

-->p22=p21*p21;

-->G11=(1+(17/450)*p22)*p21/(1+(1/100)*p22)+(p22/4);

-->p23=log(1+F11);

-->p24=p23*p23;

-->G12=(1+(17/450)*p24)*p23/(1+(1/100)*p24)+(p24/4);

-->x5=-log(1-emin)+ B*(ks/kw)*(1.15)*(-log(1-emin))+B/2*(G11-G12)-NTU;

-->y5=B/2*(p21/F10-(1-emin)*p23/(1+F11));

-->F12=F10-x5/y5
 F12 =

   5.9101173

-->

-->F13=(1-emin)*F12;

-->p25=log(1+F12);

-->p26=p25*p25;

-->G13=(1+(17/450)*p26)*p25/(1+(1/100)*p26)+(p26/4);

-->p27=log(1+F13);

-->p28=p27*p27;

-->G14=(1+(17/450)*p28)*p27/(1+(1/100)*p28)+(p28/4);

-->x6=-log(1-emin)+ B*(ks/kw)*(1.15)*(-log(1-emin))+B/2*(G13-G14)-NTU;
```

```
-->y6=B/2*(p25/F12-(1-emin)*p27/(1+F13));

-->F14=F12-x6/y6
 F14  =

   5.9096051

-->

-->F15=(1-emin)*F14;

-->p29=log(1+F14);

-->p30=p29*p29;

-->G15=(1+(17/450)*p30)*p29/(1+(1/100)*p30)+(p30/4);

-->p31=log(1+F15);

-->p32=p31*p31;

-->G16=(1+(17/450)*p32)*p31/(1+(1/100)*p32)+(p32/4);

-->x7=-log(1-emin)+ B*(ks/kw)*(1.15)*(-log(1-emin))+B/2*(G15-G16)-NTU;

-->y7=B/2*(p25/F14-(1-emin)*p31/(1+F15));

-->F16=F14-x7/y7
 F16  =

   5.909455

-->

-->F17=(1-emin)*F16;

-->p33=log(1+F16);

-->p34=p33*p33;

-->G17=(1+(17/450)*p34)*p33/(1+(1/100)*p34)+(p34/4);

-->p35=log(1+F17);

-->p36=p35*p35;

-->G18=(1+(17/450)*p36)*p35/(1+(1/100)*p36)+(p36/4);

-->x8=-log(1-emin)+ B*(ks/kw)*(1.15)*(-log(1-emin))+B/2*(G17-G18)-NTU;

-->y8=B/2*(p33/F16-(1-emin)*p35/(1+F17));

-->F18=F16-x8/y8
 F18  =

   5.909411
```

-->eps=abs(F18-F16)/F18
 eps =

   0.0000074

-->p37=log(1+F18)   // parameter in calculation the dimensionless time [tau]
 p37 =

   1.9328844

-->Go=(1+F18)*p37-F18 // parameter in calculation the dimensionless time [tau]
 Go =

   7.4456818

-->tau=F18/(2*B)+Go/4+F18*(ks/kw)*log (1.15)/(2) // Dimensionless time, The ratio outer
radius and inner radius of the tube exchanger is fixed at 1.15
 tau =

   9.7181409

-->

-->Ro=sqrt(ks*(Tm-Ti)*td/(tau*Ps*H)) // The outside radius of the tube [m]
 Ro =

   0.0245472

-->Ri=Ro/1.15   // The inside radius of the tube [m]. The ratio outer radius and inner radius of
the tube exchanger is fixed at 1.15
 Ri =

   0.0213454

-->h1=B*ks/Ro   // Convective heat transfer coefficient [W/m2.K]
 h1 =

   11.231016

-->Dp=2*Ro*sqrt(1+F18)// Tube pitch [m]
 Dp =

   0.1290481

-->v=(NTU*mft*Cpf)/(2*%pi*Ri*h1)// product of the number of tubes and the length of tube
 v =

   36.562048

-->L=3   // length of tube fixed at 3 m
 L =

   3.

-->n=v/L   // number of tube
 n =

```
    12.187349

-->ceil(n)
 ans  =

    13.

-->mf=mft/n // mass flow rate in a tube [kg/s]
 mf  =

    0.0013949

-->Re=(2*mf)/(%pi*Ri*nuf)  // Reynolds number in the tube( less than 2300, laminar flow rate)
 Re  =

    35.256112

-->Dt=Dp*sqrt(2*((3)^0.5)*n/%pi) // Tank diameter [m]
 Dt  =

    0.4730714

-->Vt=%pi*Dt^2*L/4  // Tank volume [m^3]
 Vt  =

    0.5273082

-->Vl=%pi*n*L*Ri^2  // Liquid volume [m^3]
 Vl  =

    0.0523344

-->Vtu=%pi*(Ro+Ri)*n*L*(Ro-Ri)// Tube volume [m^3]
 Vtu  =

    0.0168778

-->Vpcm=Vt-Vl-Vtu // Volume of PCM [m^3]
 Vpcm  =

    0.4580960

-->Vpcmt=(Vpcm/10+Vpcm) // Volume of Erythritol changes about 10% during solid to liquid
phase transition[m^3]
 Vpcmt  =

    0.5039056

-->Mpcm=Ps*Vpcmt    // mass of PCM [kg]
 Mpcm  =

    745.78032
```

APPENDIX G: SIMULATION OF THE THERMAL MODEL LATENT HEAT STORAGE UNIT (MODIFIED MODEL)

These results were obtained in the following manner:

- Since the total discharge period was 12 hours, for various instants: 0, 2, 4, 6,8,10 and 12 h, the corresponding dimensionless time is calculated as:

$$\tau_i = \frac{k_m (T_m - T_i) t_i}{H \rho_m R_O^2}$$

(G.1)

- The second step consisted of calculating the corresponding value of the fraction of solidified PCM F_O at inlet of heat exchanger by using the following equation:

$$\tau_i = \frac{F_{Oi}}{2\beta} + \frac{1}{4} G_O (F_{Oi}) + \frac{F_{Oi}}{2} \frac{k_m}{k_w} \ln s$$

(G.2)

- The calculation of corresponding effectiveness is obtained from the equation:

$$NTU_x = \frac{2\pi R_i h x}{m_f\, c_p} = -\ln(1 - e_{\min(i)}) - \frac{\beta.k_m}{k_w} \ln(1 - e_{\min(i)}) \ln s + \frac{\beta}{2} [G_1(F_{Oi}) - G_1(F)]$$

(G.3)

The axial distancex varies between 0 and 3 since the total length of the tube is fixed at 3 m.

- The fourth step was the determination of corresponding value of F_i from:

$$\varepsilon_i = \frac{T_f - T_O}{T_m - T_O} = 1 - \frac{F_i}{F_{Oi}}$$

(G.4)

Therefore,

$$F_i = F_{0i}(1 - \varepsilon_i)$$

(G.5)

- The last step is about the calculation of solidification front radius of the PCM. It is given by:

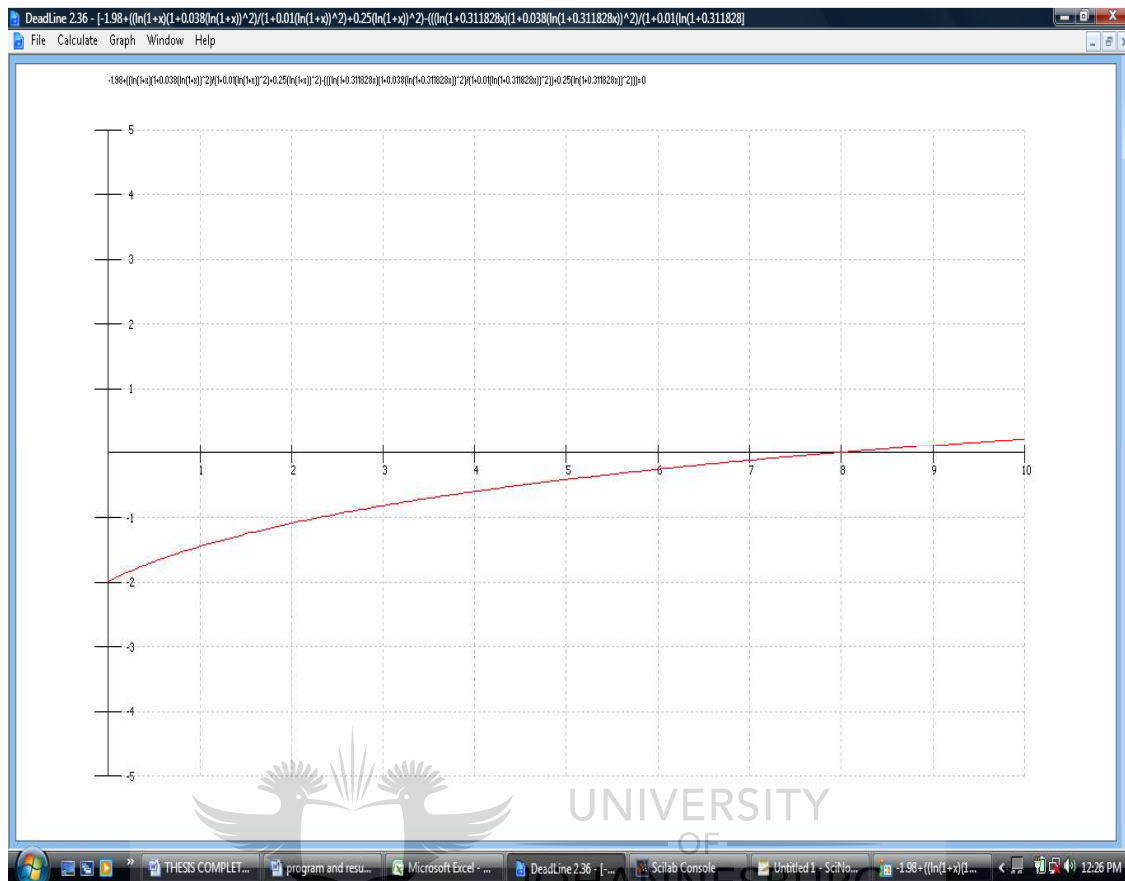$$F_i = \left(\frac{r_m^2}{R_O^2} - 1 \right)$$

(G.6)

With:

$$r_m = R_0 \sqrt{F_i + 1}$$

(G.7)

	NTU	x[m]	e	Tf[C]	F0	F	r_m	r_m [mm]
	0	0	0	25	0	0	0.0244	24.4
0h	0.496	1	0.39	61.27	0	0	0.0244	24.4
	0.769	1.5	0.54	75.22	0	0	0.0244	24.4
	0.992	2	0.63	83.59	0	0	0.0244	24.4
	1.24	2.5	0.71	91.03	0	0	0.0244	24.4
	1.488	3	0.77	96.61	0	0	0.0244	24.4
	0	0	0	25	1.235	1.235	0.03648	36.48
	0.496	1	0.36	58.48	1.235	0.7904	0.03265	32.65
2h	0.769	1.5	0.5	71.5	1.235	0.6175	0.03103	31.03
	0.992	2	0.59	79.87	1.235	0.50635	0.02995	29.95
	1.24	2.5	0.68	88.24	1.235	0.3952	0.02882	28.82
	1.488	3	0.74	93.82	1.235	0.3211	0.02805	28.05
	0	0	0	25	2.1721	2.1721	0.04346	43.46
	0.248	0.5	0.185	42.205	2.1721	1.77026	0.04061	40.61
	0.496	1	0.34	56.62	2.1721	1.43359	0.03806	38.06
4h	0.769	1.5	0.48	69.64	2.1721	1.12949	0.03561	35.61
	0.992	2	0.57	78.01	2.1721	0.934	0.03393	33.93
	1.24	2.5	0.66	86.38	2.1721	0.73851	0.03217	32.17
	1.488	3	0.72	91.96	2.1721	0.60819	0.03094	30.94
	0	0	0	25	3.158	3.158	0.04975	49.75
	0.248	0.5	0.18	41.74	3.158	2.58956	0.04623	46.23
	0.496	1	0.33	55.69	3.158	2.11586	0.04307	43.07
6h	0.769	1.5	0.47	68.71	3.158	1.67374	0.0399	39.90
	0.992	2	0.56	77.08	3.158	1.38952	0.03772	37.72
	1.24	2.5	0.64	84.52	3.158	1.13688	0.03567	35.67
	1.488	3	0.71	91.03	3.158	0.91582	0.03377	33.77
	0	0	0	25	4.1099	4.1099	0.05516	55.16
	0.248	0.5	0.175	41.275	4.1099	3.39067	0.05113	51.13
	0.496	1	0.32	54.76	4.1099	2.79473	0.04753	47.53
8h	0.769	1.5	0.46	67.78	4.1099	2.21935	0.04378	43.78
	0.992	2	0.55	76.15	4.1099	1.84946	0.04119	41.19
	1.24	2.5	0.63	83.59	4.1099	1.52066	0.03874	38.74
	1.488	3	0.7	90.1	4.1099	1.23297	0.03646	36.46
	0	0	0	25	5.0368	5.0368	0.05995	59.95
	0.248	0.5	0.17	40.81	5.0368	4.18054	0.05554	55.54
	0.496	1	0.32	54.76	5.0368	3.42502	0.05133	51.33
10h	0.769	1.5	0.45	66.85	5.0368	2.77024	0.04738	47.38
	0.992	2	0.54	75.22	5.0368	2.31693	0.04444	44.44
	1.24	2.5	0.6	82.66	5.0368	1.91398	0.04165	41.65
	1.488	3	0.69	89.17	5.0368	1.56141	0.03905	39.05
	0	0	0	25	5.943	5.943	0.06429	64.29
	0.248	0.5	0.17	40.81	5.943	4.93269	0.05943	59.43
	0.496	1	0.31	53.83	5.943	4.10067	0.05511	55.11
	0.769	1.5	0.44	65.92	5.943	3.32808	0.05076	50.76
	0.992	2	0.53	74.29	5.943	2.79321	0.04752	47.52
12h	1.24	2.5	0.62	82.66	5.943	2.25834	0.04404	44.04
	1.488	3	0.69	89.17	5.943	1.84233	0.04114	41.14

SIMULATION OF THE MODIFIED MODEL

APPENDIX H: GRAPHICAL DETERMINATION OF F_0 [SHAMSUNDAR'S MODEL]

-1.98+((ln(1+x)(1+0.038(ln(1+x))^2)/(1+0.01(ln(1+x))^2)+0.25(ln(1+x))^2)-(((ln(1+0.311828x)(1+0.038(ln(1+0.311828x))^2)/(1+0.01(ln(1+0.311828x))^2))+0.25(ln(1+0.311828x))^2))) = 0

m=0.1

[0; 10]

1 root found and the result provided the value of F_0

x_1 =7.90840829

APPENDIX I.1: PROGRAMME CODE FOR THE DESIGN OF THE LHS – SHAMSUNDAR'S MODEL

```
//  PROGRAMME FOR THE DESIGN OF THE LATENT HEAT STORAGE UNIT
Tm=118       // Melting point of Erythritol [°C]
H=339800     // Latent heat of fusion of Erythritol [°C]
Cps=1383     // Specific heat of solid Erythritol @ 20°C [ J/kg C]
Cpl=2765     // Specific heat of liquid Erythritol @ 140°C [ J/kg C]
ks=0.733     // Thermal conductivity of solid Erythritol @ 20°C [ W/m K]
kl=0.326     // Thermal conductivity of liquid Erythritol @ 140°C [W/m K]
Ps= 1480     // Density of solid Erythritol @ 20°C [kg/m^3]
Pl =1300     // Density of liquid Erythritol @ 140°C [kg/m^3]


kw=386 // Thermal conductivity of copper


// HEAT TRANSFER FLUID SELECTED : DURATHERM XLT-50
// PROPERTIES OF DURATHERM XLT-50 AT MEAN TEMPERATURE=60 °C
kf=0.131   // Thermal conductiivity of Duratherm XLT-50 [ W/m K]
Cpf=2177   // Specific heat of Duartherm XLT-50 [ J/kg C]
nuf=1.18e-3 // Dynamic viscosity of Duratherm XLT-50 [ Pa.s]
Pf=814     // Density Duratherm XLT-50 [ kg/m3]


// PARAMETER SPECIFICATIONS OF WORKING FLUID IN HEAT EXCHANGER
Ti=25
Tmax=97    // Outlet Temperature of Duratherm XLT-50 [°C] from the heat exchanger
Tmin=89    // Outlet Temperature of Duratherm XLT -50 [C] from the heat exchanger[°C]
mft=0.017   // Total mass flow rate [ kg/s]
td=43200    // Discharge period  of heat exchanger [s], 12 hours is the discharge period


emax=(Tmax-Ti)/(Tm-Ti) // maximum  effectiveness of heat exchanger
emin=(Tmin-Ti)/(Tm-Ti) // minimum  effectiveness of heat exchanger


Nu=1.83              // Nusselt Number for fully developed flow laminar ( Nu=h*Ri/kf).It is equal to
3.67 with reference to the diameter.
NTU=-log(1-emax)   // Number of Transfer Units ( 0.5< NTU >5
B=Nu*(kf/ks)// The parameter B is calculated for fully developed flow laminar, The ratio outer
radius and inner radius of the tube exchanger is fixed at 1.15


// DETERMINATION OF FRACTION OF THE PCM SOLIDIFIED AT THE INLET HEAT
EXCHANGER
p0=-log(1-emin);
x=(NTU-p0)*2/B;
y=exp(x);
F0=(y-1)/(1-y*(1-emin));
if F0 < 0 then y=exp(2*x/p0); F0=sqrt(y/(1-emin))// F0 is the approximate value of F0. In order to
find the value of F0, the Newton Raphson method is applied
end;


F1=(1-emin)*F0;
p1=log(1+F0);
p2=p1*p1;
G1=(1+(17/450)*p2)*p1/(1+(1/100)*p2)+(p2/4);// F0 is determined by iteration
p3=log(1+F1);
p4=p3*p3;
G2=(1+(17/450)*p4)*p3/(1+(1/100)*p4)+(p4/4);
x=-log(1-emin)+B/2*(G1-G2)-NTU;
y=B/2*(p1/F0-(1-emin)*p3/(1+F1));
F2=F0-x/y
```

119

```
F3=(1-emin)*F2;
p5=log(1+F2);
p6=p5*p5;
G3=(1+(17/450)*p6)*p5/(1+(1/100)*p6)+(p6/4);
p7=log(1+F3);
p8=p7*p7;
G4=(1+(17/450)*p8)*p7/(1+(1/100)*p8)+(p8/4);
x1=-log(1-emin)+ B*(ks/kw)*(1.15)*(-log(1-emin))+B/2*(G3-G4)-NTU;
y1=B/2*(p5/F2-(1-emin)*p7/(1+F3));
F4=F2-x1/y1

F5=(1-emin)*F4;
p9=log(1+F4);
p10=p9*p9;
G5=(1+(17/450)*p10)*p9/(1+(1/100)*p10)+(p10/4);
p11=log(1+F5);
p12=p11*p11;
G6=(1+(17/450)*p12)*p11/(1+(1/100)*p12)+(p12/4);;
x2=-log(1-emin)+B/2*(G5-G6)-NTU;
y2=B/2*(p9/F4-(1-emin)*p11/(1+F5));
F6=F4-x2/y2

F7=(1-emin)*F6;
p13=log(1+F6);
p14=p13*p13;
G7=(1+(17/450)*p14)*p13/(1+(1/100)*p14)+(p14/4);
p15=log(1+F7);
p16=p15*p15;
G8=(1+(17/450)*p16)*p15/(1+(1/100)*p16)+(p16/4);
x3=-log(1-emin)+B/2*(G7-G8)-NTU;
y3=B/2*(p13/F6-(1-emin)*p15/(1+F7));
F8=F6-x3/y3

F9=(1-emin)*F8;
p17=log(1+F8);
p18=p17*p17;
G9=(1+(17/450)*p18)*p17/(1+(1/100)*p18)+(p18/4);
p19=log(1+F9);
p20=p19*p19;
G10=(1+(17/450)*p20)*p19/(1+(1/100)*p20)+(p20/4);
x4=-log(1-emin)+B/2*(G9-G10)-NTU;
y4=B/2*(p17/F8-(1-emin)*p19/(1+F9));
F10=F8-x4/y4

F11=(1-emin)*F10;
p21=log(1+F10);
p22=p21*p21;
G11=(1+(17/450)*p22)*p21/(1+(1/100)*p22)+(p22/4);
p23=log(1+F11);
p24=p23*p23;
G12=(1+(17/450)*p24)*p23/(1+(1/100)*p24)+(p24/4);
x5=-log(1-emin)+B/2*(G11-G12)-NTU;
y5=B/2*(p21/F10-(1-emin)*p23/(1+F11));
F12=F10-x5/y5

F13=(1-emin)*F12;
p25=log(1+F12);
p26=p25*p25;
G13=(1+(17/450)*p26)*p25/(1+(1/100)*p26)+(p26/4);
```

```
p27=log(1+F13);
p28=p27*p27;
G14=(1+(17/450)*p28)*p27/(1+(1/100)*p28)+(p28/4);
x6=-log(1-emin)+B/2*(G13-G14)-NTU;
y6=B/2*(p25/F12-(1-emin)*p27/(1+F13));
F14=F12-x6/y6

F15=(1-emin)*F14;
p29=log(1+F14);
p30=p29*p29;
G15=(1+(17/450)*p30)*p29/(1+(1/100)*p30)+(p30/4);
p31=log(1+F15);
p32=p31*p31;
G16=(1+(17/450)*p32)*p31/(1+(1/100)*p32)+(p32/4);
x7=-log(1-emin)+B/2*(G15-G16)-NTU;
y7=B/2*(p25/F14-(1-emin)*p31/(1+F15));
F16=F14-x7/y7

F17=(1-emin)*F16;
p33=log(1+F16);
p34=p33*p33;
G17=(1+(17/450)*p34)*p33/(1+(1/100)*p34)+(p34/4);
p35=log(1+F17);
p36=p35*p35;
G18=(1+(17/450)*p36)*p35/(1+(1/100)*p36)+(p36/4);
x8=-log(1-emin)+B/2*(G17-G18)-NTU;
y8=B/2*(p33/F16-(1-emin)*p35/(1+F17));
F18=F16-x8/y8
eps=abs(F18-F16)/F18
p37=log(1+F18)      // parameter in the calculation the dimensionless time [tau]
Go=(1+F18)*p37-F18  // parameter in calculation the dimensionless time [tau]
tau=F18/(2*B)+Go/4+F18*(ks/kw)*log (1.15)/(2) // Dimensionless time, The ratio outer radius and
inner radius of the tube exchanger is fixed at 1.15

Ro=sqrt(ks*(Tm-Ti)*td/(tau*Ps*H)) // The outside radius of the tube [m]
Ri=Ro/1.15    // The inside radius of the tube [m]. The ratio outer radius and inner radius of the
tube exchanger is fixed at 1.15
h1=B*ks/Ro    // Convective heat transfer coefficient [W/m2.K]
Dp=2*Ro*sqrt(1+F18)// Tube pitch [m]
v=(NTU*mft*Cpf)/(2*%pi*Ri*h1)// product of the number of tubes and the length of tube
L=3       // length of tube fixed at 3 m
n=v/L        // number of tubes
ceil(n)
mf=mft/n // mass flow rate in a tube[kg/s]
Re=(2*mf)/(%pi*Ri*nuf)  // Reynolds number in the tube( less than 2300, laminar flow rate)
Dt=Dp*sqrt(2*((3)^0.5)*n/%pi) // Tank diameter [m]
Vt=%pi*Dt^2*L/4  // Tank volume [m^3]
Vl=%pi*n*L*Ri^2  // Liquid volume [m^3]
Vtu=%pi*(Ro+Ri)*n*L*(Ro-Ri)// Tube volume [m^3]
Vpcm=Vt-Vl-Vtu // Volume of PCM [m^3]
Vpcmt=(Vpcm/10+Vpcm) // Volume of Erythritol changes about 10% during solid to liquid phase
transition[m^3]
Mpcm=Ps*Vpcmt    // mass of PCM [kg]
```

APPENDIX I.2: RESULTS OF THE PROGRAMME CODE OF THE LATENT HEAT STORAGE UNIT [SHAMSUNDAR'S MODEL]

scilab-5.3.0-beta-5

Consortium Scilab (DIGITEO)
Copyright (c) 1989-2010 (INRIA)
Copyright (c) 1989-2007 (ENPC)

_____

Startup execution:
  loading initial environment

-->// PROGRAM DESIGN OF THE LATENT HEAT STORAGE UNIT

-->Tm=118   // Melting point of Erythritol [^{o}C]
 Tm =

   118.

-->H=339800   // Latent heat of fusion of Erythritol [^{o}C]
 H =

   339800.

-->Cps=1383   // Specific heat of solid Erythritol @ 20°C [J/kg ^{o}C]
 Cps =

   1383.

-->Cpl=2765   // Specific heat of liquid Erythritol @ 140°C [J/kg ^{o}C]
 Cpl =

   2765.

-->ks=0.733   // Thermal conductivity of solid Erythritol @ 20°C [W/m.K]
 ks =

   0.733

-->kl=0.326   // Thermal conductivity of liquid Erythritol @ 140°C [W/m.K]
 kl =

   0.326

-->Ps= 1480 // Density of solid Erythritol @ 20°C [kg/m^3]
 Ps =

   1480.

-->Pl =1300   // Density of liquid Erythritol @ 140°C [kg/m^3]
 Pl =

   1300.

```
-->

-->kw=386 // Thermal conductivity of copper
 kw  =

   386.

-->

-->// HEAT TRANSFER FLUID SELECTED: DURATHERM XLT-50

-->// PROPERTIES OF DURATHERM XLT-50 AT MEAN TEMPERATURE=60°C

-->kf=0.131   // Thermal conductivity of Duratherm XLT-50 [W/m.K]
 kf  =

   0.131

-->Cpf=2177   // Specific heat of Duratherm XLT-50 [J/kg.°C]
 Cpf  =

   2177.

-->nuf=1.18e-3 // Dynamic viscosity of Duratherm XLT-50 [Pa.s]
 nuf  =

   0.00118

-->Pf=814      // Density Duratherm XLT-50 [kg/m3]
 Pf  =

   814.

-->

-->// PARAMETER SPECIFICATIONS OF THE WORKING FLUID IN HEAT EXCHANGER

-->Ti=25
 Ti  =

   25.

-->Tmax=97   // Outlet Temperature of Duratherm XLT-50 [°C] from the heat exchanger
 Tmax  =

   97.

-->Tmin=89    // Outlet Temperature of Duratherm XLT -50 [°C] from the heat exchanger [°C]
 Tmin  =

   89.

-->mft=0.017   // Total mass flow rate [kg/s]
 mft  =

   0.017
```

-->td=43200   // Discharge period of heat exchanger [s], 12 hours is the discharge period
 td =

    43200.

-->

-->emax=(Tmax-Ti)/(Tm-Ti) // maximum effectiveness of heat exchanger
 emax =

    0.7741935

-->emin=(Tmin-Ti)/(Tm-Ti) // minimum effectiveness of heat exchanger
 emin =

    0.6881720

-->

-->Nu=1.83   // Nusselt Number for fully developed flow laminar (Nu=h*Ri/kf).It is
equal to 3.67 with reference to the diameter.
 Nu =

    1.83

-->NTU=-log(1-emax)   // Number of Transfer Units (0.5< NTU >5)
 NTU =

    1.4880771

-->B=Nu*(kf/ks) // The parameter B is calculated for fully developed flow laminar, The ratio
outer radius and inner radius of the tube exchanger is fixed at 1.15
 B =

    0.3270532

-->
-->// DETERMINATION OF THE FRACTION OF THE PCM SOLIDIFIED AT THE INLET
HEAT EXCHANGER DURING THE DISCHARGE CYCLE.

-->p0=-log(1-emin);

-->x=(NTU-p0)*2/B;

-->y=exp(x);

-->F0=(y-1)/(1-y*(1-emin));

-->if F0 < 0 then y=exp(2*x/p0); F0=sqrt(y/(1-emin))// F0 is the approximate value of F0. In
order to find the value of F0, the Newton-Raphson method is applied
 F0 =

    9.7423592
-->end;

-->

```
-->F1=(1-emin)*F0;

-->p1=log(1+F0);

-->p2=p1*p1;

-->G1=(1+(17/450)*p2)*p1/(1+(1/100)*p2)+(p2/4);// Fo is determined by iteration

-->p3=log(1+F1);

-->p4=p3*p3;

-->G2=(1+(17/450)*p4)*p3/(1+(1/100)*p4)+(p4/4);

-->x=-log(1-emin)+B/2*(G1-G2)-NTU;

-->y=B/2*(p1/F0-(1-emin)*p3/(1+F1));

-->F2=F0-x/y
 F2  =

   8.2367021

-->

-->F3=(1-emin)*F2;

-->p5=log(1+F2);

-->p6=p5*p5;

-->G3=(1+(17/450)*p6)*p5/(1+(1/100)*p6)+(p6/4);

-->p7=log(1+F3);

-->p8=p7*p7;

-->G4=(1+(17/450)*p8)*p7/(1+(1/100)*p8)+(p8/4);

-->x1=-log(1-emin)+ B*(ks/kw)*(1.15)*(-log(1-emin))+B/2*(G3-G4)-NTU;

-->y1=B/2*(p5/F2-(1-emin)*p7/(1+F3));

-->F4=F2-x1/y1
 F4  =

   7.9345991

-->

-->F5=(1-emin)*F4;

-->p9=log(1+F4);

-->p10=p9*p9;

-->G5=(1+(17/450)*p10)*p9/(1+(1/100)*p10)+(p10/4);
```

```
-->p11=log(1+F5);

-->p12=p11*p11;

-->G6=(1+(17/450)*p12)*p11/(1+(1/100)*p12)+(p12/4);;

-->x2=-log(1-emin)+B/2*(G5-G6)-NTU;

-->y2=B/2*(p9/F4-(1-emin)*p11/(1+F5));

-->F6=F4-x2/y2
 F6  =

    7.8889739

-->

-->F7=(1-emin)*F6;

-->p13=log(1+F6);

-->p14=p13*p13;

-->G7=(1+(17/450)*p14)*p13/(1+(1/100)*p14)+(p14/4);

-->p15=log(1+F7);

-->p16=p15*p15;

-->G8=(1+(17/450)*p16)*p15/(1+(1/100)*p16)+(p16/4);

-->x3=-log(1-emin)+B/2*(G7-G8)-NTU;

-->y3=B/2*(p13/F6-(1-emin)*p15/(1+F7));

-->F8=F6-x3/y3
 F8  =

    7.8765279

-->

-->F9=(1-emin)*F8;

-->p17=log(1+F8);

-->p18=p17*p17;

-->G9=(1+(17/450)*p18)*p17/(1+(1/100)*p18)+(p18/4);

-->p19=log(1+F9);

-->p20=p19*p19;

-->G10=(1+(17/450)*p20)*p19/(1+(1/100)*p20)+(p20/4);
```
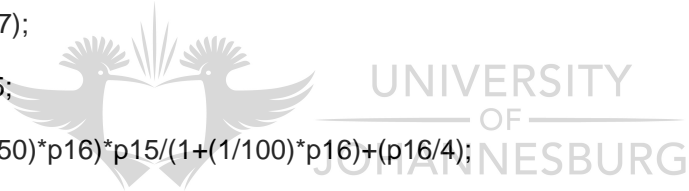
```
-->x4=-log(1-emin)+B/2*(G9-G10)-NTU;

-->y4=B/2*(p17/F8-(1-emin)*p19/(1+F9));

-->F10=F8-x4/y4
 F10  =

    7.8731

-->

-->F11=(1-emin)*F10;

-->p21=log(1+F10);

-->p22=p21*p21;

-->G11=(1+(17/450)*p22)*p21/(1+(1/100)*p22)+(p22/4);

-->p23=log(1+F11);

-->p24=p23*p23;

-->G12=(1+(17/450)*p24)*p23/(1+(1/100)*p24)+(p24/4);

-->x5=-log(1-emin)+B/2*(G11-G12)-NTU;

-->y5=B/2*(p21/F10-(1-emin)*p23/(1+F11));

-->F12=F10-x5/y5
 F12  =

    7.8721534

-->

-->F13=(1-emin)*F12;

-->p25=log(1+F12);

-->p26=p25*p25;

-->G13=(1+(17/450)*p26)*p25/(1+(1/100)*p26)+(p26/4);

-->p27=log(1+F13);

-->p28=p27*p27;

-->G14=(1+(17/450)*p28)*p27/(1+(1/100)*p28)+(p28/4);

-->x6=-log(1-emin)+B/2*(G13-G14)-NTU;

-->y6=B/2*(p25/F12-(1-emin)*p27/(1+F13));

-->F14=F12-x6/y6
 F14  =
```

7.8718918

```
-->

-->F15=(1-emin)*F14;

-->p29=log(1+F14);

-->p30=p29*p29;

-->G15=(1+(17/450)*p30)*p29/(1+(1/100)*p30)+(p30/4);

-->p31=log(1+F15);

-->p32=p31*p31;

-->G16=(1+(17/450)*p32)*p31/(1+(1/100)*p32)+(p32/4);

-->x7=-log(1-emin)+B/2*(G15-G16)-NTU;

-->y7=B/2*(p25/F14-(1-emin)*p31/(1+F15));

-->F16=F14-x7/y7
 F16  =

   7.8718195

-->

-->F17=(1-emin)*F16;

-->p33=log(1+F16);

-->p34=p33*p33;

-->G17=(1+(17/450)*p34)*p33/(1+(1/100)*p34)+(p34/4);

-->p35=log(1+F17);

-->p36=p35*p35;

-->G18=(1+(17/450)*p36)*p35/(1+(1/100)*p36)+(p36/4);

-->x8=-log(1-emin)+B/2*(G17-G18)-NTU;

-->y8=B/2*(p33/F16-(1-emin)*p35/(1+F17));

-->F18=F16-x8/y8
 F18  =

   7.8717995

-->eps=abs(F18-F16)/F18
 eps  =

   0.0000025
```

```
-->p37=log(1+F18)      // parameter in  calculation the dimensionless time [tau]
 p37  =

   2.1828776

-->Go=(1+F18)*p37-F18  // parameter in calculation the dimensionless time [tau]
 Go  =

   11.494253

-->tau=F18/(2*B)+Go/4+F18*(ks/kw)*log (1.15)/(2) // Dimensionless time, The ratio outer
radius and inner radius of the tube exchanger is fixed at 1.15
 tau  =

   14.90904

-->

-->Ro=sqrt(ks*(Tm-Ti)*td/(tau*Ps*H)) // The outside radius of the tube [m]
 Ro  =

   0.0198184

-->Ri=Ro/1.15    // The inside radius of the tube [m]. The ratio outer radius and inner radius of
the tube exchanger is fixed at 1.15
 Ri  =

   0.0172334

-->h1=B*ks/Ro   // Convective heat transfer coefficient [W/m2.K]
 h1  =

   12.096353

-->Dp=2*Ro*sqrt(1+F18)// Tube pitch [m]
 Dp  =

   0.1180603

-->v=(NTU*mft*Cpf)/(2*%pi*Ri*h1)// product of the number of tubes and the length of tube
 v  =

   42.046355

-->L=3      // length of tube fixed at 3 m
 L  =

   3.

-->n=v/L       // number of tube
 n  =

   14.015452

-->ceil(n)
 ans  =
```

15.

```
-->mf=mft/n // mass flow rate in a tube [kg/s]
 mf  =

   0.0012129

-->Re=(2*mf)/(%pi*Ri*nuf)  // Reynolds number in the tube( less than 2300, laminar flow rate)
 Re  =

   37.972556

-->Dt=Dp*sqrt(2*((3)^0.5)*n/%pi) // Tank diameter [m]
 Dt  =

   0.4641173

-->Vt=%pi*Dt^2*L/4  // Tank volume [m^3]
 Vt  =

   0.5075357

-->Vl=%pi*n*L*Ri^2  // Liquid volume [m^3]
 Vl  =

   0.0392300

-->Vtu=%pi*(Ro+Ri)*n*L*(Ro-Ri)// Tube volume [m^3]
 Vtu  =

   0.0126517

-->Vpcm=Vt-Vl-Vtu // Volume of PCM [m^3]
 Vpcm  =

   0.455654

-->Vpcmt=(Vpcm/10+Vpcm) // Volume of Erythritol changes about 10% during solid to liquid
phase transition[m^3]
 Vpcmt  =

   0.5012194

-->Mpcm=Ps*Vpcmt    // mass of PCM [kg]
 Mpcm  =

   741.80471
```

Time[h]	NTU	X[m]	e	Tf[C]	F0	F	r_m
	0	0	0	25	0	0	20
	0.49	1	0.39	61	0	0	20
0	0.74	1.5	0.52	73	0	0	20
	0.99	2	0.63	84	0	0	20
	1.24	2.5	0.71	91	0	0	20
	1.48	3	0.77	97	0	0	20
	0	0	0	25	1.5	1.5	31
	0.49	1	0.35	58	1.5	0.975	28
2	0.74	1.5	0.48	70	1.5	0.78	26
	0.99	2	0.59	80	1.5	0.615	25
	1.24	2.5	0.67	87	1.5	0.495	24
	1.48	3	0.74	94	1.5	0.39	23
	0	0	0	25	2.9	2.9	39
	0.49	1	0.33	56	2.9	1.943	34
4	0.74	1.5	0.46	68	2.9	1.566	32
	0.99	2	0.56	77	2.9	1.276	30
	1.24	2.5	0.65	85	2.9	1.015	28
	1.48	3	0.72	92	2.9	0.812	27
	0	0	0	25	4.2	4.2	45
	0.49	1	0.32	55	4.2	2.856	39
6	0.74	1.5	0.46	68	4.2	2.268	36
	0.99	2	0.56	77	4.2	1.848	33
	1.24	2.5	0.64	85	4.2	1.512	31
	1.48	3	0.71	91	4.2	1.218	29
	0	0	0	25	5.4	5.4	50
	0.49	1	0.32	55	5.4	3.672	43
8	0.74	1.5	0.45	67	5.4	2.97	39
	0.99	2	0.56	77	5.4	2.376	36
	1.24	2.5	0.63	84	5.4	1.998	34
	1.48	3	0.7	90	5.4	1.62	32
	0	0	0	25	6.6	6.6	55
	0.49	1	0.31	54	6.6	4.554	47
10	0.74	1.5	0.44	66	6.6	3.696	43
	0.99	2	0.54	75	6.6	3.036	40
	1.24	2.5	0.62	83	6.6	2.508	37
	1.48	3	0.69	89	6.6	2.046	35
	0	0	0	25	7.9	7.9	59
	0.49	1	0.31	54	7.9	5.451	50
12	0.74	1.5	0.43	65	7.9	4.503	46
	0.99	2	0.53	74	7.9	3.713	43
	1.24	2.5	0.62	83	7.9	3.002	40
	1.48	3	0.69	89	7.9	2.449	37

SIMULATION SHAMSUNDAR'S MODEL

APPENDIX J.1: ANALYTICAL APPROXIMATION [QUASI STATIONARY METHOD]

METHOD 1

The first method referred to as "Yu's method" and the results obtained using this model are also given.

In quasi stationary (quasi-static) method, the heat conduction equation is replaced by the steady-state equation at the same time the phase change front is varied.

Yu's method consisted in determining the outlet temperature of the HTF flowing inside the tube of heat exchanger as well as the solidification front radius (for the discharging process) and the melting front radius for the charging process). It is established from the *conservation of energy* principle.

Consider a hollow cylinder along the x-axis of inner radius R_i and outer radius R_0, filled with PCM with the melting temperature T_m. Heat is transferred from the PCM by pumping a HTF through the inner tube at desired velocity v and the inlet temperature T_i at x=0. If $T_i \rangle T_m$ the PCM is charged, whereas $T_i \langle T_m$ the PCM being discharged (Alexiades V.,Solomon A.D; 1993). The problem is to evaluate the interface r_m and temperature of HTF T_f as function of velocity v and the inlet temperature.

The following assumptions are made:

- The thermo-physical properties of the liquid and the solid phase of PCM are the same. All the properties remain constant with respect to temperature;
- Effect of natural convection in the liquid phase of PCM was not taken into account;
- Conduction in the PCM and tube wall is circumferential, and the conduction in axial direction is neglected. The problem is axisymmetric;
- Initial temperature of the thermal energy storage unit is uniform;
- Adiabatic outer wall is assumed.

Initial and boundary conditions:

    (1) Initial condition:

$$r_m(x, t = 0) = R_o$$
$$T_f(x, t = 0) = T_m$$

    (2) Boundary condition: $T_f(x, t = 0) = T_i$

The following equations are obtained from the *conservation of energy* principle:

$$T_f = T_m - [T_m - T_i].\exp\left[-\frac{\pi D_i h}{C_{P,f}\dot{m}_f}.\frac{R_h}{R_h + R_w + R_m(x,t)}.x\right] \tag{J.1}$$

132

$$r_m(x,t) = \sqrt{R_0^2 + \int_0^t \frac{hD_i}{H\rho_m} \times \frac{R_h}{R_h + R_w + R_m(x,t)} \times [T_m - T_i]dt}$$ (J.2)

Where T_f = outlet temperature of HTF;

T_m = melting point of PCM;

T_i = inlet temperature of HTF;

D_i = inner diameter of the tube heat exchanger;

R_0 = outer radius of the tube heat exchanger;

h = convective heat transfer coefficient;

$C_{p,f}$ = heat specific capacity of HTF;

x = distance along the axial direction;

H = latent heat of fusion of PCM;

ρ_m = density of the PCM;

t = time;

$R_h = \dfrac{1}{h} =$ convective thermal resistance of HTF;

$R_w = \dfrac{D_i}{2k_w} \ln \dfrac{D_0}{D_i} =$ conductive thermal resistance of tube wall, $k_w =$ thermal

conductivity of the tube wall;

$R_m(x,t) = \dfrac{D_i}{2k_m} \ln \dfrac{D_m(x,t)}{D_0} =$ The conduction thermal resistance of the PCM, $D_0 =$

outer diameter of the tube heat exchanger; $k_m =$ thermal conductivity of the PCM   and

$D_m(x,t) =$ solidification front diameter of the PCM as a function of time and distance along

the axial direction.

$r_m(x,t)$ = the solidification front radius of the PCM as a function of x and t.

 By making use of the software Engineering Equation Solver (EES), the results obtained

using this mathematical model are given in the following table:

Time t=[h]	Temp.=Tf[C]	PCM Front radius rm [mm]	Axial distance x= [m]
2	25	34	0
	45	32	0.5
	61.1	31	1
	73.92	29	1.5
	84.03	28	2
	91.92	27	2.5
	98.03	27	3
4	25	40	0
	44.14	38	0.5
	59.8	36	1
	72.56	34	1.5
	82.76	32	2
	90.85	30	2.5
	97.19	29	3
6	25	46	0
	43.56	43	0.5
	58.94	40	1
	71.55	37	1.5
	81.78	35	2
	89.98	33	2.5
	96.47	31	3
8	25	51	0
	43.14	47	0.5
	58.27	44	1
	70.77	41	1.5
	80.99	38	2
	89.25	36	2.5
	95.85	33	3
10	25	55	0
	42.8	51	0.5
	57.73	47	1
	70.12	44	1.5
	80.32	41	2
	88.62	38	2.5
	95.3	35	3
12	25	59	0
	42.53	55	0.5
	57.27	51	1
	69.58	47	1.5
	79.75	43	2
	88.08	40	2.5
	94.81	37	3

APPENDIX J.2: ANALYTICAL APPROXIMATION
[QUASI STATIONARY METHOD]

METHOD 2

This method is also a quasi stationary analytical method. The problem statement and the unknowns are the same as in the method 1.

The following assumptions were made:

- Heat conduction is negligible in the fluid, which is at steady state thermally, so that its temperature depends only on x: $T_f(x)$

- Radial heat transfer is dominated in the PCM, so the axial one could be ignored;

- Latent heat and radial thermal conductivity of the PCM are so large that the surface temperature of the PCM at the tube wall could be as essentially equal to T_m during the entire freezing process.

$$T_f(x) = T_m - [T_m - T_i] \times \exp[-\gamma.x] \qquad \text{(J.3)}$$

$$r_m(x,t) = \sqrt{R_0^2 + \frac{2R_i h}{\rho_m H} \times \exp(-\gamma x)[T_m - T_f]t} \qquad \text{(J.4)}$$

where $\gamma = \dfrac{2h}{R_i v \rho_f C_{p,f}}$

T_f = outlet temperature of HTF;

T_m = melting point of PCM;

T_i = inlet temperature of HFT;

$r_m(x,t)$ = solidification front radius of the PCM as a function of x and t;

h = convective heat transfer coefficient;

$C_{p,f}$ = heat specific capacity of HTF;

x = distance along the axial direction of the tube heat exchanger;

ρ_m = density of the PCM;

t = time;

R_0 = outer radius of the tube heat exchanger;

R_i = inner radius of the tube heat exchanger;

v = velocity of HTF.

Using EES, the results obtained from the mathematical model used are given in the following table:

Time t=[h]	Temp.Tf=[C]	PCM solid Front radius rm=[mm]	axial distance.x=[m]
2	25	35	0
	46.65	31	0.5
	63.26	28	1
	76	26	1.5
	85.78	25	2
	93.28	25	2.5
	99.03	24	3
4	25	43	0
	46.65	36	0.5
	63.26	32	1
	76	29	1.5
	85.78	27	2
	93.28	26	2.5
	99.03	25	3
6	25	50	0
	46.65	41	0.5
	63.26	35	1
	76	31	1.5
	85.78	28	2
	93.28	27	2.5
	99.03	26	3
8	25	56	0
	46.65	45	0.5
	63.26	38	1
	76	33	1.5
	85.78	30	2
	93.28	27	2.5
	99.03	26	3
10	25	61	0
	46.65	49	0.5
	63.26	41	1
	76	34	1.5
	85.78	31	2
	93.28	28	2.5
	99.03	27	3
12	25	66	0
	46.65	52	0.5
	63.26	43	1
	76	38	1.5
	85.78	32	2
	93.28	29	2.5
	99.03	27	3